STUDIES OF
COPPER(II) COMPLEXES OF BIOACTIVE PEPTIDES

by

Rong Meng

BS, University of Science and Technology of China, 1997

MS, University of Science and Technology of China, 1999

Submitted to the Graduate Faculty of

Art and Science in partial fulfillment

of the requirements for the degree of

Doctor of Philosophy

University of Pittsburgh

2006

UNIVERSITY OF PITTSBURGH

FACULTY OF ARTS AND SCIENCES

This dissertation was presented

by

Rong Meng

It was defended on

Apr. 27th, 2006

and approved by

Billy Day

Adrian Michael

Stephane Petoud

Stephen G. Weber
Dissertation Director

STUDIES OF
COPPER(II) COMPLEXES OF BIOACTIVE PEPTIDES

Rong Meng, PhD

University of Pittsburgh, 2006

Separation-based determinations of peptides hold the promise of measuring the concentrations of many peptides and their metabolites. However, typical chromatographic methods bear disadvantages in their selectivity and/or sensitivities. Thus, means for lowering detection limits are needed. The biuret reaction, the coordination of Cu(II) and peptides in basic solutions, provides a sensitive detection method based on the reversible Cu(III)/Cu(II) electrochemistry in peptide-bonded states.

Thyrotropin-releasing hormone (TRH) is an important neuropeptide that undergoes the biuret reaction. The cationic form of TRH is not retained in a typical reversed-phase column. We have modified the common acidic mobile phase for peptide separation with a surfactant to retain the cationic TRH. A surfactant-preconditioned packed-bed capillary serves as the sample loop to preconcentrate TRH through sequential loading. The preconcentration has improved the detection limit for TRH 50-fold in the capillary HPLC-EC system.

TRH lacks the N-terminal amine and C-terminal carboxylate that are usually required in the biuret reactions of Cu(II) and tripeptides. The unique structure of TRH affects the electrochemical behavior of the complex. We have utilized various electrochemical and spectroscopic techniques to determine the stoichiometry of the complex and to identify the binding sites in the peptide. Our data reveal that the interactions between Cu(II) and TRH are also possible under physiological pH.

The unusual structure of TRH complicates the electrochemistry of Cu(II)-TRH complex. Multiple chemical reactions accompany the redox processes. We have investigated the kinetics of the coupling reactions using a rotating ring-disk electrode. The results suggest deprotonation of the ligand and inter-molecular interactions between complexes.

Using microelectrode voltammetry, we have discovered that the octarepeat peptide of the prion protein is involved in Cu(II)/Cu(I) electrochemistry at physiological pH. This observation is relevant to the copper toxicity: Cu(II) may be reduced *in vivo* to Cu(I), which reacts with hydrogen peroxide to produce damaging oxidative radicals. The octarepeat peptide stabilizes Cu(I) by altering its redox potentials. Thus, the prion protein may have a function of anti-copper-toxicity.

TABLE OF CONTENTS

LIST OF TABLES

LIST OF FIGURES

ACKNOWLEDGEMENT

During my pursuing my degree, I have received help, support, courage and much more from many people. I could not have done it without them.

My sincere appreciation goes to Dr. Weber, my research advisor, for his elaborated mentoring through these years. It is his patient guidance and encouraging advice that pulled me out of straying and lead me to every step toward success. Thanks for having confidence in me.

I would like to thank my committee members to spend their precious time and give me valuable suggestion and comments.

I thank the current and previous Weber group members for their long time help. I will cherish all the joy, all the fun, and all the big and small achievements we have been through together.

I thank all the administrative and technical staff at Department of Chemistry. Your smiles and your work have done so much.

I thank my family for their support and tolerance. I never admit but really appreciate it.

PREFACE

To my

Daughter, Husband, and Mother.

They came to me at different stages of my life.

They are equally important to me,

and all more so than I

myself.

1. Introduction: Neuropeptides and Their Interactions with Cu(II)

1.1. Neuropeptides and Biuret Method for Peptide Analysis

The mammalian brain exerts its functions through neurons and glial cells that communicate through the release of chemicals, namely neurotransmitters, into the extracellular space. Over 100 neurotransmitters, some of which are peptides, have been identified [1]. It is of great importance and interest to monitor these chemical messengers to understand behavior, disease and mental illness and how such malfunctions might be corrected.

Since neuropeptides always coexist with many other neurotransmitters, separation is usually required to perform sensible and reliable analysis of peptides. Reversed-phase High Performance Liquid chromatography (RP-HPLC) is a popular technique that bears a number of advantages. It is the ideal separation method for polar and non-volatile samples with a wide range of molecular weights and ionic properties. These features are characteristic of many biological molecules. Development of capillary HPLC has allowed the use of sample sizes down to sub-microliters and also led to lower mass detection limits [2,3]. Reversed-phase LC with 0.1% TFA and an acetonitrile gradient has worked satisfactorily for the separation of peptides. Using these conditions, high resolution separations with 100-150 peaks per chromatogram can be achieved.

Most neuropeptides exist in mammalian brains in the low μM range [4]. The extracellular concentrations are typically 1 – 100 pM. A useful detection method should be capable of detecting attomole levels in microliter samples. Commonly used detection techniques for LC include ultraviolet [5,6], fluorescence [7,8], mass spectrometry [9], immunoassay [10] and electrochemical detection [3,5,8]. UV absorbance detection lacks sensitivity towards small peptides (10^{-8} - 10^{-6} M detection limit [5,6]) because of poor selectivity. Considering the small light path length in capillary separation systems which additionally lowers the sensitivity,

absorbance detection is not suitable for neuropeptide determinations. Table 1-1 compares the selectivities and sensitivities of the other methods.

Table 1-1. Characteristics of commonly used detection method for peptides following HPLC separation.

Detector	Derivatization	Detection Limit (M)	Selectivity	References
Fluorescence	Pre-column	10^{-11} - 10^{-9}	Amine or Thiol	[7,8]
Mass Spec	None	10^{-9} - 10^{-7}	Universal	[9]
Immunoassay	Off-line	10^{-13} - 10^{-10}	Epitope	[10]
Electrochemistry	None	10^{-12} - 10^{-9}	Trp, Tyr, Cys	[3,5,8]

Table 1-1 implies disadvantages associated with the listed methods despite their high sensitivity. The specificity of immunoassay is low in the presence of cross-reactive species [11]. Necessary modifications, such as truncation and deamidation, may lead to peptide microheterogeneity and influence data interpretation [12]. Fluorescence detection depends on the derivatization of amine or thiol groups, thus the reaction is not specific for peptides. Multiple derivatization sometimes occurs on peptides bearing multiple amine groups and interferes with quantification. Electrospray mass spectrometry is well suited for coupling with microseparation techniques. Yet, since its sensitivity is closely related to the spray rate, the interface, the operation mode, the m/z ratio, and the solution matrix [13], this detection method is better for qualification purposes rather than quantification, unless coupled with clean-up/preconcentration procedures to improve ionization efficiency and sensitivity [2]. Direct electrochemical methods apparently have very limited application.

Few methods among the above allow for both sensitive and selective peptide detection. Another detection scheme that is peptide-specific and characterized by low detection limits is electrochemical detection based on the biuret reaction.

The biuret reaction refers to the coordination of Cu(II) ion with deprotonated amide nitrogens in alkaline solutions. The name “biuret” came from half a century ago. Cu(II) forms a complex with biuret, H_2N-CO-NH-CO-NH_2, in pH > 13 aqueous alkali [14]. In the 1980s, the analytical value of the biuret reaction were recognized [15,16] -- in the form of a biuret complex, Cu(II) is reversibly oxidized to Cu(III) at practical potentials, typically 0.5 – 0.8 V vs Ag/AgCl at pH 10. With excess Cu(II), the oxidation is quantitative with respect to peptide concentrations. Based on the reversibility of the redox reaction, dual electrode detectors in flow systems provide additional selectivity toward peptides and high signal-to-noise ratios on the downstream electrode. The biuret detection scheme is compatible with the most common mobile phase for peptide analysis, namely 0.1% TFA in water-acetonitrile gradient [15]. The reaction takes place in a few seconds for most peptides investigated [15], meaning post-column derivatization is possible. With post-column derivatization, the detection does not interfere with the separation mechanism. Detection limits for non-electroactive peptides at the cathode range from 20 - 200 fmol (100 μL of a 0.2 - 1 nM solution) and 6 - 40 fmol (100 μL of a 60 - 400 pM solution) at the anode for electroactive peptides [17].

Biuret detection of peptides for HPLC thus provides good selectivity for peptides as well as high sensitivity. However, neuropeptides are diverse in structures and ionic properties. It is necessary to explore the applicability of biuret detection method on some special yet important neuropeptides. To allow low sample volume analysis necessary for some biological samples, a capillary HPLC system is ultimately preferred. This brings in new requirements for the separation, post-column reaction and detection.

1.2. Biuret complexes: structure and electrochemical implications

In the HPLC system, a post-column derivativatization reaction needs to be quantitative and fast enough to take place within a limited flow path (so as to avoid band broadening). It is necessary to study the coordination and electrochemical kinetics of biuret complexes for a better understanding of the applicability of the detection method.

1.2.1. Regular peptides

Metal-, especially Cu(II)-, complexes of peptides have been studied to a great extent. Initial interest arose from the surprising ability of Cu(II) to promote amide deprotonation. Amide deprotonation typically occurs at pH 15, while the biuret reaction takes place around pH 10 [18]. Figure 1-1 shows a typical structure of a copper complex of a tripeptide.

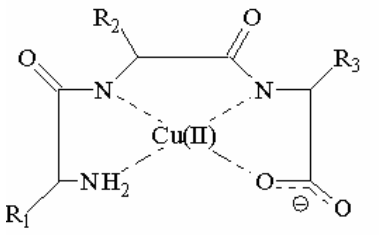

Figure 1-1. Typical structure of Cu(II)-tripeptide complex.

Side chains R_1 – R_3 do not participate in the coordination.

Typical peptides, which we define as having an N-terminal amine group, C-terminal carboxyl group, and non-coordinating sidechains, bind Cu(II) initially from the primary amine nitrogen. As shown in Figure 1-2, the binding at first involves the amide carbonyl oxygen and facilitates the deprotonation of the nearby amide nitrogen which replaces the oxygen to bind Cu(II). For N-blocked peptides, the coordination is slower and may require other conditions such as higher pH or higher temperature [19]. In this case, the C-terminal carboxylate group has been suggested to initiate the coordination [20].

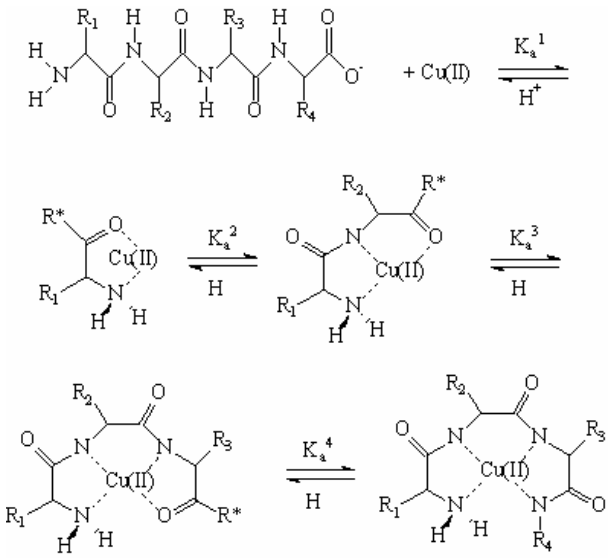

Figure 1-2. Typical procedure of Cu(II)-tripeptide coordination.

Side chains R_1 – R_3 do not participate in the coordination.

Cu(II)-peptide complexes usually are square planer structures with four equatorial ligands, resulting from Jahn-Teller effects. The equatorial donors determine most of the characteristics of the complex, including optical and electrochemical properties. Depending on the actual conditional pK_a values of each amide nitrogen and the environmental pH, components of NNOO (one amine nitrogen, one deprotonated peptide amido nitrogen, and two carbonyl oxygens or one carbonyl and one carboxylate oxygen), NNNO (one amine nitrogen, two deprotonated peptide amido nitrogen, and one carbonyl/carboxyle oxygen) and NNNN (one amine nitrogen and three deprotonated peptide amido nitrogens) equatorial binding modes can co-exist.

The strong nitrogen ligating brings the Cu(III)/Cu(II) redox potential down to practical values. At pH 9.8, a Cu(II)-peptide complex with the NNNN binding mode is oxidized at 0.4 – 0.6 V and a complex of NNNO binding mode at 0.7 – 0.9 V, all vs. Ag/AgCl [18,19]. For regular

peptides, the coordination is fast enough to be used in a post-column detection method in an HPLC system [15].

The Cu(III)/Cu(II) redox couple when bonded to peptides is not a simple case. The rotating ring-disk electrode (RRDE) has proven powerful in elucidating the electrochemical kinetics of Cu(II) complexes of model peptides [21]. Homogeneous chemical reactions exist both prior to and after the oxidation. The chemical reactions following oxidation are related to peptide backbone and have been observed in the redox processes of Cu(II)-polyglycine complexes [21,22].

By comparing the diffusion layer thickness at an electrode surface in a channel-type flow cell and at a rotating disc electrode (RDE), RDE experiments can be used to investigate flow cell behavior. With regular peptides there are no following chemical reactions in the typical microbore or capillary HPLC systems [15,23,24].

However, many neuropeptides are not “regular”. Electron-donating side chains are common as many peptides contain residues such as His, Cys, Glu, etc. Some peptides lack a free amine or carboxylate at the termini. The diversity of neupeptides adds a challenge and excitement to the biuret reaction-based electrochemical detection method.

1.2.2. Peptides containing His residues

Some sidechains are electron donating. These include the imidazole in His, the carboxylate in Asp and Glu, and the nitrogens in Arg in their deprotonated state. These side chains, especially the former two, may participate in coordination.

The imidazole moiety of the His side chain offers a basic binding site. The pK_a ranges from 6.0 to 7.1 [25,26]. Cu(II) may promote the deprotonation through coordination. For example, a 120-mer poly-histidine binds Cu(II) with three imidazole and one peptide bond amido

nitrogen at pH 5 [27]. Coordination of Cu(II) with His-containing peptides can occur at a lower pH than required by ordinary biuret reaction (typically pH 9.8). Many proteins interact with Cu(II) under physiological conditions through their His residues, such as Cu,Zn-superoxide dismutase [28,29], bovine serum albumin [30], and the pathogenic proteins prion [31] and amyloid-β peptide [32].

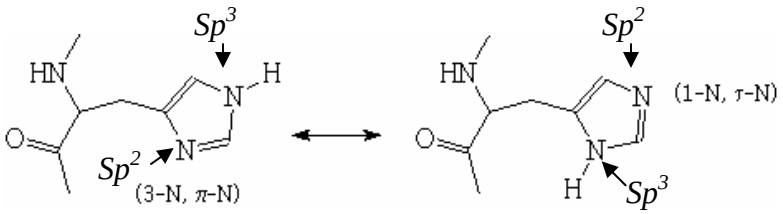

Figure 1-3. The tautomeric forms of the imidazole nitrogens.

The nitrogen that is closer to the alkyl link to the peptide backbone is often annotated as π-N, 3-N or pyridine-N. The one that is farther away is annotated as τ-N, 1-N, or pyrrole-N. They undergo rapid tautomeric exchange when not bound (Figure 1-3). When interacting with suitable metal ions, it is the 3-N that binds metal to form a six-membered ring along with other peptide backbone donors [26] (Figure 1-4). Being a stronger donor than carboxylate or carbonyl oxygen, the imidazole nitrogen can replace the oxygens to form a more stable Cu(II) complex. This is not always the case. Besides taking an equatorial binding position, the imidazole of a histidine residue may also occupy an axial position of the same [27,33], or even another Cu(II) ion to form a dimer [34].

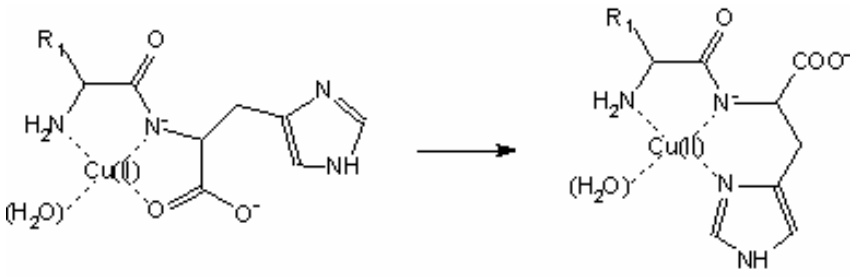

Figure 1-4. The imidazole 3-N participates in binding Cu(II).

Though not as competitive, the pyrrole nitrogen (1-N) of peptide Gly-His has been suggested to deprotonate at higher pH and bind equi-molar Cu^{2+}, Ni^{2+} or Pd^{2+} [35]. The imidazole moiety thus acts as a bridge and promoted bi-nuclear complex formation. The argument is based on a deprotonation at pH higher than 9.6 accompanied by a blue shift in the d-d transition of the Cu^{2+} and Pd^{2+} complexes. The deprotonation has been reported to be concentration dependent, which is favored by the bi-nuclear complex formation. With tripeptide Gly-Gly-His as the ligand, similar deprotonation of the pyrrole-nitrogen has been suggested. There was no shift in the d-d transition band, which was explained through the hypothesis that the deprotonated nitrogen does not bind any metal ions [36].

1.3. The octarepeat peptide of the prion protein and its interaction with Cu(II)

1.3.1. PrP and prion diseases.

Prion proteins (PrP) in the past decade have caused worldwide interest. Its misfolding and aggregation in neurons affect the nearby neurons quickly, resulting in lethal and transmissible prion diseases [37]. Prion diseases affect various mammals and exist as mad cow disease in cattle, scrapie in sheep and goats, chronic wasting disease in deer and elk, and kuru and Creutzfeldt-Jakob disease (CJD) in human [38,39]. These transmissible diseases can be spread by means of infected food, transplant tissues or blood products, all imposing a potential menace to human life. There is thus a need to understand the normal functions and misfolding mechanism of the prion proteins.

The existence of prion protein in brain was not noticed until the breakouts of prion diseases. No notable functions of the protein have been discovered other than causing the neurodegenerative diseases. PrP-knockout mice do not show considerable difference when compared to wild type mice in their behavior or brain tissue [40]. This suggested that the normal function of PrP is subtle. Moreover, the knockouts stay free of infection for twice as long as the wild type controls after being inoculated with the pathogenic prions, PrP^{SC} [41,42]. These results have convincingly pointed out that it is, critically, the conversion of normal PrP to PrP^{SC}, not the PrP^{SC} itself, that leads to prion diseases.

The pathological behavior of PrP has analogs in other neurodegenerative diseases, such as the aggregation of β-amyloid protein in Alzheimer's disease [43,44] and of α-synuclein in Parkinson's disease [45-47]. In both diseases, metal ions have been found to play important roles [48-51]. In 1995, Hornshaw's study of Cu(II)'s binding with synthetic PrP repeat units [52] started the exploration of the interaction of PrP with metal ions, especially Cu(II).

1.3.2. PrP as a metal binding protein.

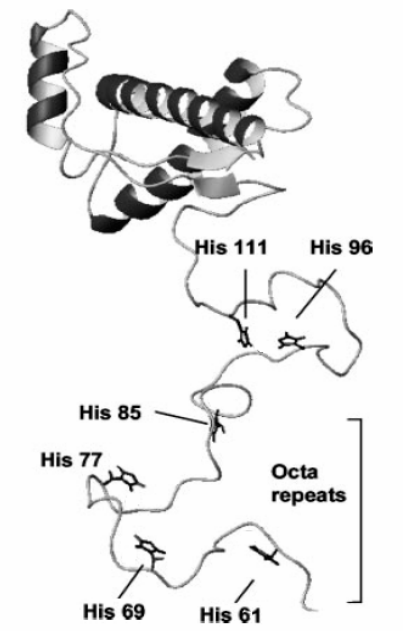

Prion protein is a glycoprotein of about 230 residues, variation depending on the actual species, with residues 1-22 attached to the cell membrane. The C-terminus of the protein adopts a highly conserved alpha-helical structure, while the N-terminus is more flexible.

Figure 1-5. Metal binding regions in full length prion protein.

Several regions of the prion molecule have shown substantial affinity for transition metal ions. These regions include segments 92-96, 106-126 and the N-terminal octarepeats 59-91 [53-56]. Their metal-binding ability is attributed to the histidine residues [57]. Figure 1-5 shows a normal prion protein molecule and the N-terminal histidines where metal ions are often found to bind [55]. The octarepeat region features multiple tandem copies of the eight-residue sequence PHGGGWGQ. Most interestingly, this domain is highly conserved across species [58], suggesting roles in possible PrP function.

The metal-binding property of the octarepeat region gave rise to the hypothesis that prion protein may have metal-related functions. Suggestions surrounding this hypothesis, including transporting extracellular copper ion into the cell interior and maintaining cellular copper balance [59-62] and protecting neurons in excessive oxidative stress [63-65], have been proposed.

1.3.3. Cu(II)-octarepeat coordination.

Many techniques have served in the studies of Cu(II)-octarepeat coordination. These include electron paramagnetic resonance spectroscopy (EPR) [66], nuclear magnetic resonance

spectroscopy [67], x-ray crystallography [62], x-ray absorption spectroscopy [68], circular dichroism (CD) [54,66], potentiometry and spectroscopy [69] and mass spectrometry [57,70].

Cu(II) is unique among all the transition metal ions that have been reported to bind PrP or its fragments: it displays quenching effect in Trp fluorescence spectroscopy while other metal ions do not [54], and the interactions between Cu(II) and a couple of metal-binding fragments of PrP are much stronger than those of Ni(II), Zn(II) and Mn(II), etc. [61]. A full length PrP picks up at most six Cu(II) ions. The main Cu(II) binding domain is the less folded N-terminal part, especially the octarepeats. Much evidence exists to show that each repeat unit binds one Cu(II) at physiological pH [66,70,71]. But at lower pH, one Cu(II) may need two repeat units to complete complexation [70]. In a single octarepeat, the five residue fragment Ac-HGGGW-NH_2 acts as the fundamental binding unit [66]. A resolved crystal structure is shown in Figure 1-6. The crystal structure suggests indirect communication between the metal center and the tryptophan residue. Other authors argue that Trp does not exert any weak interaction with the metal center, and the apical oxygen donor is more likely an oxygen from either the amide carbonyl in front of His residue or the one of the third Gly [72]. The argument comes from both spectroscopic and electrochemical observations: the Cu(II) complex of single octarepeat at around pH 7 displays biuret-like absorption at 614 nm; it blue-shifts as pH increases to 10; at around neutral pH the complex displays a reduction signal at – 0.299 V (NHE); at pH 10, it shifts to – 0.308 V (NHE). These data can be explained when an axial water ligand is replaced by carbonyl oxygen, which is a rather stronger donor.

Cu(II) binding motifs within the octarepeat domain have not been isolated. It has been suggested that the cooperative effects among octarepeat units [69,73] lead to stronger and more structured interaction than single octarepeat.

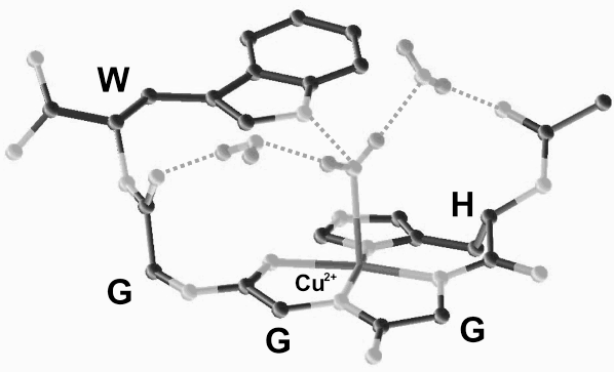

Figure 1-6. Crystal structure of Cu(II)-Ac-HGGGW-NH_2 illustrating Cu(II) binding mode with the octarepeat unit peptide.

Adopted from ref. [58].

With normal functions of the prion protein being unclear, more and more people have come to believe the protein works closely with metal ions. More interest focuses on copper. The notion comes not only from the comprehensive roles of copper in mammalian body, but also has to do with the highly conserved octarepeat region in mammal species [58].

1.4. Goals

Peptides may react with metal ions. Study of the metal complexes will help to understand the roles, functions, and mechanism, etc., of important bioactive peptides or proteins, and pathways of important physiological processes.

A number of techniques can be used to measure the spectroscopic, electrochemical, and/or magnetic properties of the metal complex of interest. These properties are often reflective of the electron configuration of the metal center, the donors, and the structure of the ligands. There have been documented correlations between metal-peptide complex structures and their signals of UV-Vis [74], nuclear magnetic resonance [75,76], electron spin resonance [77], voltammetry [17,18], and circular dichroism [78], etc. Since the properties of the complex depend greatly on the donors for a given metal ion, the fragment of a protein that interacts with the metal is often studied before the full length protein. Examples include the amyloid-β peptide 1- 40 in the amyloid-β protein [79], the octarepeats 59 - 91 of the prion protein [66], and the His-containig sequences in Cu, Zn-superoxide dismutatse [80].

In the following chapters, I will demonstrate the utilization of electrochemical methods, mainly rotating ring-disk electrode and microelectrode voltammetry and chronoamperometry, with help of various spectroscopic tools in solving a series of question regarding biuret complexes of a couple of bioactive peptides. Solutions to these questions help to extend the application of biuret detection scheme of neuropeptides to wider ranges of peptides, to elucidate the coordination nature of non-ordinary peptides, and to explore the Cu(II)-related functions of the prion protein octarepeat unit peptide.

BIBLIOGRAPHY

[1]. Kennedy, R. T.;Watson, C. J.;Haskins, W. E.;Powell, D. H.;Strecker, R. E. *Cur. Opi. Chem. Biol.* **2002**, *6*, 659-665.

[2]. Haskins, W. E.;Wang, Z.;Watson, C. J.;Rostand, R. R.;Witowski, S. R.;Powell, D. H.;Kennedy, R. T. *Anal. Chem.* **2001**, *73*, 5005-5014.

[3]. Shen, H.;Lada, M. W.;Kennedy, R. T. *J. Chromatogr. B* **1997**, *704*, 43-52.

[4]. Mcilwain, H.;Bachelard, H. S., *Biochemistry and the Central Nervous System. 5th Ed.* **1985**. 668 pp.

[5]. Ranta, V.-P.;Urtti, A.;Auriola, S. *J. Chromatogr. A* **1997**, *766*, 85-97.

[6]. Shah, P. K.;Borchardt, R. T. *J. Pharm. Biomed. Anal.* **1990**, *8*, 457-461.

[7]. Kanazawa, H.;Nagatsuka, T.;Miyazaki, M.;Matsushima, Y. *J. Chromatogr. A* **1997**, *763*, 23-29.

[8]. Larsimont, V.;Bogaards, M.;Mulleneers, P.;Hochhaus, G. *J. Pharm. Biomed. Anal.* **1999**, *19*, 855-864.

[9]. Moseley, M.A.; Deterding, L. J.; De Wit, J. S. M.; Tomer, K.B.; Kennedy, R.T.; Bragg, N. Jorgenson, J.W., *Anal. Chem.* **1989**, 61(14), 1577-1584.

[10]. Venn, R. F. *J. Chromatogr.* **1987**, *423*, 93-104.

[11]. Lovelace, J. L.;Kusmierz, J. J.;Desiderio, D. M. *J. Chromatogr.* **1991**, *562*, 573-584.

[12]. Nilsson, C. L.;Karlsson, G.;Bergquist, J.;Westman, A.;Ekman, R. *Peptides* **1998**, *19*, 781-789.

[13]. Crowther, J.;Adusumalli, V.;Mukherjee, T.;Jordan, K.;Abuaf, P.;Corkum, N.;Goldstein, G.;Tolan, J. *Anal. Chem.* **1994**, *66*, 2356-2361.

[14]. Freeman, H. C.;Smith, J. E. W. L.;Taylor, J. C. *Nature* **1959**, *184*, 707-711.

[15]. Chen, J.-G.;Weber, S. G. *Anal. Chem.* **1995**, *67*, 3596-3604.

[16]. Warner, A. M.;Weber, S. G. *Anal. Chem.* **1989**, *61*, 2664-2668.

[17]. Chen, J.-G.;Woltman, S. J.;Weber, S. G. *J. Chromatogr. A* **1995**, *691*, 301-315.

[18]. Margerum, D. W. *Pure Appl. Chem.* **1983**, *55*, 23-34.

[19]. Chen, J.-G.;Logman, M.;Weber, S. G. *Electroanalysis* **1999**, *11*, 331-336.

[20]. Shi, F.;Woltman, S. J.;Weber, S. G. *Anal. Chim. Acta.* **2002**, *474*, 1-9.

[21]. Woltman, S. J.;Alward, M. R.;Weber, S. G. *Anal. Chem.* **1995**, *67*, 541-551.

[22]. Kurtz, J. L.;Burce, G. L.;Margerum, D. W. *Inorg. Chem.* **1978**, *17*, 2454-2460.

[23]. Meng, R.;Weber, S. *Ubpublished work.*

[24]. Beisler, A. T., *Development of Capillary Separation Systems for the Analysis of Proteins and Peptides*, in *Chemistry, Ph.D.* 2003, University of Pittsburgh: Pittsburgh. p. 97-117.

[25]. Grant, I. J.;Hay, R. W. *Aus. J. Chem.* **1965**, *18*, 1189-1195.

[26]. Sundberg, R. J.;Martin, R. B. *Chem. Rev.* **1974**, *74*, 471-517.

[27]. Levitzki, A.;Pecht, I.;Berger, A. *J. Am. Chem. Soc.* **1972**, *94*, 6844-6849.

[28]. Beem, K. M.;Richardson, D. C.;Rajagopalan, K. V. *Biochemistry* **1977**, *16*, 1930-1936.

[29]. Myari, A.;Malandrinos, G.;Deligiannakis, Y.;Plakatouras, J. C.;Hadjiliadis, N.;Nagy, Z.;Sovago, I. *J. Inorg. Chem.* **2001**, *85*, 253-261.

[30]. Bradshaw, R. A.;Shearer, W. T.;Gurd, F. R. N. *J. Biol. Chem.* **1968**, *243*, 3817-3825.

[31]. Brown, D. R., Qin, K., Herms, J. W., Madlung, A., Manson, J., Strome, R., Fraser, P. E., Kruck, T., Bohlen, A. V., Schulz-Schaeffer, W., Giese, A., Westaway, D., and Kretzschmar, H. *Nature* **1997**, *390*, 684-687.

[32]. Syme, C. D.;Nadal, R. C.;Rigby, S. E. J.;Viles, J. H. *J. Biol. Chem.* **2004**, *279*, 18169-18177.

[33]. Sportelli, L.;Neubacher, H.;Lohmann, W. *Biophys. Struc. Mech.* **1977**, *3*, 317-326.

[34]. Freeman, H. C.;Szymanski, J. T. *Acta Crystallogr.* **1967**, *22*, 406-417.

[35]. Morris, P. J.;Bruce Martin, R. *J. Inorg. Nucl. Chem.* **1971**, *33*, 2913-2918.

[36]. Aiba, H.;Yokoyama, A.;Tanaka, H. *Bull. Chem. Soc. Jpn* **1974**, *47*, 1437-1441.

[37]. Dobson, C. M. *Tr. Biochem. Sci.* **1999**, *24*, 329-332.

[38]. Prusiner, S. B. *Science* **1997**, *278*, 245-251.

[39]. Prusiner, S. B. *Proc. Nat. Acad. Sci. USA* **1998**, *95*, 13363-13383.

[40]. Bueler, H.;Fischer, M.;Lang, Y.;Bluethmann, H.;Lipp, H.-P.;Dearmond, S. J.;Prusiner, S. B.;Aguet, M.;Weissmann, C. *Nature* **1992**, *356*, 577-.

[41]. Bueler, H.;Aguzzi, A.;Sailer, A.;Greiner, R.-A.;Autenried, P.;Aguet, M.;Weissmann, C. *Cell* **1993**, *73*, 1339-1347.

[42]. Sailer, A.;Bueler, H.;Fischer, M.;Aguzzi, A.;Weissmann, C. *Cell* **1994**, *77*, 967-968.

[43]. Pike, C. J.;Burdick, D.;Walencewicz, A. J.;Glabe, C. G.;Cotman, C. W. *J. Neurosci.* **1993**, *13*, 1676-1687.

[44]. Lorenzo, A.;Yankner, B. A. *Proc. Nat. Acad. Sci. USA* **1994**, *91*, 12243-12247.

[45]. Gibb, W. R.;Lees, A. J. *J. Neurol. Neurosurg. Psych.* **1988**, *51*, 745-752.

[46]. Spillantini, M.;Schmidt, M.;Vm-Y, L.;Trojanowski, J.;Jakes, R.;Goedert, M. *Nature* **1997**, *388*, 839-840.

[47]. Spillantini, M. G.;Crowther, R. A.;Jakes, R.;Hasegawa, M.;Goedert, M. *Proc. Nat. Acad. Sci. USA* **1998**, *95*, 6469-6473.

[48]. Uversky, V. N.;Li, J.;Fink, A. L. *J. Biol. Chem.* **2001**, *276*, 44284-44296.

[49]. Paik, S. R.;Shin, H. J.;Lee, J. H. *Arch. Biochem. Biophys.* **2000**, *378*, 269-277.

[50]. Deibel, M. A.;Ehmann, W. D.;Markesbery, W. R. *J. Neurol. Sci.* **1996**, *143*, 137-142.

[51]. Dexter, D.;Carayon, A.;Javoy-Agid, F.;Agid, Y.;Wells, F.;Daniel, S.;Lees, A.;Jenner, P.;Marsden, C. *Brain* **1991**, *114*, 1953-1975.

[52]. Hornshaw, M. P.;Mcdermott, J. R.;Candy, J. M.;Lakey, J. H. *Biochem. Biophys. Res. Commun.* **1995**, *214*, 993-999.

[53]. Zong, X. H.;Zhou, P.;Shao, Z. Z.;Chen, S. M.;Chen, X.;Hu, B. W.;Deng, F.;Yao, W. H. *Biochemistry* **2004**, *43*, 11932-11941.

[54]. Stockel, J.;Safar, J.;Wallace, A. C.;Cohen, F. E.;Prusiner, S. B. *Biochemistry* **1998**, *37*, 7185-7193.

[55]. Jones, C. E.;Abdelraheim, S. R.;Brown, D. R.;Viles, J. H. *J. Biol. Chem.* **2004**, *279*, 32018-32027.

[56]. Gaggelli, E. B., Francesca; Molteni, Elena; Pogni, Rebecca; Valensin, Daniela; Valensin, Gianni; Remelli, Maurizio; Luczkowski, Marek; Kozlowski, Henryk. *J. Am. Chem. Soc.* **2005**, *127*, 996-1006.

[57]. Qin, K.;Yang, Y.;Mastrangelo, P.;Westaway, D. *J. Biol. Chem.* **2002**, *277*, 1981-1990.

[58]. Wopfner, F.;Weidenhofer, G.;Schneider, R.;Brunn, A. V.;Gilch, S.;Schwarz, T. F.;Werner, T.;Schatzl, H. M. *J. Mole. Biol.* **1999**, *289*, 1163-1178.

[59]. Rossi, L.;Lombardo, M. F.;Ciriolo, M. R.;Rotilio, G. *Neurochem. Res.* **2004**, *29*, 493-504.

[60]. Ji, H. F.;Zhang, H. Y. *Chem. Res. Toxicol.* **2004**, *17*, 471-475.

[61]. Jackson, G. S.;Murray, I.;Hosszu, L. L. P.;Gibbs, N.;Waltho, J. P.;Clarke, A. R.;Collinge, J. *Proc. Nat. Acad. Sci. USA* **2003**, *98*, 8531-8535.

[62]. Burns, C. S., Aronoff-Spencer, E., Dunham, C. M., Lario, P., Avdievich, N. I., Antholine, W. E., Olmstead, M. M., Vrielink, A., Gerfen, G. J., Peisach, J., Scott, W. G., and Millhauser, G. L. *Biochemistry* **2002**, *41*, 3991-4001.

[63]. Brown, D. R.;Wong, B.-S.;Hafiz, F.;Clive, C.;Haswell, S. J.;Jones, C. E. *Biochem. J.* **1999**, *344*, 1-5.

[64]. Tabner, B. J.;Turnbull, S.;El-Agnaf, O. M. A.;Allsop, D. *Cur. Med. Chem.* **2003**, *3*, 299-308.

[65]. Vassallo, N.;Herms, J. *J. Neurochem.* **2003**, *86*, 538-544.

[66]. Aronoff-Spencer, E.;Burns, C. S.;Avdievich, N. I.;Gerfen, G. J.;Peisach, J.;Antholine, W. E.;Ball, H. L.;Cohen, F. E.;Prusiner, S. B.;Millhauser, G. L. *Biochemistry* **2000**, *39*, 13760-13771.

[67]. Viles, J. H.;Donne, D.;Kroon, G.;Prusiner, S. B.;Cohen, F. E.;Dyson, H. J.;Wright, P. E. *Biochemistry* **2001**, *40*, 2743-2753.

[68]. Morante, S.;Gonzalez-Iglesias, R.;Potrich, C.;Meneghini, C.;Meyer-Klaucke, W.;Menestrina, G.;Gasset, M. *J. Biol. Chem.* **2004**, *279*, 11753-11759.

[69]. Valensin, D.;Luczkowski, M.;Mancini, F. M.;Legowska, A.;Gaggelli, E.;Valensin, G.;Rolka, K.;Kozlowski, H. *Dalton Trans.* **2004**, 1284-1293.

[70]. Whittal, R. M.;Ball, H. L.;Cohen, F. E.;Burlingame, A. L.;Prusiner, S. B.;Baldwin, M. A. *Protein Sci.* **2000**, *9*, 332-343.

[71]. Viles, J. H.;Cohen, F. E.;Prusiner, S. B.;Goodin, D. B.;Wright, P. E.;Dyson, H. J. *Proc. Nat. Acad. Sci. USA* **1999**, *96*, 2042-2047.

[72]. Bonomo, R. P.;Cucinotta, V.;Giuffrida, A.;Impellizzeri, G.;Magri, A.;Pappalardo, G.;Rizzarelli, E.;Santoro, A. M.;Tabbi, G.;Vagliasindi, L. I. *Dalton Trans.* **2005**, *1*, 150-158.

[73]. Garnett, A. P.;Viles, J. H. *J. Biol. Chem.* **2003**, *278*, 6795-6802.

[74]. Billo, E. J. *Inorg. Nucl. Chem. Lett.* **1974**, *10*, 613-617.

[75]. Gaggelli, E.;D'amelio, N.;Gaggelli, N.;Valensin, G. *ChemBiochem* **2001**, *2*, 524-529.

[76]. Basosi, R.;D'amelio, N.;Gaggelli, E.;Pogni, R.;Valensin, G. *J. Chem. Soc. Perkin Trans.* **2001**, 252-257.

[77]. Peisach, J.;Blumberg, W. E. *Arch. Biochem. Biophys.* **1974**, *165*, 691-708.

[78]. Wilson, E. W. J.;Kasperian, M. H.;Martin, R. B. *J. Am. Chem. Soc.* **1970**, *92*, 5365-5370.

[79]. Atwood, C. S.;Scarpa, R. C.;Huang, X.;Moir, R. D.;Jones, W. D.;Fairlie, D. P.;Tanzi, R. E.;Bush, A. I. *J. Neurochem.* **2000**, *75*, 1219-1233.

[80]. Myari, A.;Malandrinos, G.;Plakatouras, J.;Hadjiliadis, N.;Sovago, I. *Bioinorg. Chem. Appl.* **2003**, *1*, 99-112.

2. Online Preconcentration of Thyrotropin-Releasing Hormone (TRH) By SDS-Modified Reversed Phase Column for Microbore and Capillary High Performance Liquid Chromatography (HPLC)

(This chapter contains materials from publication R. Meng, W. Xia, M. Sandberg, R. Stephens, S.G. Weber, J. Chromatogr. A 1071 (2005) 179.

2.1. Abstract

Thyrotropin-releasing hormone (TRH, pGlu-His-Pro-amide) is an important tripeptide existing in biological systems at low concentrations. It is a fairly hydrophilic peptide, cationic in acidic solutions. Preconcentration online before reversed phase chromatography separation can enhance concentration detection limits of hydrophobic, but not hydrophilic species. The Hydrophilic TRH can be preconcentrated using a reversed phase precolumn charged with sodium dodecyl sulfate (SDS). The separation also uses SDS. The preconcentration is effective for a microbore system, achieving detection limit of 250 pM for a sample size of 500 μl with electrochemical detection of the biuret complex formed post column. Preconcentration using an online precolumn is also effective in packed capillary HPLC with a detection limit of 3 nM in 24 μl.

2.2. Introduction

Thyrotropin-releasing hormone (TRH) is an important neuropeptide originally discovered in the hypothalamus as a releasing factor for pituitary hormones such as Thyrotropin and prolactin [1,2]. From a therapeutic perspective, administration of TRH and some of its stable analogs, appear to have neuroprotective and anti-convulsive effects [3-8]. It is also present in other brain areas with proposed additional, although not yet fully elucidated, functions [9-11].

Radioimmunoassay (RIA) has been used for TRH assays in serum and various tissues from rat [12-16]. Though powerful, RIA suffers from the drawbacks that it is too selective to be useful for determining all the members in a family of related peptides, but may not be selective enough to determine a single peptide accurately. In fact, analogs of TRH that displayed similar immunoactivity as TRH have been found in various rat tissues [17-21]. Therefore, a "separate-and-detect" approach is preferred. High-performance liquid chromatography (HPLC) with UV-Vis detection only works at low sensitivity [22-25]. While fluorescence detection following HPLC or CZE separations is a powerful technique for the determination of amino acids and peptides, it typically requires a primary amine or thiol group in the targeted molecule to be derivatized. Neither of these two functional groups exists in TRH. Mass spectrometry (MS) coupled to chromatography has been used qualitatively in characterizing this peptide [20] and to determine the sequence of some of its analogs that may not be distinguishable in RIA [21,26,27]. There are very few works on quantification of TRH by MS and these are not routine methods. Reports were found on field-desorption ionization following LC [28] and on fast atom bombardment ionization following GC by looking at the fragments [29]. A simpler detection method with high sensitivity and selectivity is still desirable.

Selective chromatographic detection of peptides has been established based on the reversible electrochemistry of the Cu(II)/Cu(III) couple in polydentate peptide complexes [30-33]. The detection relies on the coordination reaction of peptides and Cu(II), also called the biuret reaction [34,35]. TRH forms electroactive complex with Cu(II) thus is proposed to be detectable with the above method. In rat brain, TRH concentration ranges from roughly 2 nM (cerebellum) to 350 nM (hypothalamus) [11]. The targeted sample for dialysate analysis – extracellular fluid, is expected to contain lower concentrations of TRH. The low endogenous levels in biological samples have been a challenge for the detection of bioactive peptides. One method to improve sensitivity is to preconcentrate the analytes. Moreover, on-line preconcentration is preferred over off-line for higher efficiency.

Works on online preconcentration methods for liquid separations are limited, especially for capillary LC. For hydrophobic analytes (e.g. hydrophobic peptides), reversed phase precolumns as injection loops trap and preconcentrate the analytes [36,37]. A simpler alternative is to inject a large volume of sample in a lower strength solvent, and elute the retained analytes with the higher strength mobile phase [38-40]. This method evidently will not apply to hydrophilic molecules. TRH is a hydrophilic cation in weak acidic solution, while the general mobile phases for peptide separation have acidic pH due to trifluoroacetic acid (TFA). This makes preconcentration on the reversed-phase column head not very promising. For charged analytes, a few works about strong ion exchange precolumns have been reported. In an analysis of trypsin digested BSA, strong cationic peptide fragments which featured Arg or Lys as terminal residues were trapped in a 250 μm i.d. strong ion exchange precolumn and eluted by a neutral buffer prior to a microbore HPLC system [41]. In the present work, we describe an online preconcentration method to enrich TRH through sorption in the presence of a surfactant. Ionic

interactions have been widely used in liquid chromatography to achieve better separation on reversed phase columns [42,43]. To our best knowledge, no works have been reported on surfactant-assisted online preconcentration of cationic peptides.

2.3. Experimental

2.3.1. Microbore HPLC

Reagents and sources were as follows: Sodium carbonate, sodium bicarbonate, cupric sulfate pentahydrate, disodium tartrate dihydrate, and sodium dodecyl sulfate (SDS) were from Sigma (St. Louis, MO, USA) and used without further purification. TFA was from Avocado (Heysham, Lancs, UK). TRH was from Sigma and stored at - 20°C. Doubly deionized water used in all solutions was obtained through a Milli-Q system (Millipore, Bedford, MA, USA). All other common reagents were of AR grade or better and purchased from commercial sources.

The chromatographic apparatus included a LC-10AD Shimadzu pump (Kyoto, Japan) delivering mobile phase (0.1% TFA, 2% 1-propanol, 20% acetonitrile and 3.0 mM SDS in water), a Rheodyne injector, and a Jupiter 150 × 1.0 mm C_{18} reversed phase column from Phenomenex (Torrance, CA, USA). The postcolumn biruet reagent (0.50 mM CuSO4, 3.0 mM sodium tartrate, and 1 M carbonate, pH 9.8) was delivered by a 100 DM syringe pump from ISCO (Lincoln, NE, USA). The typical flow rates were 50 μl/min in the column and 20 μl/min for the biuret reagent. All necessary fittings and tubings are from Upchurch (Oak harbor, Washington, USA). A mixing tee and teflon tubing with 100 μm i.d. and 12.5 μl volume were used as the postcolumn reactor. Both the column and the reactor were put in a temperature controller (model LC-23A, BAS, W. Lafayette, IN, USA) which was maintained at 50 °C.

A 4.0×2.0 mm C_{18} guard column from Phenomenex was used as the preconcentration column (also called precolumn or preconcentration loop in this work). It was connected to the injector by a 16 cm 62 μm i.d. PEEK (polyetheretherketone) tube (about 0.5 μl). Before each loading, the precolumn was preconditioned with 1250 μl of 0.1 % TFA and 3.0 mM SDS solution. Then about 500 μl of analyte solution were loaded into the precolumn. For brain slice

experiment 470 μl was loaded. There was a 2 minute or longer delay time before the injector was switched to injection position.

The electrochemical detector was a BAS LC-4C thin layer flow cell, with a dual glassy carbon electrode (3.0 mm diameter) and a 13 μm thick teflon spacer (both from BAS). Detection potential was + 0.9 V at the upstream electrode, + 0.1 V at the downstream electrode vs. Ag/AgCl reference electrode (3 M NaCl, BAS). Data were collected and processed with EZChrom software (Sci. Software, San Ramon, CA, USA).

2.3.2. Capillary HPLC

Reagents and sources were as follows: TFA and 1-propanol were from Sigma; disodium tartrate dihydrate and sodium hydroxide were from Baker (Phillipsburgh, NJ, USA); copper sulfate pentahydrate was from Fisher (Pittsburgh, PA, USA); acetonitrile (ACN), sodium carbonate, and sodium bicarbonate were from EM Science (Gibbstown, NJ, USA); TRH was from Bachem (King of Prussia, PA, USA); SDS was from Fluka (Switzerland). The copper sulfate pentahydrate and disodium tartrate dihydrate were recrystallized once from water. All other reagents were used without further purification, but purities were taken into account in preparation. De-ionized water from a Millipore A10 Synthesis system was used for all solutions. All mobile phases and biuret reagent solutions were filtered through 0.45 mm nylon membranes (Osmonics, Minnetonka, MN, USA) before use.

The chromatographic instrumentation included a Waters 600 E quaternary pump for mobile phase (0.1% TFA, 3% 1-propanol, 20% acetonitrile, and 2.2 mM SDS), a split tee for low flow rates, a VICI injector (Valco Instrument Company, Houston, TX, USA), and a home-packed capillary column. Injections were made through 100 μm silica capillary with an Upchurch inline filter (part # M-520) to one of the injector ports. A Harvard Model 11 syringe

pump (Harvard Apparatus, Inc. Holliston, MA, USA) was used to pump the biuret reagent (2.5 mM $CuSO_4$, 12.0 mM sodium tartrate, and 0.6 M carbonate, pH 9.83). Typical flow rates were 800 nl/min for the HPLC and 250 nl/min for the biuret. The two streams were mixed for post-column reaction in a home-made device [44]. At the end of the reactor, the copper(II)-peptide complexes were detected at + 0.80 V versus Ag/AgCl (3 M NaCl) with a 10 μm carbon fiber electrode 1.0 mm in length. The potential was controlled with a BAS Epsilon potentiostat.

Capillary columns were slurry packed with the technique described previously [45]. Typically 100 μm silica capillaries were slurry packed with 2.0 μm prototype bridged hybrid C_{18} (Waters, Milford, MA, USA) reversed-phase particles. The packed length was typically 6 to 8 cm. The preconcentration loop was packed in a 7.0 cm long 75 μm i.d. silica capillary with 5 μm C_{18} packing material. The packed length was 2 mm. Before each loading it was preconditioned with a solution containing 0.1% TFA and 3.0 mM SDS. Reactors were constructed with 50 μm silica capillaries and 18 μm tungsten wires, according to previously published procedures [44]. The mixing length was 6 or 6.6 cm, stated in figure captions.

All necessary fittings and tubings are from Upchurch. All syringes used are from Hamilton (Reno, NV, USA).

2.3.3. Brain tissue samples

The tissue samples were supplied by Prof. Mats Sandberg. The detailed preparation procedures have been previously described [43,46,47]. Briefly, rat hippocampus is homogenized and extracted with 90% (v/v) methanol. Lyophilized extracts are stored frozen until use. Before injection, samples were reconstituted in 500 μl water, sonicated 6 min, centrifuged for 10 min (Jouan, Winchester VA, 12,000 rpm), and filtered (0.2 μm). Typically, somewhat less than 500 μl were recovered for injection.

2.4. Results and discussion

In the dual electrode detection mode, the downstream (cathode) electrode typically has a better baseline and signal to noise ratio than the upstream (anode) electrode. We will focus our discussion on the downstream electrode signals in microbore HPLC.

As the post-column reaction is essential in the detection scheme, the mixer had to be optimized for complete reaction yet minimal band broadening. Preferably, the radial diffusion in the tubing needs to be predominant over axial diffusion and convection. We will call this regime of convective dispersion the Taylor regime [44,48]. It allows for good mixing when two flow streams come into one open tube without excessive band spreading. For microbore HPLC, a combine-and-split reactor achieved good mixing of eluents and biuret reagent. Figure 2-1 shows a sketch of this reactor. It operates in the Taylor regime under the employed flow rate of 70 μl/min. Because of the three crosses employed, the reactor provides additional mixing over that in a single open tube with the same volume. The total reaction volume was 12.5 μl. This reactor was used throughout the microbore HPLC work. In the capillary HPLC experiments, staying in the Taylor regime, efficient mixing took place in a 120 nl capillary (50 μm i.d., 6.0 cm).

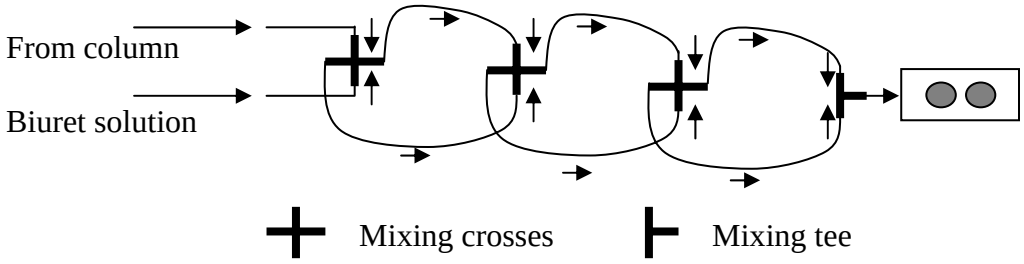

Figure 2-1. Sketch of the combine-split reactor for microbore HPLC.

The tubings connecting the crosses were 65 μm i.d., 40 cm long each. Crosses and the Tee have 0.05 cm through holes. Dimensions of the detection cell are in the experimental section.

TRH is not retained in a typical TFA/ACN mobile phase (data not shown). This is due to the low molecular weight and high polarity of TRH. A hydrophobic anionic additive, heptafluorobutyric acid (HFBA), is able to shift the retention of TRH to longer times. Unfortunately, it was found that the added HFBA deactivated the electrode very quickly, making the detection irreproducible.

Alternatively, 2 - 3 mM SDS retained TRH as an additive in the mobile phase. Acetonitrile had to be included in the mobile phase to achieve a practical retention time. Figure 2-2 shows the signal and retention time of TRH standard at various fractions of ACN in the SDS-containing mobile phase. In a 10% ACN mobile phase, TRH was not eluted within 40 minutes. Higher ACN level of 20% brought the TRH k' to a reasonable value of 2 - 3. In capillary HPLC, this percentage of ACN gives a similar k' value.

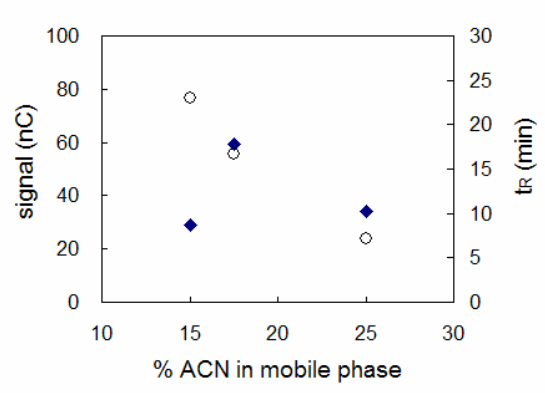

Figure 2-2. Optimizing acetonitrile content in the SDS-containing mobile phase.

Mobile phase contained 0.1% TFA, 2% 1-propanol, 3.0 mM SDS, and stated amount of ACN. TRH concentration: 500 nM. Sample loop: 20 µl. ♦: Peak area; ○: Retention time.

Under the above conditions, TRH displayed a linear response in the range of 100 to 500 nM. The regression of peak area in nC vs TRH mass in pmol gave an intercept much smaller than its uncertainty. Regression with the calibration curve forced through zero yields y = 0.22x

(R^2 = 0.9845). The detection limit (3σ) is 4.8 nM. (S/N value for 100 nM injection was about 55, for 500 nM injection was about 400).

In an effort to push the concentration detection limit to a lower level, we attempted to use the column head to preconcentrate TRH by analogy to reversed phase LC. However, because the large volume of low strength solvent (usually water) disturbed the equilibrium of SDS between the mobile and stationary phases, a long equilibration time, at least several hours, was found necessary to get reproducible separation.

A postulated solution to this problem is to put a small C_{18} precolumn in the injection loop, which is preconditioned with SDS-containing aqueous solution. The SDS generates a negatively charged layer on the stationary phase by hydrophobic interaction. When the sample prepared in aqueous solution is loaded into the preconditioned precolumn, molecules partition between the "mobile phase" water and the SDS-modified stationary phase. During this procedure the anionic and neutral hydrophilic and weakly hydrophobic species go through the precolumn to waste, while the cations and hydrophobic species stay in the precolumn. When the loop is switched into the separation system, the mobile phase desorbs the TRH (and some SDS). One of the advantages of this strategy is that it removes the interfering species such as salts which commonly exist in biologic samples.

It is interesting to find that the solvent composition of sample has a great effect on the preconcentration. Shown in Figure 2-3, TRH in water gave a much narrower peak than in 0.1 % TFA/3 mM SDS (the precondition solution). This implies that biological samples such as microdialysates could be directly introduced to the precolumn.

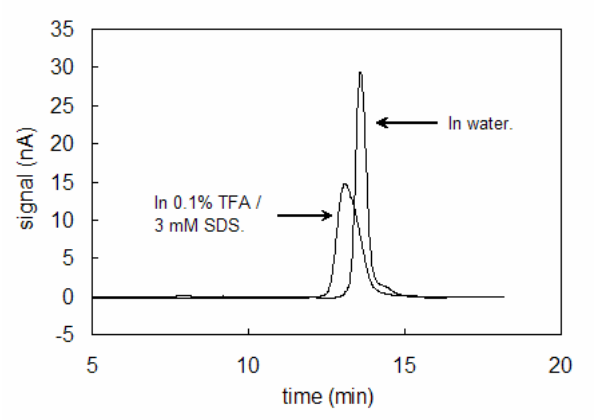

Figure 2-3. Comparison of preconcentrated TRH signals in SDS-containing solution and water.

TRH concentration: 500 nM. Loaded volume: 500 µl.

As a demonstration of the preconcentration approach, 500 µl of TRH standard solutions from 5 nM to 100 nM were loaded each time and detected. In Figure 2-4 the chromatograms show that both the retention time and peak width of TRH are consistent. Similar to the case without preconcentration, the intercept from regression (nC vs pmol) was also smaller than the associated standard error. Regression anew gave a calibration curve of $y = 143.1x$ ($R^2 = 0.9490$).

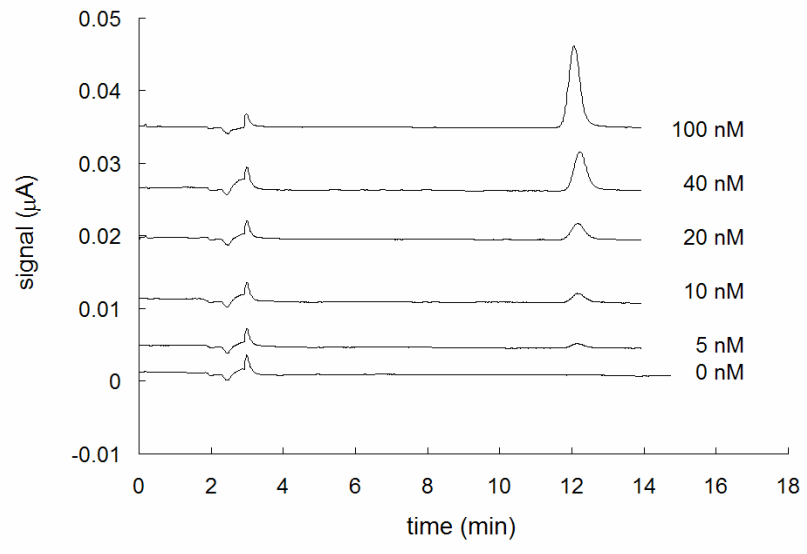

Figure 2-4. Signals of preconcentrated TRH at different concentrations in microbore HPLC.

The detection limits (3σ in each case) from chromatograms of 5 nM, 10 nM and 20 nM injections were 142 pM, 340 pM and 250 pM (S/N values are 105, 90 and 250 respectively). We conclude that 250 pM is the detection limit of this technique for TRH.

The low detection limit obtained from this detection approach made analysis in biological samples promising. Homogenized rat brain tissue was then introduced into the setup. In Figure 2-5, a clear peak is observed at the same retention time that TRH is eluted. It corresponds to 0.3 pmol TRH per mg of hippocampus tissue. This value was within the concentration range from the literature [11,49,50]. The chromatogram is fairly clean because the preconcentration step removed many interfering species.

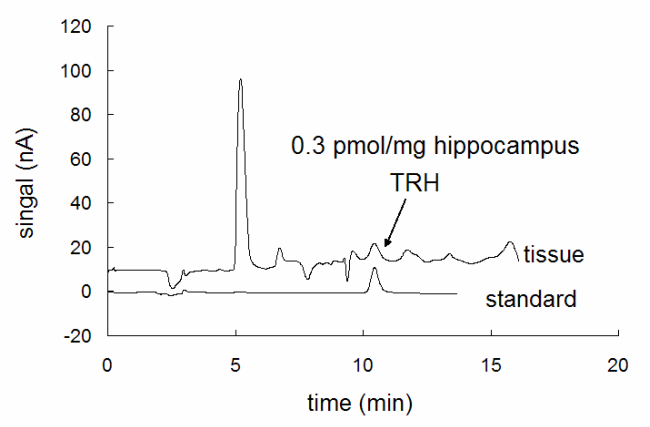

Figure 2-5. TRH determination in a homogenized rat brain tissue sample by microbore HPLC.

Sample was centrifuged, filtered and then diluted to 470 μl for loading and injection.
The standard was 100 nM TRH.

It could be concluded that the above preconcentration method was successful in terms of detection limit and compatibility with biological samples. Sensitivity was enough for physiological analysis, and selectivity was assured by the use of precolumn and dual electrode cell. However, there is a very serious drawback, which is the large sample size required for the

determination. The loaded volume in the brain tissue analysis was 470 μl. This is not practical for many samples. In this perspective, the system volume had to be decreased to accommodate much smaller sample sizes. Accordingly, the preconcentration strategy had to be carried out in a capillary format. The chemistry behind it should work regardless of the size of the column.

In a capillary chromatography systems there are two potential sources of extracolumn band spreading: precolumns and post column reactors. A locally developed post column reactor [44] has been demonstrated to meet the requirement of low sample volume and virtually no band broadening post column.

As for the precolumn, there are no commercial guard columns to use as the precolumn to match the much smaller size of the separation column. In preparing precolumns with capillaries, not surprisingly, the system brought up some engineering issues. The most important concern was the void volume of the tubing that connects the precolumn to the injector relative to the volume of the precolumn. For uniform sample loading, the void volume should be negligible compared to that of the precolumn. However, it is extremely hard to achieve because the packed precolumn will already be very small. At the same time, the port-to-port distance of the injector determines the minimum length that can be used. If the capillary loop/precolumn is too short, the strain will lead to breakage. Larger i.d. capillaries, though providing lower back pressure and therefore allowing for easy manual injection, are easily broken at the frit. In order to reduce the unpacked void volume, shorter, smaller i.d. capillaries are preferred.

Loop/precolumns that failed (broke at the frit) were (o.d./i.d., μm) 360/250, 330/180, and a system that was 360/40 in series with a < 1cm packed 360/250 and another 360/40. In the latter system, a single high pressure connector (LC Packings TF-250) covered the precolumn and overlapped with the 360/40 on both sides. On the other hand, loop/precolumns with thicker walls,

360/75, were successful. For 75 μm i.d. silica capillary, a 7 cm total length preconcentration loop did not break on being connected to the injector. Only a 2 mm length at the end of this capillary was packed. The back pressure was low enough to be permit injection with a 50 μl Hamilton gastight syringe.

To test if such a packed preconcentration loop works, TRH standard solutions of the same concentration were loaded into the loop at different loading volumes. Loaded volumes were corrected for the volume of the tubing from injection port to injector and the dead volume of an inline filter (1.5 μl total). After each loading, the loaded loop was switched into the system for analysis. The signals from Cu(II)-TRH were proportional to the loaded volume as expected, with a rather good correlation coefficient (see Figure 2-6). The bands were tailing to some extent, but the tailing did not get worse as loaded volume increased. This implied that the band shape was not affected by overloading of the precolumn, but by other parameters, most likely the construction of the precolumn.

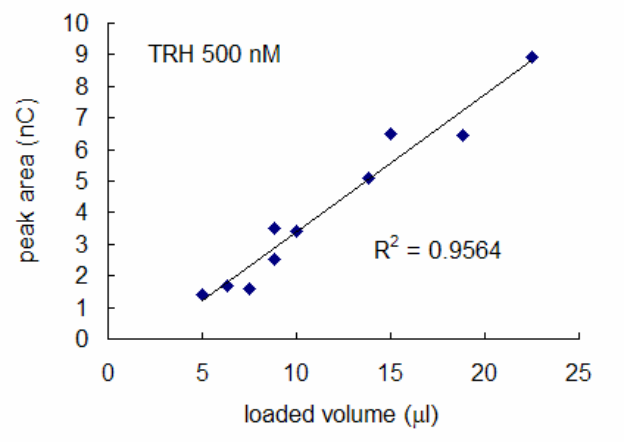

Figure 2-6. Responses of 500 nM TRH standard of different loaded volumes.
Sample undergoes preconcentration in capillary HPLC.

Figure 2-7 gives a comparison of the TRH signal before and after the preconcentration column was introduced. The 5 μM and 100 nM TRH standards gave similar signal to noise ratio (approximately 100 in both cases). Figure 2-7b signal corresponds to a detection limit of 3 nM. It can be concluded that after preconcentration the concentration sensitivity of the current detector to TRH could be increased up to 50 fold.

Injection to injection repeatability is function of the amount injected for the microbore experiments. Coefficients of variation range from 3% for 5 nM (500 μl) injected to 21% for 100 nM (500 μl) injected. For the capillary system, the coefficient of variation is about 20% for volumes of 8.5 and 13.5 μl (500 nM).

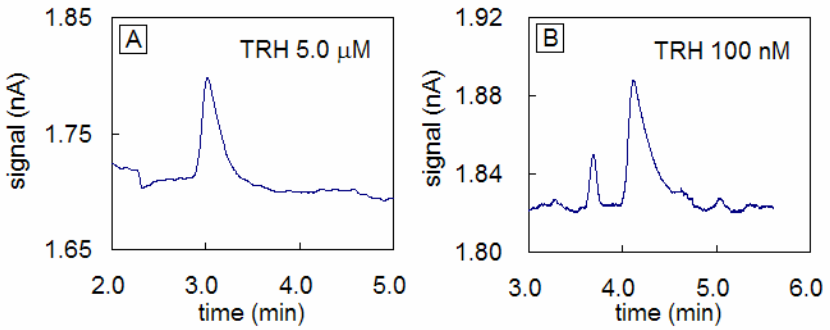

Figure 2-7. TRH signals before and after preconcentration in capillary HPLC.

The postcolumn mixing length was 6.0 cm in Figure 2-7a and 6.6 cm in Figure 2-7b. Other conditions are listed in experimental section.

The precolumn can be improved by optimizing its construction. The packed length should not be too short, in that sufficient partition process was required to stack TRH molecules into the precolumn. On the other hand, the packed length could not be too long, otherwise the back pressure introduced in loading the precolumn would be hard to handle. Large i.d. tubings

can be used for larger packed volumes, if ways can be found to prevent the thinner-wall capillaries from snapping. To limit void volume is also very important. Currently, the volume ratio of the precolumn and the separation column is much smaller than that in the microbore HPLC. This is mostly due to the engineering restrictions associated with compromising between better mechanical strength as well as smaller void volume and bigger precolumn capacity.

2.5. Conclusions

SDS-modified precolumn as a preconcentration sample loop is successful. The same chemistry worked on both microbore and capillary HPLC systems. Introducing of preconcentration column improved the detection limit of TRH 30 – 50 fold in both systems.

Analysis of biological samples, especially microdialysates, is ultimate in the study of neuropeptides. The capillary HPLC system has to be improved for this purpose. Two feasible ways are improvement of the precolumn construction and improvement of the electrochemical detector.

ACKNOWLEDGEMENTS

The authors are grateful to the NIH for funding through grant GM44842. We are also grateful to Dr. Ed Bouvier (Waters, Corp.) for providing us with the packing materials.

BIBLIOGRAPHY

[1]. Boler, J.; Enzmann, F.; Folkers, K.; Bowers, C. Y.; Schally, A. V. *Biochem. Biophys. Res. Commun.* **1969**, *37*, 705-710.

[2]. Bowers, C. Y.; Friesen, H. G.; Hwang, P.; Guyda, H. J.; Folkers, K. *Biochem. Biophys. Res. Commun.* **1971**, *45*, 1033-1041.

[3]. Faden, A. I. *Arch. Neurol.* **1986**, *43*, 501-504.

[4]. Prange, A. J., Jr.; Lara, P. P.; Wilson, I. C.; Alltop, L. B.; Breese, G. R. *Lancet* **1972**, *2*, 999-1002.

[5]. De Marinis, L.; Mancini, A.; Valley, D.; Bianchi, A.; Gentilella, R.; Liberale, I.; Mignani, V.; Pennis, M.; Della Corte, F. *Clin. Endocrinol.* **1999**, *50*, 741-747.

[6]. Manaka, S.; Sano, K. *Neurosci. Lett.* **1978**, *8*, 255-258.

[7]. Stocca, G.; Nistri, A. *Neurosci. Lett.* **1995**, *184*, 9-12.

[8]. Ujihara, H.; Xie, R. M.; Sasa, M.; Ishihara, K.; Fujita, Y.; Yoshimura, M.; Kishimoto, T.; Serikawa, T.; Yamada, J.; Takaori, S. *Eur. J. Pharmacol.* **1991**, *196*, 15-19.

[9]. Kachidian, P.; Poulat, P.; Marlier, L.; Privat, A. *J. Neurosci. Res.* **1991**, *30*, 521-530.

[10]. Iverfeldt, K.; Serfozo, P.; Arnesto, L. D.; Bartfai, T. *Acta Physiol. Scand.* **1989**, *137*, 63-71.

[11]. Winokur, A.; Utiger, R. D. *Science* **1974**, *185*, 265-267.

[12]. Fuse, Y.; Polk, D. H.; Lam, R. W.; Fisher, D. A. *Endocrinology* **1990**, *127*, 2501-2505.

[13]. Nillni, E. A.; Vaslet, C.; Harris, M.; Hollenberg, A.; Bjorbaek, C.; Flier, J. S. *J. Biol. Chem.* **2000**, *275*, 36124-36133.

[14]. Mohari, K.; Janoki, G.; Korosi, L. *Izotoptechnika, Diagnosztika* **1991**, *34*, 137-139.

[15]. Leppaluoto, J.; Suhonen, A. S. *J. Clin. Endocrinol. Metab.* **1982**, *54*, 914-918.

[16]. Nagai, H.; Morise, K.; Mitsuma, T.; Furusawa, A.; Kaneko, H.; Uchida, K.; Yamamoto, H. *J. Gastroenterol.* **1995**, *30*, 142-148.

[17]. Ghilchik, M. W.; Tobaruela, M.; Del Rio-Garcia, J.; Smyth, D. G. *Biochim. Biophys. Acta* **2000**, *1475*, 55-60.

[18]. Gkonos, P. J.; Kwok, C. K.; Block, N. L.; Roos, B. A. *Prostate* **1993**, *23*, 135-147.

[19]. Gkonos, P. J.; Kwok, C. K.; Block, N. L.; Roos, B. A. *Peptides* **1994**, *15*, 1281-1283.

[20]. Graham, E. S.; Webster, C. A.; Hazlerigg, D. G.; Morgan, P. J. *J. Neuroendocrinol.* **2002**, *14*, 945-954.

[21]. Bilek, R. *Physiol Res.* **2000**, *49*, s19-s26.

[22]. Rao, G. N. S.; Sutherland, J. W.; Menon, G. N. *Pharm. Res.* **1987**, *4*, 38-41.

[23]. Waterfall, A. H.; Clarke, R. W.; Bennet, G. W. *Neurosci. Lett.* **1993**, *151*, 97-100.

[24]. Sheward, W. J.; Harmar, A. J.; Fraser, H. M.; Fink, G. *J. Chromatogr.* **1983**, *222*, 381-387.

[25]. Spindel, E.; Pettibone, D.; Fisher, L.; Fernstrom, J.; Wurtman, R. *J. Chromatogr.* **1981**, *222*, 381-387.

[26]. Gibson, B. W.; Poulter, L.; Williams, D. H. *J. Nat. Prod.* **1986**, *49*, 26-34.

[27]. Lackey, D. B. *J. Biol. Chem.* **1992**, *267*, 17508-17511.

[28]. Desiderio, D. M.; Stein, J. L.; Cunningham, M. D.; Sabbatini, J. Z. *J. Chromatogr.* **1980**, *195*, 369-377.

[29]. Heki, N.; Noto, M.; Hosojima, H. *Nippon Naibunpi Gakkai Zasshi* **1977**, *53*, 690-702.

[30]. Warner, A. M.; Weber, S. G. *Anal. Chem.* **1989**, *61*, 2664-2668.

[31]. Chen, J.-G.; Weber, S. G. *Anal. Chem.* **1995**, *67*, 3596-3604.

[32]. Tsai, H.; Weber, S. G. *J. Chromatogr.* **1990**, *515*, 451-457.

[33]. Woltman, S. J.; Chen, J.-G.; Weber, S. G.; Tolley, J. O. *J. Pharm. Biomed. Anal.* **1995**, *14*, 155-164.

[34]. Margerum, D. W.; Wong, L. F.; Bossu, F. P.; Chellappa, K. L.; Czarnecki, J. J.; Kirksey, S. T., Jr.; Neubecker, T. A. *Adv. Chem. Ser.* **1977**, *162*, 281-303.

[35]. Noda, Y. *Bull. Chem. Soc. Jpn.* **1967**, *40*, 1264-1265.

[36]. Frommberger, M.; Schmitt-Kopplin, P.; Ping, G.; Frisch, H.; Schmid, M.; Zhang, Y.; Hartmann, A.; Kettrup, A. *Anal. Bioanal. Chem.* **2004**, *378*, 1014-1020.

[37]. Shintani, Y.; Zhou, X.; Furuno, M.; Minakuchi, H.; Nakanishi, K. *J. Chromatogr. A* **2003**, *985*, 351-357.

[38]. Shen, H.; Witowski, S. R.; Boyd, B. W.; Kennedy, R. T. *Anal. Chem.* **1999**, *71*, 989-994.

[39]. German, I.; Roper, M. G.; Kalra, S. P.; Rhinehart, E.; Kennedy, R. T. *Electrophoresis* **2001**, *22*, 3659-3667.

[40]. Mitulovic, G.; Smoluch, M.; Chervet, J.-P.; Steinmacher, I.; Kungl, A.; Mechtler, K. *Anal. Bioanal. Chem.* **2003**, *376*, 946-951.

[41]. Zhang, G.; Fan, H.; Xu, C.; Bao, H.; Yang, P. *Anal. Chem.* **2003**, *313*, 327-330.

[42]. Chen, J.-G.; Weber, S. G.; Glavina, L. L.; Cantwell, F. F. *J. Chromatogr. A* **1993**, *656*, 549-576.

[43]. Xia, W.; Sandberg, M.; Weber, S. G. *J. Chromatogr. B* **1998**, *705*, 251-259.

[44]. Beisler, A. T.; Sahlin, E.; Schaefer, K. E.; Weber, S. G. *Anal. Chem.* **2004**, *76*, 639-645.

[45]. Kennedy, R. T.; Jorgenson, J. W. *Anal. Chem.* **1989**, *61*, 1128-1136.

[46]. Mohammed, J. R.; Saska, T. A.; Chi, J.; Stephens, R. L. J. *Brain Res.* **1995**, *695*, 100.

[47]. Xia, W.; Sandberg, M.; Weber, S. G. *J. Pharm. Biomed. Anal.* **1999**, *19*, 261-268.

[48]. Probstein, R. F., *Physicochemical Hydrodynamics*. **1994**, New York: John Wiley & Sons. 82-96.

[49]. Mendez, M.; Joseph-Bravo, P.; Cisneros, M.; Vargas, M. A.; Charli, J. L. *Peptides* **1987**, *8*, 291-298.

[50]. Griffiths, E. C.; Bennett, G. W., *Thyrotropin-Releasing Hormone*, ed. E.C. GriffithsG.W. Bennett. **1983**, New York: Raven Press.

3. Binding of Copper Ion to Thyrotropin-Releasing Hormone (TRH) and Its Analogs

(This chapter contains materials from publication R. Meng, J. Becker, F.-T. Lin, S. Saxena, S.G. Weber, Inorg. Chim. Acta 358 (2005) 2933.)

3.1. Abstract

Spectroscopy (UV-Vis, ^{1}H-NMR, ESR) and electrochemistry revealed details of the structure of the Cu(II)-TRH (pyroglutamyl-histidyl-prolyl amide) complex. The ^{1}H-NMR spectrum of TRH has been assigned. NMR spectra of TRH in presence of Cu(II) showed that Cu(II) initially binds TRH through the imidazole. TRH analogs, pGlu-His-Pro-OH, pGlu-(1-Me)His-Pro-amide, pGlu-His-(3,4-dehydro)Pro-amide, pGlu-His-OH, pGlu-Glu-Pro-amide, and pGlu-Phe-Pro-amide provided comparison data. The stoichiometry of the major Cu(II)-TRH complex at pH 7.45 and greater is 1:1. The conditional formation constant (in pH 9.84 borate with 12.0 mM tartrate) for the formation of the complex is above 10^{5} M^{-1}. The coordination starts from the 1-N of the histidyl imidazole, and then proceeds along the backbone involving the deprotonated pGlu-His amide and the lactam nitrogen of the pGlu residue. The fourth equatorial donor is an oxygen donor from water. Hydroxide begins to replace the water before the pH reaches 11. Minority species with stoichiometry of Cu-$(TRH)_x$ (x = 2 – 4) probably exist at pH lower than 8.0. In non-buffered aqueous solutions, TRH acts as a monodentate ligand and forms a Cu(II)-$(TRH)_4$ complex through imidazole nitrogens. All the His-containing analogs behave like TRH in terms of the above properties.

3.2. Introduction

The neuropeptide Thyrotropin-releasing hormone improves functional recovery after neurologic dysfunctions, such as brain trauma and epilepsy [1-3]. Produced in the hypothalamus, TRH has been found to exist in significant quantities in other brain regions in rats [4,5], which implies other bioactivities. The effects of regulating body temperature [6] and stimulating hepatic blood flow [7] have been reported recently.

TRH exerts its effects through interactions with a membrane-bound receptor which has been found to be a member of the G-protein coupled receptor family [8]. Perlman et al. modeled TRH binding to its receptor. They claim that the carbonyl and NH of the pyroglutamyl moiety, the imidazole and the C-terminal amide are all involved in the interaction with receptor [9-11]. At the same time, these sites are potential electron donors for metal ions in that C=O, -NH-, and imidazole nitrogen atoms are known to be electron-rich. Ogawa et al. found that synaptic membranes carrying TRH receptors lose their function after pretreatment with metal ions in the absence of TRH, indicating irreversible changes [12]. Moreover, of the divalent ions they studied, Ni(II) was found to decrease TRH-receptor binding, while Cu(II) and Zn(II) were found to increase the binding at physiological serum concentrations (20 μM). The authors suggested that metal ions are important modulators of TRH activity.

A few studies have been carried out on the coordination of TRH and analogs with biologically active metal ions, e.g. Cu(II) and Ni(II), using techniques including potentiometric titration and spectroscopic methods such as UV-Vis, CD and ESR [13,14]. In the case of coordination with Cu(II) at pH 9.5 - 10, there was a major disagreement on the number of coordinated nitrogens (2 nitrogens in ref. [13], 3 nitrogens in ref. [14]). While both works

reported 1:1 stoichiometry of the complex, in ref. 14 the authors also claimed a major 1:2 metal-ligand binding stoichiometry when ligand was in 5-fold excess.

TRH-metal binding is important in another context. The sensitive and selective HPLC-based method for peptides is well established, based on the reversible electrochemistry of the Cu(III)/Cu(II) couple in polydentate peptide complexes, or biuret complexes [15,16]. The concentration of the neuropeptide TRH can be determined by the above mentioned means [17]. In both cases, the interaction of TRH with its receptor and the determination of TRH concentration, it is important to understand the metal complex structure. In this aspect, the role of pH should draw significant attention.

We also briefly studied the Cu(II) complexes of five TRH analogs in order to relate the nature of the coordination to the functional groups in the peptide side chain. These analogs are (abbreviations listed in parentheses):

pGlu-His-OH	(pEH)
pGlu-His-Pro-OH	(TRH-OH),
pGlu-(1-Me-His)-Pro-amide	(MeHis2-TRH),
pGlu-His-(3,4-dehydro-Pro)-amide	(deHPro3-TRH),
pGlu-Glu-Pro-amide	(Glu2-TRH), and
pGlu-Phe-Pro-amide	(Phe2-TRH).

The data support the view that the most prevalent complex in neutral and basic solutions has 1:1 stoichiometry. The four equatorial donor atoms are the imidazole 1-N, and the amide nitrogens resulting from the deprotonation of the amide bonds between pGlu and His and the lactam of pGlu as well as a water oxygen.

3.3. Experimental

3.3.1. Chemicals

TRH and all its analogs studied (all from Bachem, USA) were used without further purification, but purities were taken into account in preparation of solutions. All solutions were made in purified water using a Milli-Q A10 Synthesis water purification system (Millipore, USA) except for those used in NMR experiments in which D_2O (Cambridge Isotope Lab, USA) was used. The carbonate buffer is a mixture of equi-molar sodium carbonate and bicarbonate (both from EM science, USA), each at half of the concentration specified, i.e., given concentrations are for total carbonate. Borate buffers were all prepared with $Na_2B_4O_7 \cdot 10H_2O$ (Sigma, USA) in 0.25 M KNO_3 (J.T. Baker, USA). The borate concentration was 0.050 M except for the pH effect experiments, in which case the concentration was 0.10 M. The pH values were adjusted with 0.60 M boric acid or 4 M NaOH (both from EM science, USA), and measured with an Accumet® pHmeter (Fisher Sci., USA), standardized before each use. In ESR experiments, pH values were measured with pH test strips (Fisher Sci., USA) of the pH 5.5 and pH 9.0 solutions. These two pH values thus have one fewer significant figure. Na_2HPO_4 (0.126 M) - citric acid (0.037M) was used as a weakly acidic buffer. Copper-peptide solutions were prepared by adding the desired amount of stock solutions to buffer in the order of peptide then copper sulfate. Molar ratios were 1:1 (Cu(II):peptide) unless otherwise specified.

3.3.2. Instruments and procedures

Room temperature was 20 ± 2°C during all experiments.

UV-Vis spectroscopic instruments consisted of an HP 8453 spectrophotometer with HP 8453E operating software. Spectra of copper–peptide complexes in 1 cm quartz cuvettes were measured over 400 – 1000 nm with a 0.5 s integration time, using deionized water as a solvent

blank in all cases. The wavelengths of maximum absorption (λ_{max}) were identified by taking the first derivative with PeakFit (Version 4 for Win32 by Jandel Software, USA). The complex called "$Cu(H_2O)_6^{2+}$" was $CuSO_4$ in aqueous solution; the $Cu(OH)_4^{2-}$ complex was prepared by adding dropwise 4 M NaOH to $CuSO_4$ aqueous solution until the light blue $Cu(OH)_2$ precipitate cleared up and a deep blue solution was obtained; the Cu(II)-tartrate complex was a mixture of 1.0 mM $CuSO_4$ and 6.0 mM sodium tartrate in buffer; and the Cu(II)-peptide complexes were mixtures of 1.0 mM corresponding peptide and 1.0 mM $CuSO_4$ in buffer.

TRH spectra of ^1H-^1H 2-D and ^1H-^{13}C 2-D NMR were recorded on an AVANCE 500 NMR spectrometer from Bruker (Billerica, MA, USA). TRH spectra of ^1H, ^{13}C, DEPT (Distortionless Enhancement by Polarization Transfer) NMR and ^1H spectra of Cu(II) titration experiments were carried out on an AVANCE 300 NMR spectrometer from Bruker. The temperature was controlled at 0 °C. In copper titration experiments, the concentration of TRH was 4.0 mM in 0.20 M carbonate prepared in D_2O, with different concentrations of $CuSO_4$.

Electron spin resonance spectroscopy experiments were done with a Bruker Elexsys-E580 FT/CW spectrometer equipped with a Bruker ER 4118X-MS3 split ring resonator. Continuous wave ESR spectra were recorded with a quality factor Q of about 1600, a field-sweep of 600 Gauss, microwave power of 6.3 mW and modulation amplitude of 5 – 7 Gauss. All Cu(II)-TRH sample solutions were in 20%/80% glycerol/water (the glycerol was added as a cryoprotectant). The pH of each solution was adjusted with 2 M NaOH aqueous solution. All ESR experiments were carried out in the X-band (9.75 GHz) at a controlled temperature of 80 K.

Electrochemical instruments consisted of a DT-29 glassy carbon/glassy carbon ring-disk electrode, an ASR-2 analytical rotator, an RDE-3 potentiostat (all from Pine Instrument Co., Grove City, PA, USA), and a WaveTek 852 filter (WaveTek, San Diego, CA, USA) set for low

pass with 5 Hz cutoff frequency. A DT2802 chromatography board (Data Translation, Inc., USA) digitized the filtered analog signal to a personal computer. RRDE data were collected using EzChrom chromatography software (Scientific Software, Inc., San Raman, CA, USA). A platinum grid counter electrode and a BAS Ag/AgCl reference electrode (3 M NaCl) completed the electrochemical cell.

Complex concentrations as a function of total metal and ligand concentrations were calculated using Mathcad 2001 professional (Mathsoft, USA). Molecular simulation was carried out with the software CAChe (Fujitsu, Ltd., Japan) version 6.1.1. Structures were first checked for correct valences and hybridizations, then optimized using Allinger's standard MM3 force field model [18,19]. The following factors were taken into account when optimizing: bond stretch, bond angle, dihedral angle, improper torsion, van der Waals interaction, electrostatics interaction, hydrogen bond, torsion stretch, and bend-bend interactions.

3.4. Results and discussion

In basic Cu(II) solutions, for example pH 9.83 carbonate with tartrate in excess of Cu(II) ion, addition of TRH generates a bluish purple color with maximum absorption wavelength (λ_{max}) about 590 nm (Table 3-1). This wavelength is substantially lower than that of $CuSO_4$ aqueous solution ($Cu(H_2O)_6^{2+}$) or Cu(II)-tartrate complex, which are at 810 nm and 725 nm, respectively. Among the peptides studied, the characteristic bands are at similar wavelengths, except for Phe2-TRH and Glu2-TRH. The half wave potential is also a robust indicator for the formation of the biuret complex.

Table 3-1. Summary of spectroscopic and electrochemical properties of Cu(II) complexes of TRH and analogs.

Ligands	λ_{max} (nm)		ε_{app} [a] (cm^{-1} M^{-1})		$E_{1/2}$ (mV)	
	Carbonate	Borate	Carbonate	Borate	Carbonate	Borate
H_2O [b]	810		17		n/t	
OH^- [b]	637		n/t		n/t	
Tartrate	729	701	51	36	N/A	N/A
pGlu-His	595	585	64	65.7	n/t	780
TRH	595	588	58.7	59.6	780	785
TRH-OH	596	588	55.1	65.9	778	n/t
MeHis2-TRH	590	587	58.9	66.8	802	n/t
deHPro3-TRH	590	588	55.5	61.4	787	n/t
Glu2-TRH	730	ppt	54.4	N/A	N/A	n/t
Phe2-TRH	730	ppt	51.6	N/A	N/A	n/t

[a] Obtained by dividing the absorbance at λ_{max} by Cu(II) concentration.

[b] Not in buffer.

N/A: no detectable signal available. n/t : not tested. ppt: precipitation.

By coordination with peptides, the redox couple Cu(III)/Cu(II) has its oxidation potential significantly lowered to typically 0.5 – 0.8 V. Based on the distinguishable behavior of the two non-histidyl TRH analogs, we can conclude that for these N- and C-termini blocked peptides,

His is necessary for the formation of electrochemically active biuret complexes with Cu(II) ion. DeHPro3-TRH, TRH-OH and pGlu-His all behave like TRH, suggesting that the N-terminal Pro-NH_2 does not play an important role in the binding.

3.4.1. The binding stoichiometry

Tripeptides typically bind Cu(II) ion with 1:1 stoichiometry [20,21]. The tertiary histidyl-prolinyl amide is, however, a weak donor [22,23], thus TRH may act as a dipeptide. The molecular binding stoichiometry was determined using "the method of continuous variation", or Job's plot (Figure 3-1). The total concentrations of Cu(II) and TRH were held constant, while the relative ratios varied for each sample, from 0:1 (all TRH) to 1:0 (all Cu(II)). For pH higher than 8.0, a six-fold excess of tartrate over Cu(II) was included at the same concentration in each sample to prevent excess Cu(II) ion from precipitating. Cu(II) not bound to peptide absorbs light, so measured absorbances need to be corrected to give a measure of the concentrations of Cu(II)-peptide complex. Assuming that the molar absorptivity of unbound Cu(II) is constant, we have $C_{Cu(total)} = C_{Cu\text{-}TRH} + C_{Cu\text{-}other}$. At a certain wavelength:

$$\begin{aligned} A_{total} / l &= C_{Cu-other} \cdot \varepsilon_{Cu-other} + C_{Cu-TRH} \cdot \varepsilon_{Cu-TRH} \\ &= C_{Cu(total)} \cdot \varepsilon_{Cu-other} + C_{Cu-TRH} \cdot (\varepsilon_{Cu-TRH} - \varepsilon_{Cu-other}) \end{aligned}$$

The first term on the right side is just the absorbance of a sample with no peptide ("blank"). Thus, by subtracting a blank absorbance from the observed absorbance, a quantity A_{net} $(= A_{total} - C_{Cu\,(total)} \cdot \varepsilon_{Cu-other})$ is produced that is directly proportional to $C_{Cu\text{-}TRH}$. A_{net} values are then plotted against Cu(II) fraction in the total. The left half of each plot represents excess TRH, and the right half of the plot represents excess Cu(II). The extrapolations of both sides intersect at a Cu(II):peptide ratio indicating the complex stoichiometry.

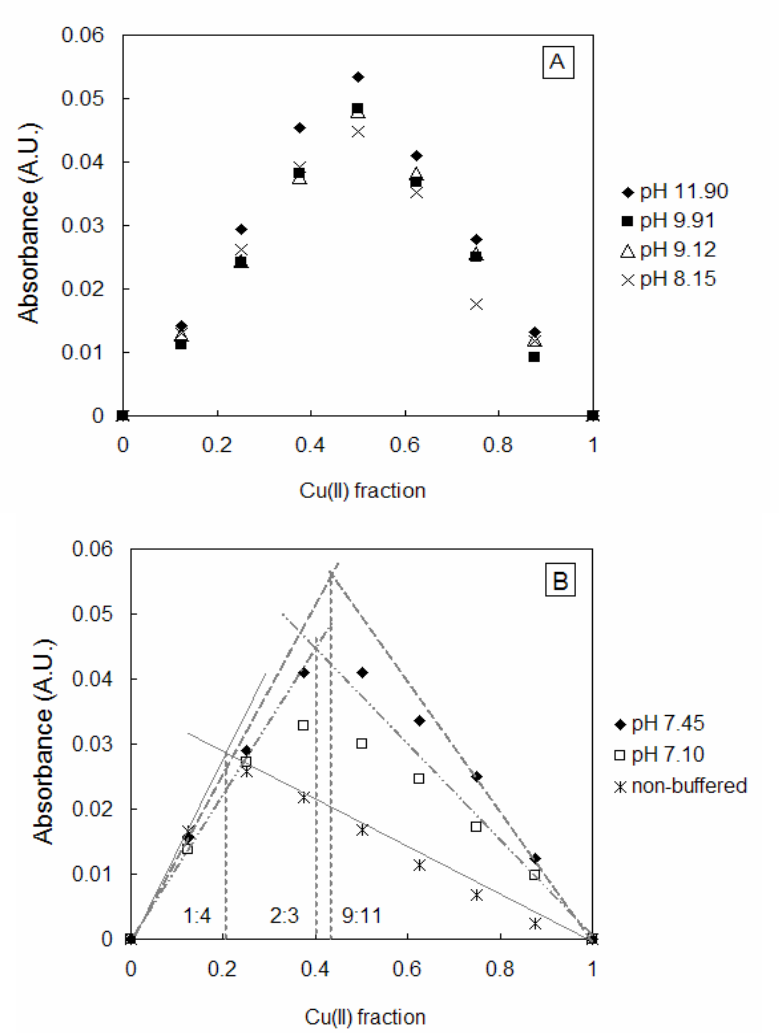

Figure 3-1. Job's plots of Cu(II)-TRH (1:1) complex at different pH.

Absorbances are normalized to 2.0 mM total concentration. A: Recorded in borate buffers containing 12.0 mM KNaTar. B: in borate-H_3BO_3 buffers, except for ∗ standing for non-buffered aqueous solutions.

The Job's plots revealed 1:1 stoichiometry from pH 8.15 to 11.90, as shown in Fig 1A. The λ_{max} and absorbance at this wavelength are also very similar from pH 8.15 to pH 9.91. Figure 3-1B shows Job's plots at lower pH values. A 1:4 stoichiometry predominates in non-buffered aqueous system (pH ranged between 5.2 – 5.7). The λ_{max} was 592 nm. No other reports about this stoichiometry have been found in the literature. At both pH 7.45 and 7.10 the apex is not well-defined. Also, in both cases the apparent binding stoichiometry involves non-integral

TRH per Cu(II) ion: 1.5 (3:2) at pH 7.10 and 1.1 (11:9) at pH 7.45. The deduction from these results at pH lower than 8 is that: 1) another component co-exists with the 1:1 complex; 2) binding is probably incomplete. The second component is a multi-peptide binding mode. A Cu-$(TRH)_2$ complex has been reported to account for ~70% of all Cu(II) between pH 7.5 and 10.0 when ligand was at 5-fold excess [14]. Our spectroscopic data can not determine the actual order of TRH in the multi-peptide binding mode. It could be 1:2, 1:3 or 1:4. Also, according to Figure 3-1B, at pH 7.45 the fraction of the second component is not as much as in the reference cited. It decreases with increasing pH, from a substantial fraction of the entire complex at pH 7.10, to a negligible amount at pH 8.15. At pH 7.45 it only represents a small fraction. Considering the pH dependence of the total apparent stoichiometry, deprotonation is involved in the formation of the 1:1 complex.

It draws interest that the binding of Cu(II) to TRH through amide groups can occur at physiological pH. Metal ions affect TRH-receptor interaction and TRH bioactivity. These observations were related to the tertiary conformation of TRH upon chelation [12,24]. The biuret complex of Cu(II) and TRH should play a significant role if the observed 1:1 binding exists at the much lower concentrations of both TRH and Cu(II) in biological environment. The molar absorptivity of the d-d transition investigated is too low at physiological concentrations to make measurements. Knowledge of the formation constant is required to predict the extent of coordination. In principle, our Job's plots contain information on the formation constants. However, in practice this method only works at a concentration range where binding is not complete. At the sub-milimolar concentrations adopted in typical visible spectroscopic measurements, the binding of Cu(II) and TRH is completed to a great extent, shown by the well-defined sharp apexes in Job's plots of pH 8.15 to pH 11.90. The observed formation constant

K_{obs} ($K_{obs} = \frac{[complex]}{([Cu_{total}] - [complex]) \cdot ([TRH_{total}] - [complex])}$) is estimated as no lower than 10^5 M^{-1}, but more accurate determination is not possible from these data.

Yamada et al. [14] reported the formation constants of 1:1 and 1:2 Cu(II)-TRH complexes which agreed with a few other values [25,26]. The average values are $\log\beta_1$=-7.70 for $MH_{-2}L$ and $\log\beta_2$ = -5.42 for $MH_{-2}L_2$ (M – metal, L – ligand, H_{-2} – two deprotonations). These numbers were obtained from pH titration experiment at tens of mM concentrations and 5-fold excess ligand. Under these conditions, the authors saw more than 70% of Cu(II) as a 1:2 complex in the pH range of 7.5 - 10. Based on their formation constant values, the corresponding conditional formation constants at pH 7.45 were calculated (by multiplying each β by $[H^+]^{-2}$) and used in a calculation of Job's experiment. In the calculation it was assumed that the 1:1 and 1:2 stoichiometry are the only forms of coordination. The result showed the fraction of 1:2 stoichiometry decreased dramatically with decreasing concentration and peptide:Cu(II) ratio.

At the concentrations used in our Job's experiments, $MH_{-2}L$ (1:1) predominates. When TRH is in excess, no more than 10% of Cu(II) exists as $MH_{-2}L_2$. When Cu(II) is in excess, there is virtually no $MH_{-2}L_2$. Physiologically, Cu(II) is in large excess of TRH. TRH exists in rat brain at nM concentrations [4], while Cu(II) has been determined with values ranging from approximately 40 to 150 μM [27,28]. At this excess, TRH forms predominantly a 1:1 complex with Cu(II). As calculated for 5 nM TRH and 50 μM Cu(II), 99.9% of TRH is bound with Cu(II) at 1:1 ratio. In the brain, the Cu(II) *activity* is certainly less than 50 μM, however, the complex is still predominantly 1:1. For example, with 5 nM TRH and 50 nM Cu(II), about 40% of TRH is bound with Cu(II) at 1:1 ratio. The concentration of the 1:2 species is 10^{-6} times lower.

For the computations above we used literature values for the binding constants. Our estimate of the formation constant of the 1:1 species is somewhat lower than the one used. The discrepancy is likely due to the difference in Cu(II) activity coefficients. Our measurements involved coordinating ions, nitrate and tartrate, and as such, the conditional constants derived from the data have little meaning in general. Nonetheless, the 1:1 coordination of Cu(II) and TRH can not be ruled out as an important process occurring biologically.

3.4.2. The equatorial donors

Billo [29] developed a correlation between the absorption maxima for Cu(II) complexes and the number and type of equatorial donors. With slight modification of the factors, the correlation worked well on multidentate ligands such as peptides [30]. According to this equation, the experimental λ_{max} data (pH 9.84) from the four histidyl-containing peptide complexes in Table 3-1 are consistent with the NNNO binding mode, in which each Cu(II) ion has three nitrogen atoms and one oxygen atom as equatorial donors. In fact, from pH 7.45 to 9.91, Cu(II)-TRH coordination fell in the NNNO binding region.

Electron Spin Resonance (ESR) can also give evidence of the number of nitrogen donors in Cu(II) complexes, often of peptides and proteins [31-33]. For Cu(II), the four features due to the parallel component of the hyperfine interaction ($A_{\|}$, with the nucleus of spin 3/2) can often be resolved near the $g_{\|}$ (the parallel component of the axially symmetric g-tensor) region of the spectrum. The magnitude of $A_{\|}$ and $g_{\|}$ are dependent on, among many factors, the ligand environment of Cu(II). Peisach and Blumberg [33] showed the dependence of $A_{\|}$ and $g_{\|}$ values and total charge of Cu(II) complexes on the ligand environment. Generally, as the number of nitrogen donors increases, all the four peaks shift to higher field. The $A_{\|}$ value also increases, from 120 G to 220 G when all four oxygen donors are replaced with nitrogen. At the same time,

$g_{\|}$ value decreases from 2.4 to 2.1. Millhauser et al. reported the binding modes of a Cu(II) complex and the prion protein octarepeats change from OOOO to NNNN in the pH range of 4.10 to 11.6 [32]. Their correlation between $A_{\|}$ and $g_{\|}$ values and the binding mode agreed with Peisach's.

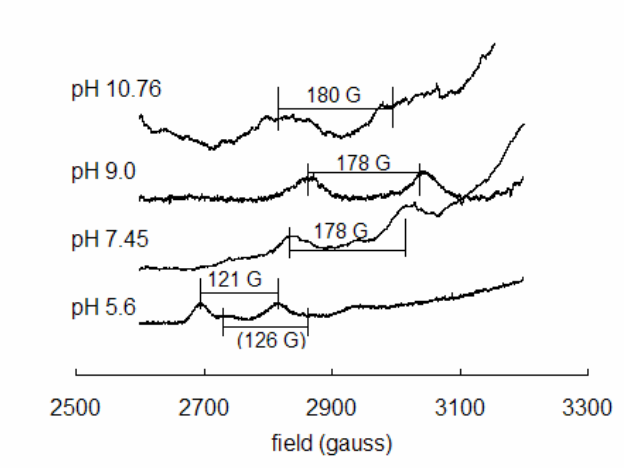

Figure 3-2. The $g_{\|}$ region of Cu(II) ESR spectra in presence of TRH.

Cu(II) and TRH were 1.0 mM each. The $A_{\|}$ value at pH 10.76 was obtained by simulating the spectrum with Bruker WINEPR simulation package because the peaks are very broad making direct reading difficult. The $A_{\|}$ value of the "shoulder" component at pH 5.5 was roughly estimated because the second peak was not well-defined.

ESR spectra were obtained for Cu(II) ion in presence of TRH at pH 5.5, 7.45, 9.0 and 10.76. $A_{\|}$ and $g_{\|}$ values were extracted. As shown in Figure 2 and Table 3-2, the main binding mode at pH 5.5 is OOOO. There is a minor component other than OOOO at slightly higher field. Due to the ambiguity of the second peak, it is difficult to assign any binding mode to this component. Based on the position of the first peak, one nitrogen binding is estimated. From 7.45 to 10.76, the Cu(II) ion hyperfine structure did not change significantly, suggesting the same equatorial binding. Shown in Table 3-2, the $A_{\|}$ and $g_{\|}$ values for all these pH values very well fit the NNNO binding mode. These results also are in good agreement with the visible spectroscopic data.

Table 3-2. ESR and UV-Vis parameters for Cu(II) signals in presence of TRH at different pH values.

pH	$A_{\parallel}$ (G)	$g_{\parallel}$	λ_{max} [a] (nm)	Equatorial binding
5.5	121 ± 2	2.41 ± 0.01	743	OOOO
7.45	178 ± 2	2.26 ± 0.01	589	NNNO
9.0	178 ± 2	2.26 ± 0.01	590	NNNO
10.76	175 ± 5	2.27 ± 0.01	586	NNNO

[a] pH 6.24, 7.01, 8.97 and 11.01, respectively.

Potential nitrogen donors in the TRH molecule include one lactam nitrogen from the pyroglutamyl residue, 1-N (pyridine) and 3-N (pyrrole) of the imidazole ring, two amide nitrogens from the two peptide bonds, and one amide nitrogen at the blocked C-terminus. The oxygen donor could be any one of the carbonyls, a water or a hydroxide. As mentioned above, the Pro residue does not seem to take part in the coordination. The tertiary amide is a weak donor. Furthermore, the nitrogen lone pair and the carbonyl group should be in the same plane [20]. This is extremely difficult for a prolinyl amide. As for the C-terminal amide, formation of a 5- or 6-membered fused ring structure does not seem possible. At the same time, the spectroscopic properties of TRH, deHPro3-TRH and TRH-OH are very close to each other. All the above argue against the participation of Pro in the binding. Despite all this, TRH does not act as a di-peptide. It forms a 1:1 complex with Cu(II) ion with three nitrogen donors, as do tripeptides. The His residue is known to have an electron-rich side-chain that can act as metal ligand [26,34,35]. If we do not consider Pro as having a donor, the three nitrogen donors are possibly the 1-N of imidazole, the lactam nitrogen of pGlu, and the amide nitrogen between the pGlu and His residues.

In general, biuret coordination starts at the N-terminal amine nitrogen of the peptide. The peptide amide bonds undergo deprotonation following that to form stable fused ring structures

[20,21]. In a TRH molecule, there is no amine group. The C-terminus, known to play a role when the N-terminus is blocked [36], is also blocked. It is of interest to find out how the coordination starts in a peptide with both termini blocked.

Selective broadening of proton and carbon resonances of ligands in NMR spectroscopy by a paramagnetic metal ion, such as Cu(II), can help locate the binding sites. Such ions increase fluctuations in the local magnetic field and reduce the both the longitudinal (T_1) and transverse (T_2) relaxation times of other nuclei nearby [37], thus altering their NMR signals. As line width is proportional to T_2^{-1}, an affected signal could be broadened and shortened, or even eliminated depending on the magnetic ion concentration [38]. By comparing the NMR spectra of ligands in the presence and absence of metal ion, one can deduce the most-affected protons or carbons in the ligand molecules. In a selective broadening experiment, the metal ion is usually held at 1/1000 or less of the ligand concentration. For peptide complexes in basic solutions, however, the binding at this molar ratio is very often not the same as at stoichiometric conditions. The main reason is that the relatively rare Cu(II) ions associate with and dissociate from the peptides rapidly before any peptide amide deprotonation or ring closure occurs [39]. In other words, the peptide acts as a monodentate ligand. The NMR signal changes under this condition will only indicate where the coordination begins, as the N-termini of glycyl di- or tri- peptides [40].

Figure 3-3 shows the ^{1}H NMR spectra of intact TRH and Cu(II)-titrated TRH solutions. Assignments of the peaks in both spectra required the TRH spectra of ^{1}H-^{1}H 2-D, ^{1}H-^{13}C 2-D NMR and DEPT (Distortionless Enhancement by Polarization Transfer, which records ^{13}C spectra that are edited with respect to the number of protons directly bonded to the carbons). As shown in Figure 3-3B, the imidazole protons respond most sensitively, showing signs of broadening and lowering when Cu(II) is present at only 1/4000 equivalents of TRH. This result

suggests that the imidazole acts as the initiating site during the binding, analogous to the primary $-NH_2$ group in most peptides. The two nitrogen atoms are both good donors, while the 1-N does have the advantage to form 6-membered ring structure. Therefore, 1-N is thermodynamically favored.

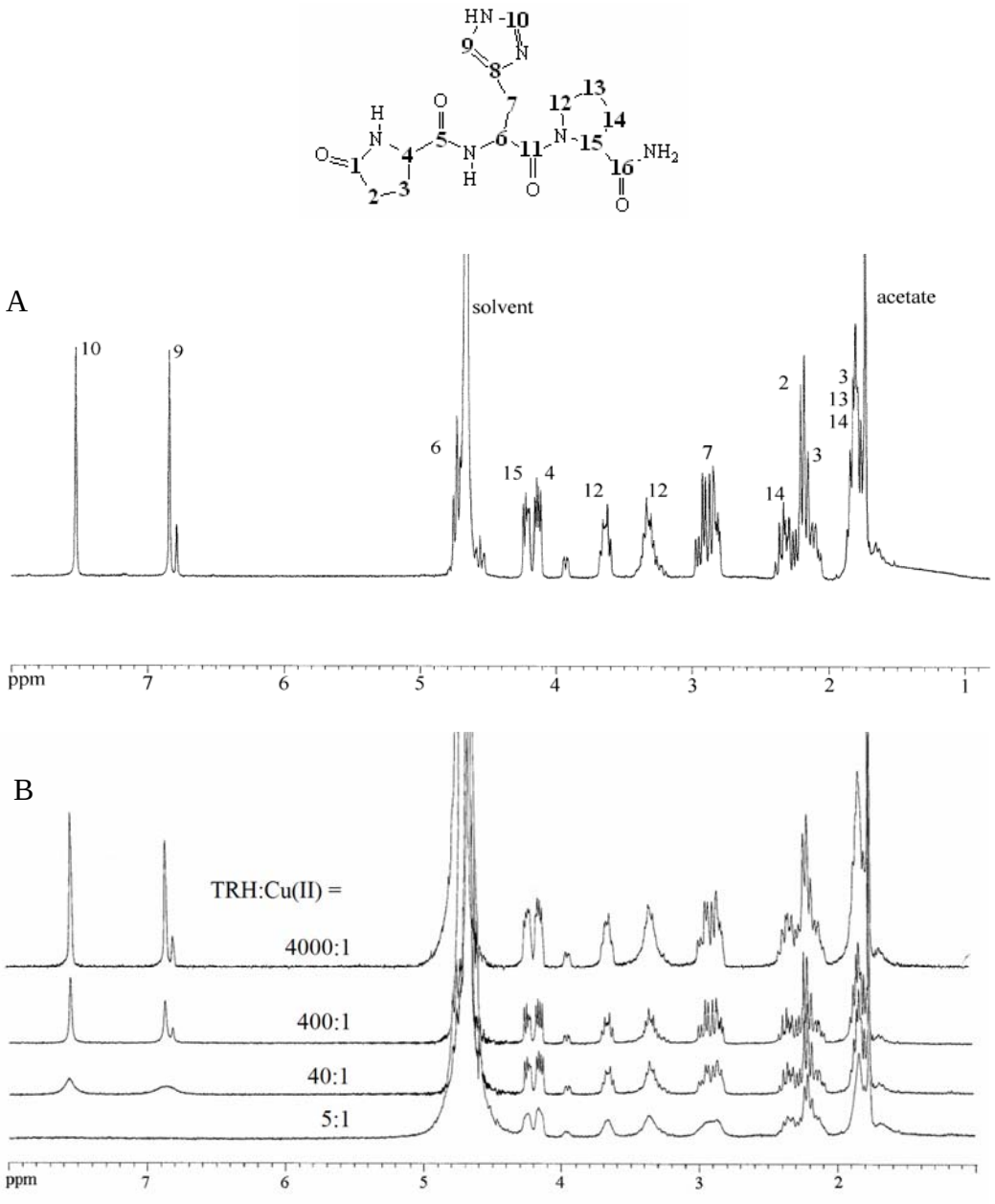

Figure 3-3. ^{1}H NMR spectra of TRH in absence and presence of Cu(II) ion..

To sum up, the NNNO binding is a reasonable structure and consistent with experimental data. Amide deprotonation propagates along the peptide backbone toward pGlu residue once the 1-N of imidazole coordinates with Cu(II). As for the fourth donor, the oxygen, Billo's equation is not able to distinguish a carbonyl, water or hydroxide. The computational software CAChe helped to verify the feasibility of some possible structures and to exclude some. The structure with a carbonyl oxygen either from the His-Pro peptide bond or from the C-terminal amide yielded structures with no reasonable Prolyl C-terminal carbonyl bond length or reasonable tetragonal complex structure. The fourth donor has to be a water or a hydroxide from this point of view. Figure 3-4 is an optimized structure by CAChe. The four donors are the deprotonated pGlu lactam nitrogen, the deprotonated pGlu-His peptide amide nitrogen, the His 1-N and H_2O. Cu(II)-peptide biuret complexes are square planar [41,42]. The two axial water ligands are placed 3 Å from Cu(II). Atoms at this distance hardly affect the spectra. The simulation also suggested that there may be a hydrogen bond between the C-Terminal amide carbonyl oxygen and the equatorial water proton.

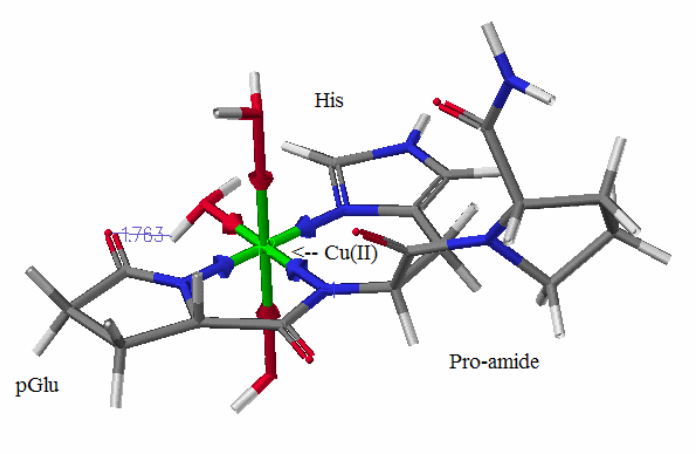

Figure 3-4 . CAChe simulation of Cu(II)-TRH complex of NNNO binding mode.

Structure was optimized by the beautify function on valence, hybridization and geometry. The 1.763 (Å) labels the O-H distance of a possible hydrogen bond.

3.4.3. The effect of pH

As deprotonation is a crucial step in Cu(II) and peptide binding, the pH of the solution is expected to affect significantly the complex formation. Figure 3-5 shows the band shift with increasing pH of Cu(II)-TRH in borate buffers. From the Job's plots and ESR results at various values of pH, we acquired the knowledge that in buffered systems, TRH starts to bind Cu(II) ion in an NNNO mode at pH slightly over 7.0. At least through pH 10.8 the equatorial binding mode is always NNNO. There is no evidence for NNOO binding. The pH range for existence of an NNOO binding mode, if there should be one, is expected to be very narrow, within pH 6 – 7. This likely results from the cooperativity in the serial binding of the three nitrogen donors.

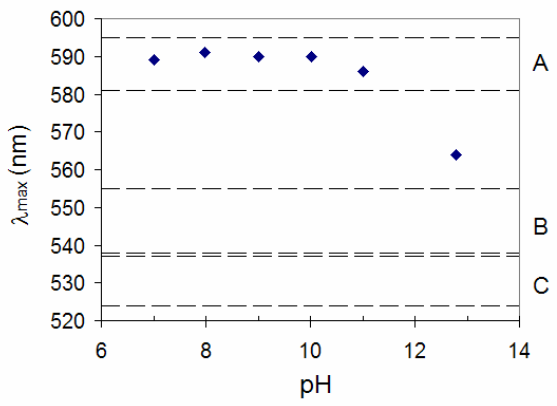

Figure 3-5. Band shift of Cu(II)-TRH with increasing pH in borate buffer.

Dashed lines define the following wavelength ranges:
A - NNNO (one imidazole, two deprotonated amides, one water or hydroxide); B - NNNN (two imidazoles, two deprotonated amides); C - NNNN (one imidazole, three deprotonated amides).

There are signs of multiple TRH binding at lower pH. The histidine is a basic residue. The pK_a of protonated imidazole has reported values ranging from 6.0 to 7.1 [43,44]. In about neutral solutions with Cu(II) present, one of the two imidazole nitrogens undergoes deprotonation and binds Cu(II). In this way the TRH acts as a monodentate ligand. This possibly

accounts for the donor in non-buffered solutions, in which one Cu(II) ion binds four TRH molecules. From a steric aspect, this seems easier for the 3-N (pyrrole). The non-buffered Job's experiment of one of the analogs, MeHis2-TRH, should differentiate the two imidazole nitrogens. The MeHis2-TRH molecule bears a methyl group at the 3-N. As a monodentate ligand, the only available nitrogen donor is the imidazole 1-N. If the His 1-N sees substantial steric hindrance, this analog would not bind Cu(II).

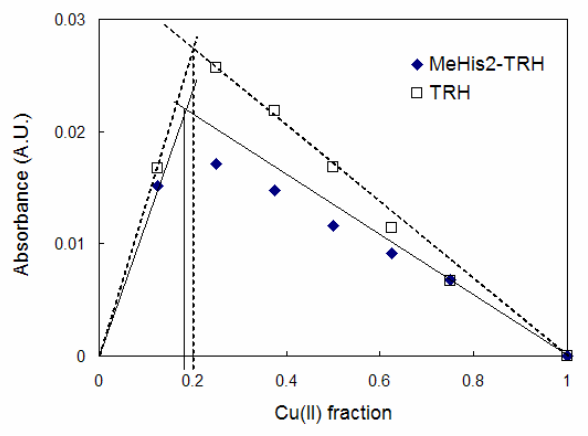

Figure 3-6. Job's plots of Cu(II)-TRH and Cu(II)-MeHis2TRH in non-buffered solutions.
The perpendicular line indicates Cu(II) fraction 0.20, which corresponds for Cu(II):peptide = 1:4.

The Job's experiment with MeHis2-TRH yielded a similar plot as the one with TRH (see Figure 3-6). The λ_{max} was 590 nm. The apparent stoichiometry was about 1:4, too. Obviously the 1-N of His imidazole is capable of binding Cu(II). The apex of MeHis2-TRH plot was lower than that of TRH. The apparent binding constant for MeHis2-TRH in this case is smaller than that of the native peptide. At this point, we are not able to identify the nitrogen donor when TRH acts as a monodentate ligand. It could be either the 1-N or the 3-N of the imidazole. Figure 3-7 shows the CAChe simulation of Cu(II)-(TRH)4 (via imidazole 3-N) and Cu(II)-(MeHis2-TRH)4 (via imidazole 1-N). The relative stabilities of the two divalent complex ions are indicated by

their “current energy” calculated by CAChe of the optimized structures. The two numbers are only a few percent different. They show relatively equal stability.

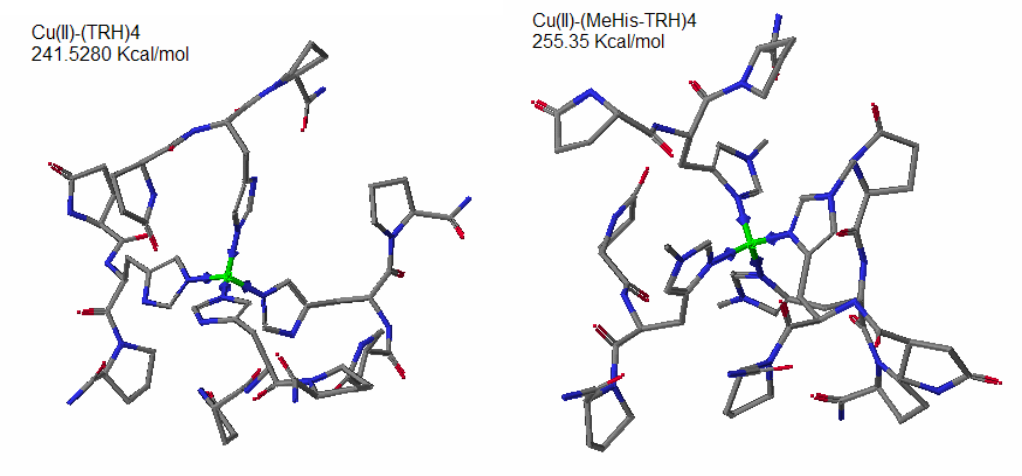

Figure 3-7. CAChe simulation of Cu(II)-TRH_4 and Cu(II)-$(MeHis2TRH)_4$.

TRH binds Cu(II) at imidazole 3-N. MeHis2TRH binds Cu(II) at imidazole 1-N. The listed energy values were “current energy” of geometry and hybridization beautified structures.

The pH 7.10 Job’s plot reveals a mixture of 1:1 stoichiometry and complexes with higher peptide:Cu(II) ratios. At pH 7.45 the 1:1 complex predominates. This means that in the presence of Cu(II) the pK_a of the two amides is not much higher than that of the imidazole. The 1:1 and 1:4 binding modes give very close λ_{max} values: 588 nm for the 1:1 binding and 592 nm for the 1:4 binding. One would deduce that for any transitional binding mode between these two the absorption band is within the range of 588 – 590 nm. This is why the Cu(II)-TRH d-d band does not shift significantly with increasing pH from 7.01 to 11.01 (< 10 nm when Cu(II) and TRH were at 1:1 molar ratio, Figure 3-5).

As pH further increases to over 12.0 the band shifts to 564 nm. This sharp shift of absorption band indicates deprotonation. There are two possible deprotonations that could cause band shifting: 1) deprotonation of an amide, which binds Cu(II) as the fourth donor; 2)

deprotonation of the 3-N (pyrrole) of the imidazole, which may or may not bind Cu(II). Hypothesis 1 was invalidated by CAChe simulation. The only available amide, the C-terminal amide is not able to reach the equatorial position while keeping reasonable bond angles and lengths. For hypothesis 2, Cu(II)-binding-facilitated proton loss from an imidazole pyrrole nitrogen has been reported widely. It has been reported to occur at various pH values depending on the actual ligand structure, as low as pH 9.6 in some cases with TRH [45,46]. The deprotonated pyrrole nitrogen of imidazole may or may not coordinate with Cu(II) ion [44,47]. However, shown by Figure 3-8, all the five His-containing TRH-like peptides including MeHis2-TRH which is not capable of pyrrole deprotonation display very similar pH-dependent band-shifting. This is a strong evidence against hypothesis 2. For TRH the pyrrole nitrogen deprotonation is still possible and consequently may lead to polymerization of Cu(II)-TRH [45] (but the stoichiometry will still be 1:1). However, this deprotonation is not the main cause of the band shifting at high pH.

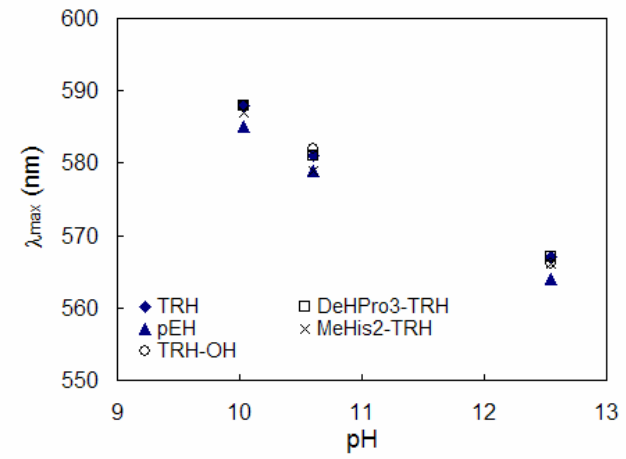

Figure 3-8. Band shift of Cu(II) complexes of TRH analogs with increasing pH.

Only His-containing analogs were included. All solutions were in borate buffer.

Another possible deprotonation is the deprotonation of the equatorial water, or replacement of the water by a hydroxide. Billo did not distinguish the contributions of carbonyl, water or hydroxide oxygen in his equation [29]. In a later regression by Sigel and Martin, the three types of oxygen donors also had the same contribution to Cu(II) complex absorption [30]. While the above two set of factors agree closely and work relatively well on general Cu(II) complexes of nitrogen-containing ligands, attention should be drawn to the generally different donating abilities of the three oxygen donors, especially the water which is a known weak donor compared to the other two. Prenesti et al. [48] studied over 100 Cu(II) complexes and came up with refined factors. Important to their discussion, they found a bigger contribution from carbonyl and hydroxide (0.39), while their factor for water is in agreement with Billo and Sigel and Martin (0.296). Our absorption data of $[Cu(OH^-)_4]^{2-}$ (see Table 3-1) gives a factor of 0.391 for OH- in this complex in agreement with Prenesti et al. The increased contribution factor of hydroxide shifts the calculated Cu(II)-TRH band (NNN(OH-)) to 553 nm. This deprotonation of water ligand does not depend on the actual peptide structure, which is consistent with Figure 3-8.

3.5. Conclusions

TRH and its analogs lack a primary amine group which is generally the initiating site of coordination with Cu(II) ion. In TRH, the imidazole nitrogen initiates complexation. Coordination of Cu(II) ion and TRH starts from 1-N of the imidazole and proceeds along the peptide backbone toward the N-terminus, involving the deprotonated amide between pGlu and His, and the deprotonated lactam amide in the pGlu residue. A water molecule completes the ligand set. Binding in this way occurs at pH as low as 7.10 in buffered systems. There should be considerable Cu(II)-TRH interaction under physiological conditions (pH 7.4), which may affect TRH-receptor interaction. The 1:1 stoichiometry is expected to predominate at physiological concentrations of Cu(II) and TRH.

ACKNOWLEDGEMENTS

This work was funded by the National Institutes of Health grant GM44842. Dr. Marco Bonora has provided great help with ESR data acquisition.

The published paper was dedicated to Prof. Rex Shepherd for his many enthusiastic and insightful comments and discussion on inorganic chemistry.

BIBLIOGRAPHY

[1]. Kastin, A. J.; Ehrensing, R. H.; Schalch, D. S.; Anderson, M. S. *Lancet* **1972**, *2*, 740-742.

[2]. Prange, A. J., Jr.; Breese, G. R.; Cott, J. M.; Martin, B. R.; Cooper, B. R.; Wilson, I. C.; Plotnikoff, N. P. *Life Sci.* **1974**, *14*, 447-455.

[3]. Prange, A. J., Jr.; Lara, P. P.; Wilson, I. C.; Alltop, L. B.; Breese, G. R. *Lancet* **1972**, *2*, 999-1002.

[4]. Winokur, A.; Utiger, R. D. *Science* **1974**, *185*, 265-267.

[5]. Winokur, A.; Utiger, R. D. *Thyrotropin-releasing hormone in the central nervous system: distribution and degradation*. in *Cent. Nerv. Syst. Eff. Hypothal. Horm. Other Pept., [Symp.]*. **1979**: Raven, New York.

[6]. Bird, J. A.; Clarke, L.; Symonds, M. E. *Biol. Neonate* **1998**, *73*, 52-59.

[7]. Hashimoto, T., Yoneda, M., Kojima, K., Murohisa, T., Tamano, M., Iijima, M., Shimada, T., Sugaya, H., Terano, A., Tamori, K., Nakade, Y., Yokohama, S., Nakamura, K., and Makino, I. *Jpn. Pharmacol. Ther.* **2001**, *29*, s189-s192.

[8]. Yamada, M.; Monden, T.; Satoh, T.; Satoh, N.; Murakami, M.; Iriuchijima, T.; Kakegawa, T.; Mori, M. *Biochem. Biophys. Res. Commun.* **1993**, *195*, 737-745.

[9]. Perlman, J. H.; Laakkonen, L.; Osman, R.; Gershengorn, M. C. *J. Biol. Chem.* **1994**, *269*, 23383-23386.

[10]. Perlman, J. H.; Thaw, C. N.; Laakkonen, L.; Bowers, C. Y.; Osman, R.; Gershengorn, M. C. *J. Biol. Chem.* **1994**, *269*, 1610-1613.

[11]. Laakkonen, L. J.; Guarnieri, F.; Perlman, J. H.; Gershengorn, M. C.; Osman, R. *Biochemistry* **1996**, *35*.

[12]. Ogawa, N.; Mizuno, S.; Kishimoto, T.; Mori, A.; Kuroda, H.; Ota, Z. *Neurosci. Res.* **1984**, *1*, 363-368.

[13]. Formicka-Kozlowska, G.; Kozlowski, H.; Jezowska-Trzebiatowska, B.; Kupryszewski, G.; Przybylski, J. *Inorg. Nucl. Chem. Lett.* **1979**, *15*, 387.

[14]. Yamada, Y.; Nakasuka, N.; Tanaka, M. *Inorg. Chim. Acta* **1991**, *185*, 49-56.

[15]. Chen, J.-G.; Woltman, S. J.; Weber, S. G. *J. Chromatogr. A* **1995**, *691*, 301-315.

[16]. Warner, A. M.; Weber, S. G. *Anal. Chem.* **1989**, *61*, 2664-2668.

[17]. Meng, R.; Xia, W.; Sandberg, M.; Stephens, R.; Weber, S. G. *submitted to J. Chromatogr. A* **2004**.

[18]. Lii, J. H.; Allinger, N. L. *J. Am. Chem. Soc.* **1989**, *111*, 8576-8582.

[19]. Lii, J.-H.; Allinger, N. L. *J. Comput. Chem.* **1998**, *1998*, 9.

[20]. Margerum, D. W. *Pure Appl. Chem.* **1983**, *55*, 23-34.

[21]. Margerum, D. W.; Wong, L. F.; Bossu, F. P.; Chellappa, K. L.; Czarnecki, J. J.; Kirksey, S. T., Jr.; Neubecker, T. A. *Adv. Chem. Ser.* **1977**, *162*, 281-303.

[22]. Bataille, M.; Formicka-Kozlowska, G.; Kozlowski, H.; Pettit, L. D.; Steel, I. *J. Chem. Soc. Chem. Commun.* **1984**, *4*, 231-232.

[23]. Formicka-Kozlowska, G.; Kozlowska, H.; Siemion, I. Z.; Sobczyk, K.; Nawrocka, E. *J. Inorg. Biochem.* **1981**, *15*, 201-212.

[24]. Tonoue, T.; Minagawa, S.; Kato, N.; Kan, M.; Terao, T.; Nonoyama, K.; Ohki, K. *Pharmacology Biochemistry and Behavior* **1979**, *10*, 201-204.

[25]. Formicka-Kozlowska, G.; Bezer, M.; Pettit, L. D. *J. Inorg. Biochem.* **1983**, *18*, 335-347.

[26]. Farkas, E.; Sovago, I.; Kiss, T.; Gergely, A. *J. Chem. Soc. Dalton Trans.* **1984**, 611-614.

[27]. Hanig, R. C.; Aprison, M. H. *Anal. Biochem.* **1967**, *21*, 169-177.

[28]. Andrasi, E.; Farkas, E.; Scheibler, H.; Reffy, A.; Bezur, L. *Arch. Gerontol. geriat.* **1995**, *21*, 89-97.

[29]. Billo, E. J. *Inorg. Nucl. Chem. Lett.* **1974**, *10*, 613-617.

[30]. Sigel, H.; Martin, R. B. *Chem. Rev.* **1982**, *82*.

[31]. Burns, C. S., Aronoff-Spencer, E., Dunham, C. M., Lario, P., Avdievich, N. I., Antholine, W. E., Olmstead, M. M., Vrielink, A., Gerfen, G. J., Peisach, J., Scott, W. G., and Millhauser, G. L. *Biochemistry* **2002**, *41*, 3991-4001.

[32]. Aronoff-Spencer, E.; Burns, C. S.; Avdievich, N. I.; Gerfen, G. J.; Peisach, J.; Antholine, W. E.; Ball, H. L.; Cohen, F. E.; Prusiner, S. B.; Millhauser, G. L. *Biochemistry* **2000**, *39*, 13760-13771.

[33]. Peisach, J.; Blumberg, W. E. *Arch. Biochem. Biophys.* **1974**, *165*, 691-708.

[34]. Boka, B.; Myari, A.; Sovago, I.; Hadjiliadis, N. *J. Inorg. Biochem.* **2004**, *98*, 113-122.

[35]. Sovago, I.; Farkas, E.; Bertalan, C.; Lebkiri, A.; Kowalik-Jankowska, T.; Kozlowski, H. *J. Inorg. Biochem.* **1993**, *51*, 715-726.

[36]. Shi, F.; Woltman, S. J.; Weber, S. G. *Anal. Chim. Acta* **2002**, *474*, 1-9.

[37]. Bertini, I.; Luchinat, C. *Coord. Chem. Rev.* **1996**, *150*, 77-110.

[38]. Emsley, J. W.; Feeney, J.; Sutcliffe, L. H., *High Resolution NMR Spectroscopy*, ed. J.W. Emsley; J. FeeneyL.H. Sutcliffe. Vol. I. **1965**, New York: Pergamon Press, Ltd.

[39]. Espersen, W. G.; Martin, R. B. *J. Am. Chem. Soc.* **1976**, *98*, 40-44.

[40]. Li, N. C.; Scruggs, R. L.; Becker, E. D. *J. Am. Chem. Soc.* **1962**, *84*, 4650-4654.

[41]. Nolan, K. B.; Soudi, A. A.; Hay, R. W. *Amino Acids, Peptides, and Proteins* **1994**, *25*.

[42]. Nolan, K. B.; Soudi, A. A.; Hay, R. W. *Amino Acids, Peptides, and Proteins* **1996**, *27*, 282-332.

[43]. Grant, G.; Ling, N.; Rivier, J.; Vale, W.; Butcher, M.; Hewitt, W. *Biochemistry* **1972**, *11*, 3070-3073.

[44]. Sundberg, R. J.; Martin, R. B. *Chem. Rev.* **1974**, *74*, 471-517.

[45]. Morris, P. J.; Bruce Martin, R. *J. Inorg. Nucl. Chem.* **1971**, *33*, 2913-2918.

[46]. Osz, K.; Varnagy, K.; Suli-Vargha, H.; Sanna, D.; Micera, G.; Sovago, I. *Dalton Trans.* **2003**, *10*, 2009-2016.

[47]. Aiba, H.; Yokoyama, A.; Tanaka, H. *Bull. Chem. Soc. Jpn.* **1974**, *47*, 1437-1441.

[48]. Prenesti, E.; Daniele, P. G.; Prencipe, M.; Ostacoli, G. *Polyhedron* **1999**, *18*, 3233-3241.

4. The Rotating Ring-Disk Electrochemistry of Copper Complexes of Thyrotropin-releasing Hormone

4.1. Abstract

The C- and N-termini blocked neuropeptide Thyrotropin-releasing Hormone (TRH) forms electroactive Cu(II) complex. Rotating ring-disk electrode (RRDE) acts as a powerful tool in investigating the reversible electrochemistry of the Cu(III)/Cu(II) couple as complex of TRH in alkaline solution. Oxidation occurs on the disk electrode and reduction on the ring electrode. Varying rotation frequency helps to discover chemical kinetics associated with the electrochemistry. The plot of limiting current vs. square root of rotation frequency deviates from theoretical Levich's equation, indicating preceding chemical reactions. The deviation is more pronounced at higher initial concentration. A non-electroactive complex, dimer $Cu(II)_2$-TRH_2, is postulated. Simulation of RRDE behavior of the postulated Cu(II)-TRH system by DigiSim software has succeeded in matching experimental data. Capillary electrophoresis implies negative charge on the dimer. It is suggested that an hydroxo-bridge may link the two Cu(II) centers. CAChe program proves that the bi-nuclear $Cu(II)_2$-TRH_2 complex is possible.

4.2. Introduction

The selective chromatographic detection of peptides has been established based on the reversible electrochemistry of the Cu(III)/Cu(II) couple in polydentate peptide complexes [1,2], also called biuret complexes. In support of this detection method, the RRDE has been used to study the electrochemical kinetics of Cu(II) complexes of oligoglycines as model peptide ligands [3]. The results revealed effects of pH, buffer and rotation frequency on the electrochemistry of Cu(II)-oligoglycine complexes. While oligoglycine complexes serve to teach us about the essential chemistry of the peptide backbone with Cu(II), their study is not sufficient to teach the complexities of bioactive peptides. Additional features in peptide structures including side chains and modified termini add complexity to the coordination reactions and thus the electrochemical kinetics of the complexes.

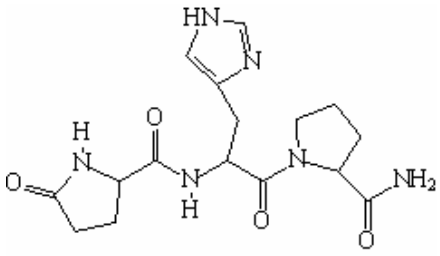

Figure 4-1. TRH molecule.
It is neutral at pH 9.8.

Thyrotropin-releasing Hormone (TRH), or pyroglutamyl-histidyl-prolyl amide, is a tripeptide blocked at both C- and N-termini (the termini are both amides). TRH has been shown to improve functional recovery after neurologic dysfunctions, such as brain trauma and epilepsy, in both humans and animals such as rats, mice and cats [4-8]. We believe that, coupled with

online microdialysis and preconcentration, the concentration of TRH can be monitored. Further, the unique structure of TRH makes it interesting from a coordination chemistry and electrochemistry perspective. The probable structure of Cu(II)-TRH has been determined by spectroscopic and electrochemical means [9]. Briefly, Cu(II) binds to TRH through the pGlu amide nitrogen, the pGlu-His peptide bond nitrogen, the 1-N of the His imidazole and a water. The electrochemistry of Cu(II)-TRH is much more complicated than that of the Cu(II)-polyglycines. This chapter reports on the electrochemistry of the Cu(II) complex of TRH.

The rotating ring-disk electrode (RRDE) has proven to be powerful in studies of homogeneous kinetics and equilibria [10], and is particularly suited to modeling dual electrode detection [3]. The disk electrode serves as the anode and the ring electrode as the cathode. The flow pattern introduced by the rotation of the electrode draws solutes first over the central disk electrode and then over the ring electrode. The disk electrode signal obtained for a simple, mass transport-limited electron-transfer process obeys the Levich equation [10]:

$$i_D = nFADC^*/\delta = 0.620nFAC^* D^{2/3}\nu^{-1/6}\omega^{1/2} \qquad \text{Eq. (4-1)}$$

where i_D (disk current) is in mA, C* (concentration of the analyte) is in M, D (diffusion coefficient of the solute) is in cm^2/s, ν (kinematic viscosity of the solution) is in cm^2/s, ω (rotation frequency) is in rad/s, n is the number of electrons transferred per molecule of solute, and F is the Faraday constant. The ratio of current at the ring to current at the disc is known as the collection efficiency, N_0.

Homogeneous chemical reactions preceding and following the disk electrode reaction affect the current profile vs. rotation frequency. The model biuret complex tetraglycine, decomposes following oxidation [11]. The effect of this ECE (electrochemical-chemical-electrochemical) process is seen from extra disk current and reduced ring current at low rotation

frequencies. Preceding reactions (CE) include amide deprotonation or ligand exchange [3]. They often cause lower current than expected at high rotation frequencies. For simple peptides such as G_4 and G_5, these effects can be eliminated by choosing the right pH and buffer systems to obtain a plot of limiting current vs. $\omega^{1/2}$ that obeys the Levich equation [3].

4.3. Experimental

4.3.1. Chemicals

Thyrotropin-releasing hormone from Bachem (King of Prussia, PA, USA) was used without further purification, but the purity (96%) was taken into account in solution preparation. Copper sulfate pentahydrate (J.T. Baker, Phillipsburg, New Jersey, USA) was re-crystallized once from water. Borate buffers were all prepared in 0.25 M KNO_3 (J.T. Baker, USA) with $Na_2B_4O_7 \cdot 10H_2O$ from Sigma (St. Louis, MO, USA). In pH effect experiments, the borate concentration was 0.10 M. In all other experiments using borate, the borate concentration was 0.05 M. All pH values were adjusted with 0.40 M boric acid (EM science, Gibbstown, NJ, USA) and/or 4 M NaOH (EM science), and measured with an Accumet® pH-meter (Fisher Sci, Fairlawn, New Jersey, USA), standardized before each use. Copper-peptide solutions were prepared by diluting a desired amount of stock solution in the order of peptide then copper sulfate in buffer. Molar ratios were 1:1 unless mentioned.

All water used was from a Milli-Q A10 Synthesis water purification system (Millipore, Billerica, Massachusetts, USA).

4.3.2. Instruments and procedures

The rotating ring-disk apparatus consisted of a DT-29 glassy carbon/glassy carbon ring-disk electrode, an ASR-2 analytical rotator, and an RDE-3 potentiostat (all from Pine Instrument Co., Grove City, PA, USA). The ring-disk electrode has a disk area of 0.2475 cm^2, and geometric collection efficiency of 0.3714. A platinum grid counter electrode and a Ag/AgCl reference electrode (3 M NaCl, Bioanalytical Systems, West Lafayette, Indiana, USA) were used. All potentials here are reported relative to this reference electrode. Before each run the working electrodes were wet polished with 0.05 μm γ-alumina powder (Buehler Ltd., Lake Bluff, Illinois,

USA) and rinsed with Milli-Q deionized water from a wash bottle. The electrode was then placed in the rotator. Background current (buffer used for the sample solution) was measured first and subtracted from sample signal.

The potentiostat signals were filtered with a WaveTek 852 filter (WaveTek, San Diego, CA, USA) set for low pass with 1 Hz cutoff frequency. RRDE data were collected using EzChrom chromatography software with a DT2802 chromatography board (Data Translation, Inc., USA), or PeakSimple software with a SRI202 board (SRI Instruments, Torrance, CA, USA). Data collection was triggered manually while the voltage was simultaneously applied to the electrode. All files then were converted to ASCII format and processed with Excel.

For hydrodynamic voltammetry, the disk potential was swept linearly from 0 mV to 1000 mV. The sweep rate was always 0.5 V/min unless otherwise specified. The ring electrode was maintained at a constant potential of 0 mV. RRDE rotation frequency studies were conducted with the disk electrode potential held at 900 mV and the ring electrode at 0 mV. These potentials were identified by voltammetry as being in the limiting current region. In each run, the electrode was rotated initially at a moderate rotation frequency before potentials were applied. The non-Faradic current was permitted to decay no less than 2.5 min. The rotation frequency then was varied in a random sequence with some of them repeated 1 or 2 times. Data collected within the initial period of current decay were ignored. The rotation frequency was maintained at each value long enough to ensure steady state.

The mass transport properties of the system were tested from 10 to 5000 rpm using 0.20 mM ruthenium(III) hexamine trichloride (Aldrich, Milwaukee, WI, USA) as a reversible one-electron standard. The solution was prepared in 0.4 M carbonate buffer, pH 9.8. The complex was reduce at the disk (E_{app} = -280 mV) and then oxidized at the ring (E_{app} = 0 mV). Data

yielded a linear Levich plot (R^2 = 0.9945, n = 39) over the entire rotation frequency range tested at both disk and ring electrodes. The diffusion coefficient obtained, 4.05 $\times 10^{-6}$ cm^2/s, agreed with the value 3.91×10^{-6} cm^2/s obtained by the Taylor-Aris flow injection method.

Spectroscopic measurements employed an HP 8453 spectrophotometer with HP 8453E operating software (Agilent, USA). Spectra of copper – peptide complexes in 1 cm quartz cuvettes were measured over 400 – 1100 nm in general scanning mode at 0.5 s integration time, using Milli-Q water as a solvent blank in all cases.

Room temperature was 22 ± 2 °C during all RRDE experiments.

Determination of diffusion coefficients by laminar flow axial dispersion was according to the procedure of A. Beisler [Beisler, 2003 #14]. Briefly, a rectangular plug of solute is allowed to disperse in a 25 μm inside diameter capillary under pressure-induced flow. Analysis of the shape of the formerly rectangular zone as it passes through a downstream detector yields the diffusion coefficient. The aqueous flow solution containing 0.1% trifluoroacetic acid, 3% 1-propanol and 25% acetonitrile was pumped with a Waters 600 E quaternary pump. A splitter tee was used to decrease the flow rate to 2-5 μL/min. The TRH stock solution was diluted in mobile phase to make a concentration of 10 μM and injected with an Upchurch microinjector. After the injector the biuret solution containing 5.00 mM $CuSO_4$, 30.0 mM sodium tartrate in 1.2 M carbonate buffer was combined with flow solution mentioned above through a home-designed micromixer. The analyte was detected at 0.80 V versus Ag/AgCl with a 10 μm carbon fiber electrode 1 mm in length (CV-27 Potentiostat, BAS, W. Lafayette, IN, USA) and current was measured with a Keithly (Cleveland, OH) 427 Picoammeter. Signals from the ammeter were collected at 50 Hz by EzChrom (Scientific Software, San Ramon, CA). Data obtained were exported and smoothed using PeakFit software. The first derivative was determined in PeakFit using Savitzky-Golay

filtering. The statistical moments were determined by fitting the 5-parameter GEMG function to the data based on the least squares criterion.

The obtained diffusion coefficient of the Cu(II)-TRH complex was then corrected for solvent based on Scheibel Correlation [23]. The diffusion coefficient in aqueous solution is 5.86 $\times 10^{-6}$ cm^2/s. This value is used in the Levich equation to determine the expected current response for a diffusion controlled one-electron transfer reaction of the Cu-TRH complex.

Capillary electrophoresis experiments were carried out on an ISCO 3850 Capillary Electropherograph (ISCO Inc., Lincoln, NE), with PeakSimple Chromatography Data System with a SRI202 board (SRI Instruments Inc., Torrance, CA, USA) for data collection. The UV detector was set at either 210 nm or 590 nm. The fused silica capillary (Polymicro Tech, LLC. Phoenix, Arizona, USA) had a 50 μm inner diameter and 70 cm total length. Detecting window was 50 cm from the injecting port. A voltage of 20 kV ran through 50 mM pH 9.84 borate buffer. Sample solutions of 1.0 mM each Cu(II) and peptide prepared in the running buffer were vacuum-injected for 5 sec each run. ACN of 5% (v/v) served as a neutral marker.

4.3.3. Simulation.

Molecular simulation was carried out with the software CAChe (Fujitsu, Ltd., Japan) version 6.1.1. Structures were first checked for correct valences and hybridizations, then optimized using Allinger's standard MM3 force field model [15]. The following factors were taken into account when optimizing: bond stretch, bond angle, dihedral angle, improper torsion, van der Waals interaction, electrostatics interaction, hydrogen bond, torsion stretch, and bend-bend interactions.

Electrochemical simulation was carried out with software DigiSim (BAS, USA), version 3.03b, under hydrodynamic conditions.

4.4. Results and discussion

In pH 9.84 borate buffers, equimolar solutions of Cu(II) and TRH show a characteristic bluish-purple color, with a maximum absorbance (λ_{max}) at 588 nm. The voltammetric wave generated by RRDE gives a half-wave potential, $E_{1/2}$, of 785 mV at both disk and ring electrodes. Shown in Figure 4-2, the same set of solutions displays different pH dependence in spectroscopic and electrochemical measurements. The absorption band does not shift in the range of pH 7.4 to pH 11 [9], while the $E_{1/2}$ decreases linearly with a slope of -70 mV/pH. When either of the two reagents is in excess, the slope gets closer to -59 mV.

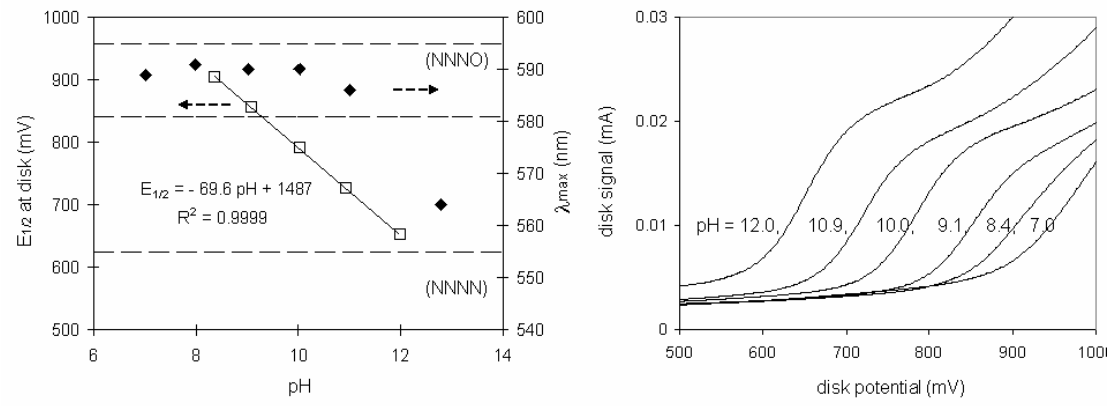

Figure 4-2. pH-dependent spectroscopy and electrochemistry of 1:1 Cu-TRH.

All solutions contain 1.00 mM (in spectroscopic measurements) or 0.10 mM (in electrochemical measurements) Cu(II) and TRH in borate buffers. Dashed horizontal lines in the left figure define the upper and lower limits of λ_{max} for NNNO- and NNNN-bound Cu(II) calculated from Billo's equation [16].

The potential shift with pH in Figure 4-2 shows a deprotonation-assisted redox reaction. The deprotonation is fast enough to catch up with the electron transfer. An example of not so fast deprotonation is that of the third peptide bond amide in Cu(II)-polyglycine complexes. The slow deprotonation causes two waves to be seen in RRDE voltammetry, representing two electroactive complexes Cu(II)-NNNO and Cu(II)-NNNN [3], the latter at a lower potential. The

deprotonation in Cu(II)-TRH is clearly not this case. We determined earlier that the equatorially bound water may lose one proton and become a hydroxide ligand [9]. This deprotonation makes a promising candidate responsible for the potential shift with pH. Since this process is fast, we will not include it in discussing preceding reactions in the later part of this work.

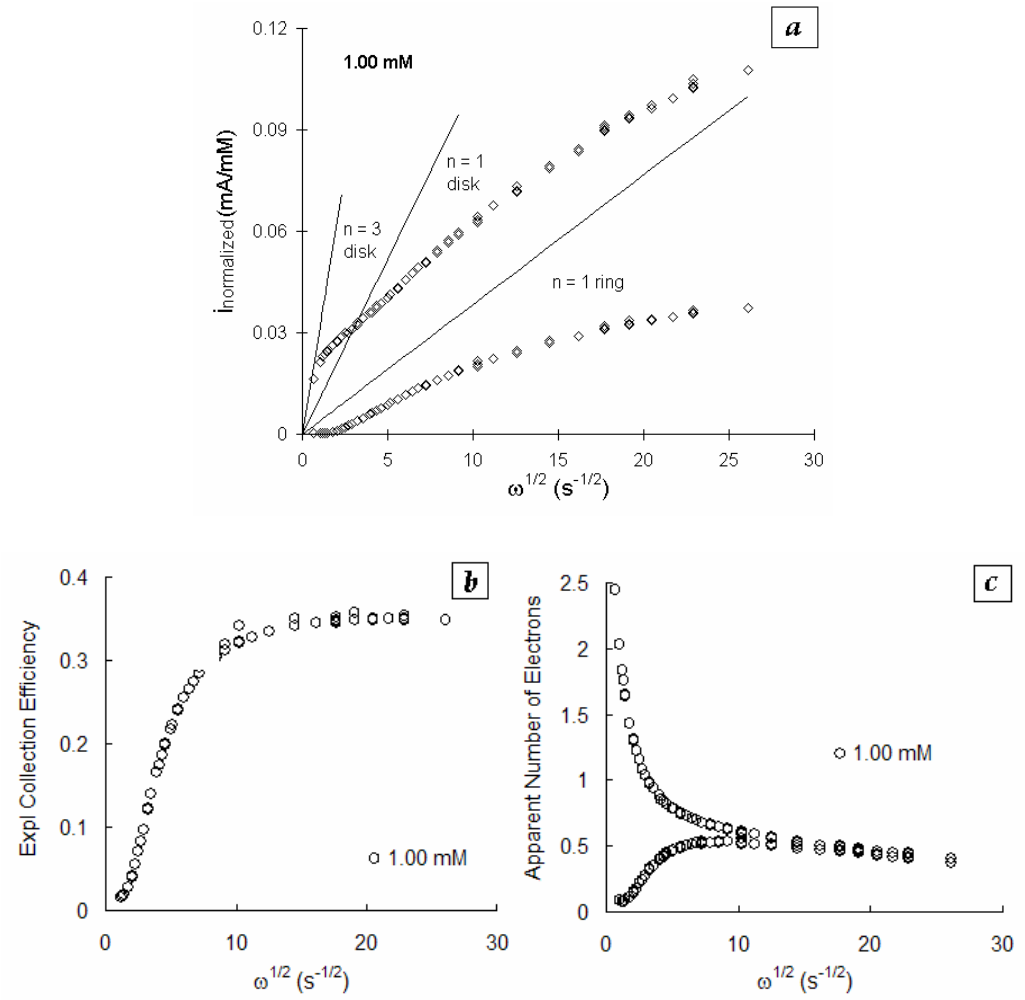

Figure 4-3. Experimental and predicted diffusion controlled currents plotted against $\omega^{1/2}$.

Solution contains 1.00 mM each Cu(II) and TRH in pH 9.84 borate buffer.
(a). Normalized currents. The upper trace is of disk signals, the bottom is of ring. Straight lines are predicted (D = 5.86 ×10-6 cm2/s) from the Levich equation, taking the total concentration of Cu(II) ion as electroactive C*. (b). Experimental collection efficiency, calculated as i_R/i_D. (c). Apparent number of electrons involved in the redox reactions on disk and ring electrode.

A Levich plot, in the case of a mass transport-limited oxidation, is a straight line with zero intercept. Figure 4-3a shows an experimental Levich plot of Cu(II)-TRH. It clearly deviates from the theoretical lines at both disk and ring electrodes. Figure 4-3b and 4-3c are replots of the same data. Figure 4-3b is the rotation frequency-dependent "experimental collection efficiency N_κ" obtained by dividing i_D (limiting current at disk) by i_R (limiting current at ring) at each rotation frequency. Figure 4-3c is the "apparent number of electrons transferred (ANE)" obtained by dividing each experimental current by the theoretical value.

Based on rotation frequency, the data set can be divided into two parts. When rotation frequency is low ($\omega^{1/2} < 10$ in the figure), N_κ is significantly less than N_o. Woltman et al. have shown similar RRDE behavior with Cu(II)-oligoglycines [3]. It is consistent with an ECE process recognized and studied by Margerum et al. [11]. Briefly, the Cu(III)-peptide as the product of the first electron transfer reaction decomposes and produces more oxidizable species. The irreversible oxidation of these species gives extra current at the disk and at the same time reduces the ring current because it removes available reactants for the ring electrode. Correspondingly, in Figure 4-3b N_κ is close to zero at low frequencies.

When the rotation frequency is greater than 1000 rpm ($\omega^{1/2} > 10$), ANE values of the disk and ring electrodes agree with each other, and N_κ reaches a plateau. Equal disk and ring ANE values and a constant N_κ represent a situation where little or no reaction occurs in the gap. Under this condition, all of the Cu(III) complex generated at the disk is reduced at the ring. The lifetime of the Cu(III) species depends on many things, one of which is substitution at the α-carbon in the amino acids making up the peptide. Glycines contribute to instability, while peptides from 2-methylalanine (i.e., no α-hydrogens) have more stability [17-19]. For triglycine, the rotation

frequency at which the plateau is reached is near 5000 rpm [3], greater than the value of 1000 seen with Cu-TRH.

As can be seen in Figure 4-3 (a and c), the number of electrons transfer at disk and ring electrodes agree with each other, but both are significantly smaller than 1 (Figure 4-3c). This behavior at high rotation frequencies is consistent with a CE (chemical-electrochemical) process. In such a process, the electroactive species is generated by a chemical reaction prior to the oxidation. As rotation becomes faster, less time is given for this reaction, so less reactant is provided to the disk electrode causing a lower disk current. Limiting current on an RRDE in this case is related to both K, equilibrium constant, and k, rate constant, of the preceding reaction. The value of K determines the fraction of electroactive species prior to the electric field application. The reaction's relaxation time determines how rapidly the equilibrium responds to the electrochemical perturbation.

The preceding reaction may have various origins. The Cu(II) and peptide binding equilibrium is the first to be considered. The conditional Cu(II)-TRH binding constant at pH 9.8 has been estimated to be at least 10^5 M^{-1} [9]. It corresponds to 90% or more bound at concentrations of 1.0 mM each Cu(II) and TRH. This value is substantially bigger than the ANE values at high ω show in Figure 4-3c. This means if Cu-peptide binding equilibrium is the only preceding reaction, even at a infinitely small rate constant, the resulted limiting current should still be higher than the experimentally obtained value. There seems to be a reaction that takes away the already produced electroactive complex in bulk solution. We recorded limiting current data at various concentrations. The deviation of the experimental Levich plot should be more severe at lower concentrations if the binding equilibrium is mainly responsible for the deviation. As shown in Figure 4-4, the result is the opposite – there is less deviation at lower concentrations.

At high rotation frequencies, the normalized limiting current decrease when concentration increases. Thus, we rule out the simple Cu-TRH binding as the preceding reaction.

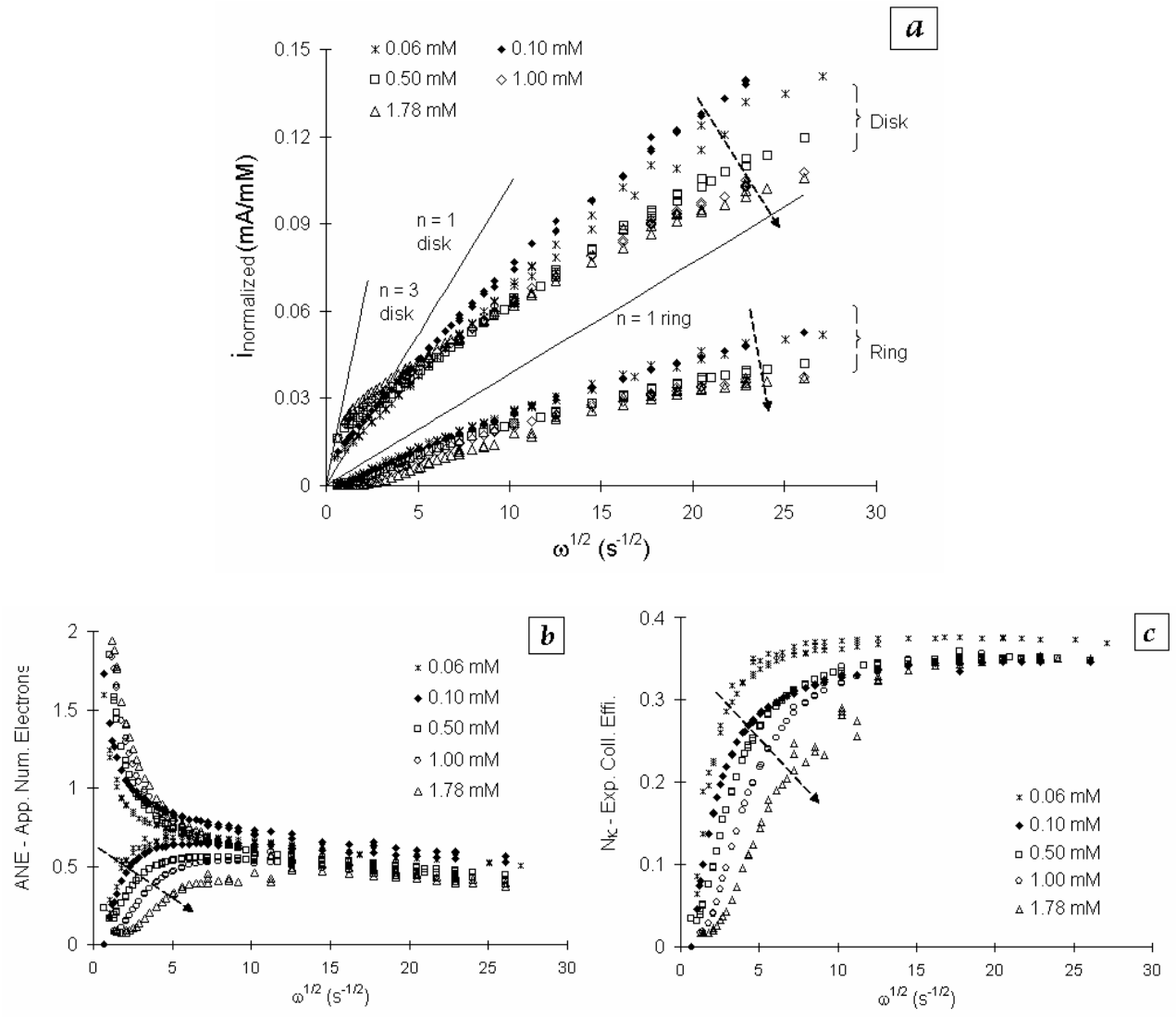

Figure 4-4. Concentration effect on RRDE behavior of 1:1 Cu(II)-TRH.

All solutions are in pH 9.8 borate buffer. Dashed arrows indicate concentration increase. (a). Normalized currents. (b). Experimental collection efficiency, calculated by i_R/i_D. (c). Apparent number of electrons involved in the redox reactions on disk and ring electrode.

Levich pointed out that with a first order preceding reaction, under conditions that $(D/\nu)^{1/6} << k/\omega$, the value $i/\omega^{1/2}$ is proportional to the value i and the Levich equation can be rewritten as [10]:

$$i/\omega^{1/2} = \frac{i_L}{\omega^{1/2}} - i\left(\frac{D^{1/6}}{1.61\nu^{1/6}Kk^{1/2}}\right) \qquad \text{Eq. (4-2)}$$

where i_L is the limiting current without a preceding reaction, K is the equilibrium constant and k is the rate constant of the preceding reaction. Because of Cu(III)-TRH decomposition, for TRH only data representing a pure CE process ($\omega^{1/2} > 10$, or $\omega > 1000$) shall be used.

Because Eq. (4-2) results from a first order process, the $Kk^{1/2}$ value is a constant regardless of concentration. It can be determined from the slope of $i_{disk}/\omega^{1/2}$ vs i_{disk}. Our "$Kk^{1/2}$" values calculated, however, vary with concentration. Figure 4-5 shows decreasing "$Kk^{1/2}$" with increasing concentration. Apparently, the C in the case of Cu(II)-TRH is not a first order reaction. Eq. (4-2) does not work in this particular case.

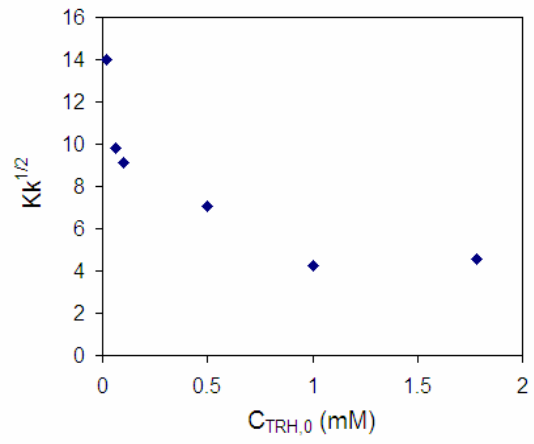

Figure 4-5. "$Kk^{1/2}$" values decrease with increasing initial concentration.
Values are derived from data in Figure 4-4 and Eq. (4-2). Cu(II):TRH = 1:1

The data are consistent with a reaction that is higher order on the reactant side than the product side, in which the product is electroinactive. This hypothesis of higher order reaction is plausible and consistent with the electrochemical and spectroscopic data. However, neither visible spectroscopy nor electrochemistry is capable of verifying it. Spectroscopy cannot distinguish the two forms while electrochemistry only recognizes one of them. Thinking of the possible donor atoms in TRH, there is really no other nitrogen or carboxyl oxygen available due to steric tension. The proposed Cu(II)-TRH structure is a neutral species [9]. If the other complex form differs in the charge that the coordination core carries, capillary electrophoresis should tell more.

We employed two TRH analogs (Figure 4-6) as comparison and charge reference. MeHisTRH and TRH-OH have the same amino acid sequence as TRH but each slightly different in one substituent. Their spectroscopic and electrochemical properties suggest identical equatorial binding under the current conditions [9]. TRH-OH and its complex should carry one more negative charge than the corresponding analogs due to the dissociation of the C-terminal carboxylic group.

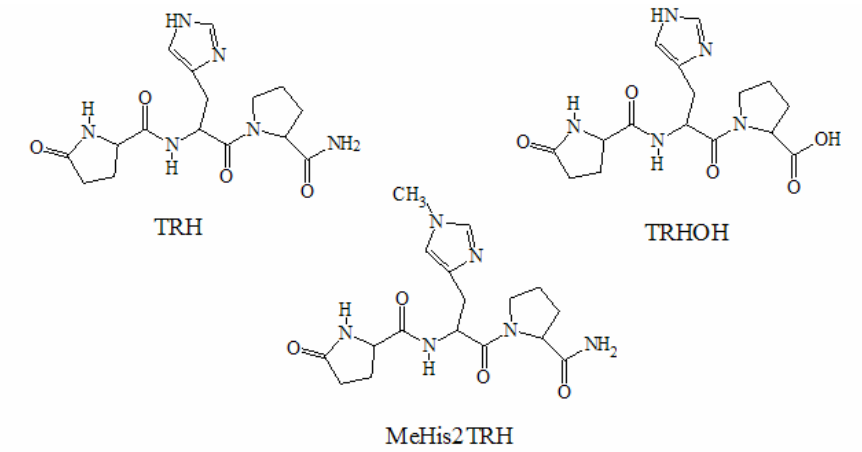

Figure 4-6. Sequences of TRH, TRHOH and Me-His2-TRH.

Both TRH and the 1:1 mixture of Cu(II) and TRH absorb maximally at 210 nm. The complex absorbs in the visible region while the peptide does not. In CE with 'normal' polarity, negatively charged species migrate at a lower velocity than the electroosmotic flow.

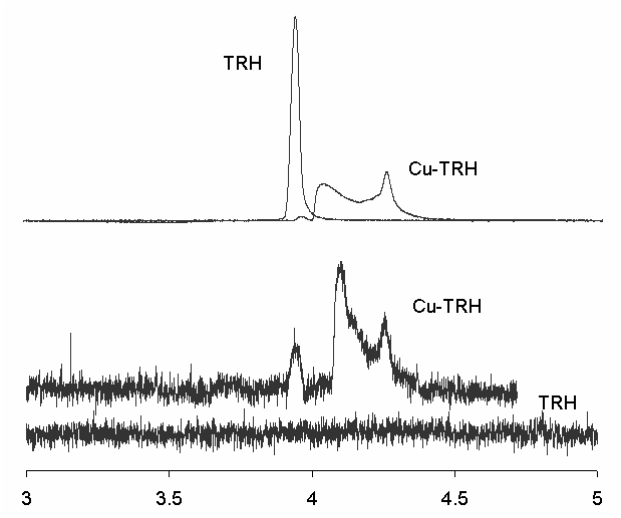

Figure 4-7. CE signals of 1:1 TRH and Cu(II)-TRH mixture.

In 50 mM pH 9.8 borate buffer. 1.0 mM each. Upper trace: detected at 210 nm. Bottom trace: detected at 590 nm.

The top electrophorograms in Figure 4-7 show a peak for TRH (Cu(II) absent) at pH 9.8 migrating with the migrating with the neutral marker (arrow). The "peak" for Cu(II)-TRH is complex. This is because we have injected a solution containing several components in an equilibrium, and the separation disturbs the equilibrium [20,21]. Krylov calls this 'non equilibrium capillary electrophoresis of equilibrium mixtures' or NECEEM. To interpret the data, it is helpful to consider the lower traces (λ = 590 nm). These traces show only Cu(II) complexes (note the lowest trace shows no response from TRH, and Cu(II) itself is not soluble at this pH). There is a small peak about 3.9 min corresponding to a neutral complex and a sharp peak at 4.25

min as well as an exponentially decaying zone with a maximum at about 4.1 min. We interpret these curves within the framework of NECEEM [20,21]. The neutral Cu(II)-TRH complex gives a peak at 3.9 min. An anionic complex also exists with its peak at 4.25 min. The exponentially-tailed peak in between represents the dissociation of the anionic complex to form the neutral complex.

Complexes formed from MeHisTRH and TRH-OH give different CE traces (Figure 4-8). The TRH-OH complex should have a charge of -1, as does the peptide itself. The CE traces are completely consistent with this. The MeHisTRH complex acts like the TRH complex.

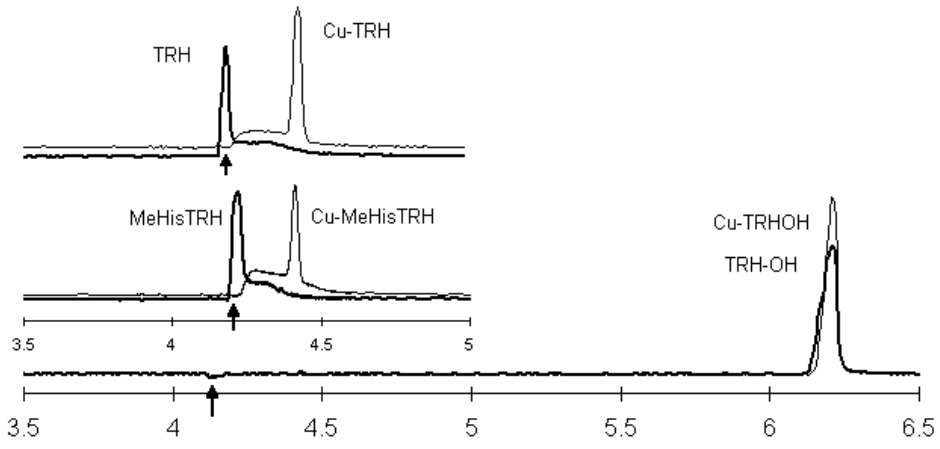

Figure 4-8. CE signals of TRH, TRHOH and MeHisTRH and their copper complexes.

All in 50 mM pH 9.8 borate buffer. All solutions contain 1.0 mM each Cu(II) and peptide. All detections are made at 210 nm. Arrows point to the neutral marker.

Hence, there is a slow equilibrium involving two different forms of Cu(II)-TRH or Cu(II)-MeHisTRH complexes. One component of the equilibrium carries one extra negative charge. TRHOH, on the other hand, binds Cu(II) with overall charge unchanged.

What proton is lost? Deprotonation of the N-terminal amide is first to be considered. Evidence for such deprotonation in a peptide is rare. The pK_a of secondary amide is usually much higher than pH 10. Coordination to Cu(II) may promote the deprotonation, as for the peptide backbone amide deprotonation in a typical biuret reaction. The argument against it is there is no fused ring formation for the deprotonated N-terminal amide to bind Cu(II), while fused ring formation is essential in stabilizing a biuret complex. We conclude that deprotonation of N-terminal amide in TRH and MeHisTRH to introduce one negative charge to their Cu(II) complexes is not likely. The best possibility lies in the equatorial water ligand, which deprotonates to become a hydroxide. Another Cu(II) center may lose a water ligand and take the place of the missing proton in this hydroxide.

We propose that a Cu(II)-TRH dimer exists, linked by an hydroxo-bridge. The presence of the dimer and the following reactions serve to explain the Levich plot curve shape of Cu(II)-TRH systems and the electrophorograms, among which Eq. (4-4) embodies the preceding reaction that holds up the redox reaction on disk electrode:

$$\text{Cu(II) + TRH} \underset{k_{f1}}{\overset{k_{b1}}{\leftrightarrows}} \text{Cu(II)-TRH} \qquad K_1 = \frac{[Cu(II)-TRH]}{[Cu(II)]\cdot[TRH]} \qquad \text{Eq. (4-3)}$$

$$2\text{Cu(II)-TRH} \underset{k_{f2}}{\overset{k_{b2}}{\leftrightarrows}} \text{Cu(II)}_2\text{-TRH}_2 \qquad K_2 = \frac{[Cu(II)_2-TRH_2]}{[Cu(II)-TRH]^2} \qquad \text{Eq. (4-4)}$$

$$\text{Cu(II)-TRH} - \text{e} = \text{Cu(III)-TRH} \qquad \text{Eq. (4-5)}$$

No simple solution of Levich equation available under this particular condition. We sought help from the simulation tool DigiSim to verify that a system following Eq. (4-3) – Eq.

(4-5) behaves similarly as we observed for Cu(II)-TRH. The following parameters have been used in the simulation:

1) Concentrations, electrode geometry, and voltammetry parameters are the same as in actual measurements.
2) Diffusion coefficients (D): D of the electroactive form of Cu(II)-TRH complex (monomer) is 5.86 $\times 10^{-6}$ cm^2/s; those of Cu(III)-TRH and TRH are assumed the same; D of $Cu(II)_{aq}$ has been calculated to be 6.5 $\times 10^{-6}$ cm^2/s based on the constant $D\eta/T = 2.23 \pm 0.37 \times 10^{-10}$ cm^2poise/Ks [22]; the value of 3.8 $\times 10^{-6}$ cm^2/s has been used for $Cu(II)_2$-TRH_2, an estimation based on the monomer value 5.86 $\times 10^{-6}$ cm^2/s and the expression D $\propto$ (molar volume)$^{-0.6}$ [23], assuming that molar volume of the dimer is twice as that of the monomer.
3) K_1 (Eq. (4-3)) is about 10^5 M^{-1} [9]. Simulation trials were made within range $1 \times 10^5 - 3 \times 10^5$ M^{-1}, and K_2 (Eq. (4-4)) within the range $2 \times 10^3 - 3.3 \times 10^3$ M^{-1}. The two parameters were then narrowed down so that the unbound Cu(II) and TRH fractions were consistent with the spectroscopic data, and the simulated current matched experimental data. The values $K_1 = 1.0 \times 10^5$ M^{-1} and $K_2 = 2.8 \times 10^3$ M^{-1} are optimum.
4) Reaction rate $v = k_f$ [reactant] $- k_b$ [product]. DigiSim simulation requires input of rate constant of the forward reaction k_f, and calculates the backward rate constant based on equation $K = k_f/k_b$. We assign subscript 1 for parameters of Eq. (4-3) and subscript 2 for those of Eq. (4-4). Thus, reaction rate for Eq. (4-3) is $v_1 = k_{f1}$ [Cu(II)][TRH] $- k_{b1}$[Cu(II)-TRH], and reaction rate for Eq. (4-4) is $v_2 = k_{f2}$ [Cu(II)-TRH]^2 $- k_{b2}$[$Cu(II)_2$-TRH_2]. Our simulation of a simple binding equilibrium as the preceding reaction confirmed that k_{f1} value from 10^{-3} to 10^5 M^{-1} s^{-1} only caused about 1% difference in the current at 0.06 mM

Cu(II) and TRH each at 3000 rpm. So a value of 500 $M^{-1}s^{-1}$ has been chosen for k_{f1}. The calculated value of k_{b1} is 0.005 s^{-1}.

5) All above parameters settled, optimal value of k_{f2} has been found to be 3.4×10^4 $M^{-1}s^{-1}$. The calculated value of k_{b2} is12.14 s^{-1}.

Figure 4-9 and Figure 4-10 compare simulated and experimental currents vs. concentration and rotation frequency. Final deviations (absolute($i_{sim} - i_{exp}$) shown are no more than 5%. Since the simulated currents match the experimental values rather well in the applicable concentration or rotation frequency range, we have demonstrated that a dimer complex of $Cu(II)_2$-TRH_2 is possible.

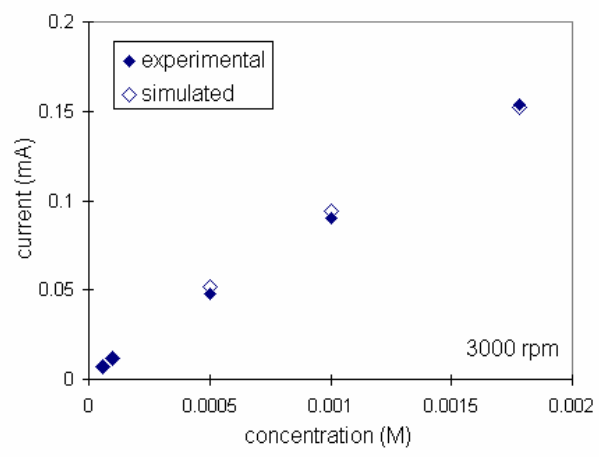

Figure 4-9. Simulated and experimental currents of CE process vs concentration.

Currents at 3000 rpm are plotted against varied concentration. Following Eq. (4-3) – Eq. (4-5): $K_1 = 1\times10^5$ M, $k_{f1} = 500$ $M^{-1}s^{-1}$, $k_{b1} = 0.005$ s^{-1}; $K_2 = 2.8\times10^3$ M^{-1}, $k_{f2} = 3.4\times10^4$ $M^{-1}s^{-1}$, $k_{b2} = 12.14$ s^{-1}.

Hydroxo-bridges in Cu(II) complexes are not rare. There are many μ-hydroxo-Cu(II) examples [24-28] with one or two hydroxo-links. Geometry around the two Cu(II) centers are not always the same in each complexes, but typically Cu-Cu distance is 2.8 – 3.1 À and bond angle at the OH is 95° – 105° [24-28]. Molecular calculation program CAChe helped to

demonstrate possible structures of $Cu(II)_2$-TRH_2 dimer. The linkage Cu-OH-Cu is bent due to the sp3 hybridization of the oxygen. Other parts of the peptide molecules may interact at convenient distances. Figure 4-9 shows one possibility, in which the lactam oxygen of one pGlu residue occupies an axial position of the other Cu(II) center. The bond geometries are in rather good agreement with literature: Cu-Cu distance: 3.06 Å, and Cu_1-OH^--Cu_2 angle: 95.1°. Water molecule may also act as a bridge bond [29,30]. Molecular calculation also suggested four member ring formed by Cu-OH-Cu-H_2O, in which the water is an apical ligand brought relatively closer to the metal center.

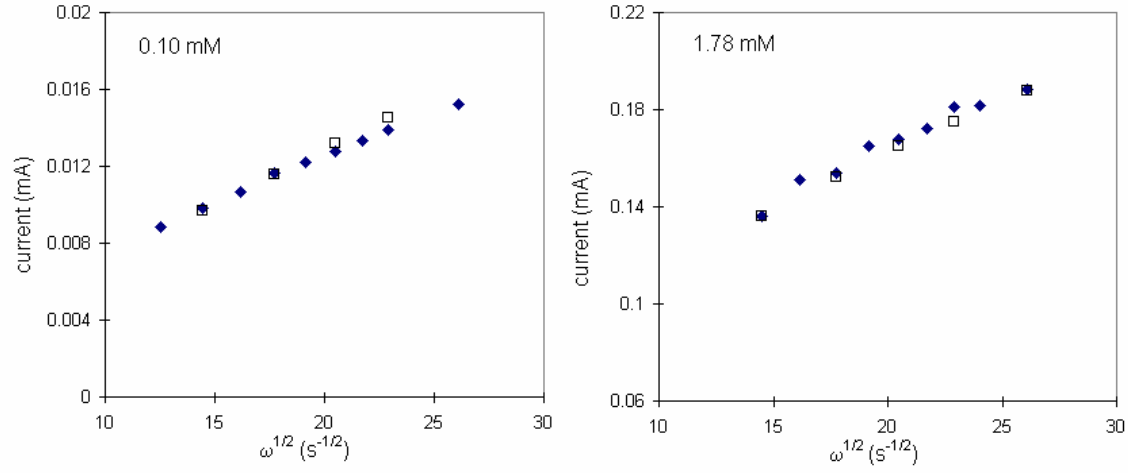

Figure 4-10. Simulated and experimental currents of CE process vs $\omega^{1/2}$.

Currents at 0.10 mM and 1.78 mM are plotted against $\omega^{1/2}$. Following Eq. (4-3) – Eq. (4-5):
$K_1 = 1\times10^5$ M, $k_{f1} = 500$ $M^{-1}s^{-1}$, $k_{b1} = 0.005$ s^{-1}; $K_2 = 2.8\times10^3$ M^{-1}, $k_{f2} = 3.4\times10^4$ $M^{-1}s^{-1}$, $k_{b2} = 12.14$ s^{-1}.

In all suggested structures, the previous "equatorial" ligands are off plain. The square planar configuration of Cu(II) is distorted. This distortion is not favored by a d^8 form of Cu(III), meaning the redox potential of the distorted form shall increase. The binuclear complex is likely to be electroinactive in the applied potential range, which fits our hypothesis.

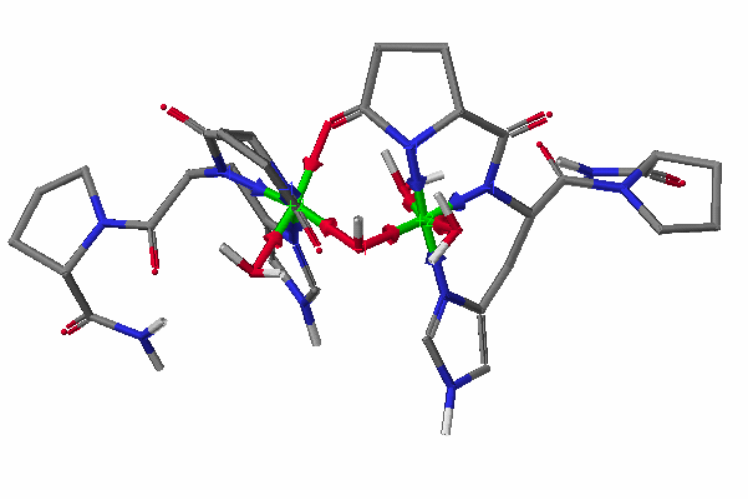

Figure 4-11. CAChe calculation of a possible structure of dimer $Cu(II)_2$-TRH_2.

An OH^- acts as a bridge. The lactam oxygen of the pGlu residue from the right monomer coordinates with Cu(II) of the left monomer in the apical position.

The hypothesis that dimer formation is responsible for the behavior of Cu(II)-TRH and the analogous MeHisTRH complex, but that there is no analogous behavior of TRHOH is consistent with the observations as well. We interpret the difference in the behavior of the latter (compared to the former two) complex based on electrostatics. In the case of TRHOH, There is an added electrostatic barrier to dimer formation, inhibiting it.

Since the simulated currents match the experimental values rather well in the applicable concentration or rotation frequency range, it shall be deduced that the values $I_{CE} / i_{E\ only}$ decreases at certain rotation frequency as concentration decreases. The simulation has verified that a dimer complex of $Cu(II)_2$-TRH_2 very possibly exists. Its carries a negative charge at the hydroxo-bridge that links the two Cu(II) centers.

4.5. Conclusions

Major Cu(II) complex of TRH formed in a still solution is not electroactive. Electric field perturbs equilirbia and gives rise to current. RRDE proves useful in the kinetics study. We have found that multiple chemical processes accompany the redox reaction of the Cu(II) complexes of TRH. A binuclear $Cu(II)_2$-TRH_2 cluster is suggested. Molecular simulation suggests distortion of the Cu(II) coordination toward square pyramidal structure, which is less favored by d^8 of Cu(III) oxidation state. The dimer is then less electroactive.

BIBLIOGRAPHY

[1]. Chen, J.-G.; Weber, S. G. *Anal. Chem.* **1995**, *67*, 3596-3604.

[2]. Warner, A. M.; Weber, S. G. *Anal. Chem.* **1989**, *61*, 2664-2668.

[3]. Woltman, S. J.; Alward, M. R.; Weber, S. G. *Anal. Chem.* **1995**, *67*, 541-551.

[4]. Prange, A. J., Jr.; Lara, P. P.; Wilson, I. C.; Alltop, L. B.; Breese, G. R. *Lancet* **1972**, *2*, 999-1002.

[5]. Faden, A. I. *Arch. Neurol.* **1986**, *43*, 501-504.

[6]. De Marinis, L.; Mancini, A.; Valley, D.; Bianchi, A.; Gentilella, R.; Liberale, I.; Mignani, V.; Pennis, M.; Della Corte, F. *Clin. Endocrinol.* **1999**, *50*, 741-747.

[7]. Koskinen, L. O. D.; Koch, M. L.; Svedberg, J. *Ups. J. Med. Sci.* **2000**, *105*, 73-83.

[8]. Manaka, S.; Sano, K. *Neurosci. Lett.* **1978**, *8*, 255-258.

[9]. Meng, R.; Becker, J.; Lin, F.-T.; Saxena, S.; Weber, S. G. *Inorg. Chim. Acta* **2005**, *358*, 2933-2942.

[10]. Albery, W. J.; Hitchman, M. L., *Ring-Disk Electrodes*. **1971**, Oxford: Clarendon Press.

[11]. Kurtz, J. L.; Burce, G. L.; Margerum, D. W. *Inorg. Chem.* **1978**, *17*, 2454-2460.

[12]. Aris, R. *Proc. Roy. Soc.* **1956**, *A252*, 538-550.

[13]. Taylor, G. I. *Proc. Roy. Soc.* **1953**, *A219*, 186-203.

[14]. Beisler, A. T.; Schaefer, K. E.; Weber, S. G. *J. Chromatogr. A* **2003**, *986*, 247-251.

[15]. Lii, J. H.; Allinger, N. L. *J. Am. Chem. Soc.* **1989**, *111*, 8576-8582.

[16]. Billo, E. J. *Inorg. Nucl. Chem. Lett.* **1974**, *10*, 613-617.

[17]. Margerum, D. W. *Pure Appl. Chem.* **1983**, *55*, 23-34.

[18]. Rybka, J. S.; Kurtz, J. L.; Neubecker, T. A.; Margerum, D. W. *Inorg. Chem.* **1980**, *19*, 2791-2796.

[19]. Bossu, F. P.; Chellappa, K. L.; Margerum, D. W. *J. Am. Chem. Soc.* **1977**, *99*, 2195-2203.

[20]. Berezovski, M.; Krylov, S. N. *Anal. Chem.* **2005**, *77*, 1526-1529.

[21]. Berezovski, M.; Krylov, S. N. *J. Am. Chem. Soc.* **2002**, *124*, 13674-13675.

[22]. Arvia, A. J.; Bazan, J. C.; Carrozza, J. S. W. *Electrochim. Acta* **1966**, *11*, 881-889.

[23]. Li, J.; Carr, W. *Anal. Chem.* **1997**, *69*, 2530-2536.

[24]. Estes, E. D.; Hatfield, W. E.; Hodgson, D. J. *Inorg. Chem.* **1974**, *13*, 1654.

[25]. Thompson, L. K. *Can. J. Chem.* **1983**, *61*, 579-583.

[26]. Sorrell, T. N. *Biol. Inorg. Copper Chem., Proc. Conf. Copper Coord. Chem., 2nd* **1986**, *2*, 41-55.

[27]. Seco, J. M.; Amador, U.; Garmendia, M. J. G. *Polyhedron* **1999**, *18*, 3605-3610.

[28]. Crawford, V. H.; Richarson, H. W.; Wasson, J. R.; Hodgson, D. J.; Hatfield, W. E. *Inorg. Chem.* **1976**, *15*, 2107-2110.

[29]. Zhou, J.-H.; Cheng, R.-M.; Song, Y.; Li, Y.-Z.; Yu, Z.; Chen, X.-T.; Xue, Z.-L.; You, X.-Z. *Inorg. Chem.* **2005**, *44*, 8011-8022.

[30]. Das Sarma, B. *J. Am. Chem. Soc.* **1956**, *78*, 892-894.

5. The Electrochemistry of Cu(II) Complex of the Octarepeat Peptide of the Prion Protein

5.1. Abstract

The octarepeat peptide of prion protein interacts with Cu(II) under physiological conditions. We have found it also binds Cu(I). The tryptophan side chain may participate. Cyclic voltammetry shows diffusion-controlled stripping-free curves of Cu(II) reduction with presence of Ac-PHGGGWGQ-NH_2, a single unit of the octarepeat region. Visible spectroscopy serves to identify any Cu(II) complex of Ac-PHGGGWGQ-NH_2 based on its absorption around 630 nm. Increasing the peptide concentration shifts the overall wave of Cu(II)/Cu(I) reduction to more positive potentials. The Cu(I) and Ac-PHGGGWGQ-NH_2 coordination does not display a single stoichiometry in the phosphate-tartrate buffer used. Multiple components and exchange processes exist.

This work is supportive of the neuro-protective function of the prion protein.

5.2. Introduction

Prion protein is believed to be responsible for a group of neurodegenerative diseases in its aggregated form [1-3]. Metal ions are found to interact with prion protein. A few binding sites have been identified, mainly around His residues [4-7]. The most interesting fragment is the N-terminal octarepeats, residues 59-91 containing tandem copies of (Ac-PHGGGWGQ-NH_2). It is a highly conserved domain in different species [8], implying roles in the normal functions of the protein. It is generally agreed by most results that each octarepeats binds one Cu(II) ion at physiological pH [9-11] and the HGGGW sequence is the fundamental binding unit [11]. Other stoichiometries at low Cu(II): peptide ratios have been noted [12]. A crystal structure of Cu(II)-HGGGW [13] indicates equatorial binding at one His nitrogen, two deprotonated peptide amide nitrogens, and the carbonyl oxygen of the second Gly.

Suggested functions of the prion protein include regulation of metal toxicities, especially those of Cu(II)[14-17]. Excess Cu(II) in mammal body is reduced by superoxide or reducing agents such as ascorbic acid and GSH to generate Cu(I). This unstable product may react with hydrogen peroxide to produce very reactive hydroxyl radicals via Habor-Weiss reaction [18, 19]:

$$Cu(I) + H_2O_2 \rightarrow Cu(II) + OH^- + OH\bullet \qquad \text{Eq. (5-1)}$$

The produced OH• is known to be damaging [20]. Shiraishi et al. have found that the octarepeat fragment binds copper resulting in suppressed copper-induced generation of reactive oxygen species [21]. A few research groups claimed that octarepeats peptide reduced cupric ion to cuprous ion, and the presence of Trp residue was critical [22-24]. Most recently, Chacon et al. showed reduced neuron density in rat brain tissues upon Cu(II) administration, and this toxicity was suppressed by Ac-PHGGGWGQ-NH_2 [17]. Moreover, replacement of the Trp but not the metal binding His residue by Ala decreased the protecting effect of the peptide.

Notably, though numerous studies have been carried out on the interaction of metal ions and the prion protein and its various fragments and redox activity is discussed, electrochemical studies are rather rare. Bonomo et al. [25] observed an irreversible reduction from Cu(II)-Ac-PHGGGWGQ-NH_2. The authors assigned this signal as coordinated Cu(II) being reduced to Cu(I) species, which partially dissociated from the peptide ligand. Little effort has been made by means of electrochemistry aside from that.

A great number of proteins interact with copper in both bivalent and monovalent states. Electrochemical methods allow insights of metal-ligand interactions and should not be excluded from the studies of prion protein and Cu(II) interactions. Cu(II) ion undergoes 2-step reduction to produce elemental copper. Because of the fast disproportion of Cu(I) ion, in aqueous solutions reduction of Cu(II) appears to be a 1-step 2-electron transfer. The reactions can be written as:

$$Cu(II) + e = Cu(I) \qquad \text{Eq. (5-2)}$$

E_0 = 0.153 V vs. NHE [22], - 0.056 V vs. Ag/AgCl

$$2Cu(I) = Cu(II) + Cu(0) \qquad \text{Eq. (5-3)}$$

Ligand existence may shift the potentials to reduce Cu(II) and Cu(I), such as acetonitrile [23]. Particularly on ligand-affected Cu(II) electrochemical reactions:

$$Cu(II)L_p + e = Cu(I)L_q + (p\text{-}q)L \qquad \text{Eq. (5-4)}$$

$$Cu(I)L_q + e = Cu(0) + qL \qquad \text{Eq. (5-5)}$$

the redox potentials and complex stability constants follow the equation [24]:

$$E_{Cu^{II}L_p/Cu^{I}L_q} - E_{Cu^{II}/Cu^{I}} = -0.0591\log\frac{K_{Cu(II)L_p}}{K_{Cu(I)L_q}} - (p-q)0.0591\log[L] \qquad \text{Eq. (5-6)}$$

$$E_{Cu^{I}L_q/Cu^{0}} - E_{Cu^{I}Cu^{0}} = -0.0591\log K_{Cu(I)L_q} - q0.0591\log[L] \qquad \text{Eq. (5-7)}$$

This chapter describes simple cyclic voltammetry technique on a microelectrode that gives us information otherwise unseen. Some comments on the neuro-toxicity and protective effects associated with Cu(II) and Ac-PHGGGWGQ-NH_2 will also be addressed.

5.3. Experimental

5.3.1. Chemicals

The prion protein octarepeat fragment (Ac-PHGGGWGQ-NH_2) and its five-residue fragment Ac-PHGGG-NH_2 were synthesized by the Peptide Synthesis Service at the University of Pittsburgh. HPLC data showed that each peptide had a purity of 99%.

Artificial cerebral-spinal fluid (aCSF) contained 145.0 mM NaCl (EMD Chemicals, Gibbstown, New Jersey), 1.2 mM $CaCl_2$ (EMD Chemicals), 2.7 mM KCl (EMD Chemicals), 1.0 mM $MgCl_2$ (Fisher Sci., Fairlawn, New Jersey), and 2.0 mM NaH_2PO_4 (J.T.Baker, Phillipsburg, New Jersey). Phosphate buffer contained 10.0 mM sodium phosphate monobasic (J. T. Baker), 3.0 mM sodium potassium tartrate (J. T. Baker, re-crystallized twice from water), and 0.10 M potassium nitrate (Acros, Morris Plaines, New Jersey). Non-buffered solution contained 0.10 M potassium nitrate (Acros). A NaOH (J. T. Baker) solution of no lower than 4 M concentration was used to bring the pH up to 7.43 - 7.46. A NaOH solution of 0.05 M was added to spectroscopic cuvette for observation of Cu(II)-Ac-PHGGGWGQ-NH_2 forming. Copper sulfate pentahydrate (J.T. Baker) was re-crystallized from water. All other reagents were used without further purification, but purities were taken into account in preparation.

All solutions were prepared using water from an A10 synthesis water system (Millipore, Billerica, Massachusetts, USA). All pH values were measured with an Accumet® pH meter (Fisher Sci.), calibrated before each use. Calibration of the pH meter typically was carried out at 36 - 37 °C.

5.3.2. Instruments:

The electrochemical cell was a two-layer glass cup with a home-made Styrofoam lid with holes. Three-electrode system consisted of a BAS Ag/AgCl reference electrode (Bioanalytical

Systems, West Lafayette, Indiana), a Platinum grid auxiliary electrode (Goodfellow, Devon, Pennsylvania), and a micro-disk working electrode made with 30 μm carbon fiber (World Precision Instruments, Inc., Sarasota, Florida). Unless stated, potentials reported in this chapter are against Ag/AgCl. The exposed electrode area of the micro-disk was calibrated with 0.301 mM ferricyanide reduction wave at room temperature. The solution was in 0.10 M KNO_3 and 0.15 M KCl. Calculated A = 8.55×10^{-6} cm^2. (Limiting current at 0.00 V = 1.36 nA. D = 7.09×10^{-6} cm^2/s in 0.10 M KNO_3 [26]).

Potentials were scanned by an Epsilon EC potentiostat (Bioanalytical Systems, Inc.). A Colora WK-5 Kryo-thermostat (Colora, Germany) provided water bath to the cell which maintained the solution at 36.7 – 37.2 degree Celsius measured in the cell. All electrochemical experiments were conducted at this temperature range. Between each two runs, working electrode was polished with 0.05 μm alumina (Buehler Ltd, Lake Bluff, Illinois, USA) slurry in water. Each solution (3.0 ml or less) was de-oxygenized with 4.8 grade argon (Valley National Gases, West Mifflin, Pennsylvania) for at least 10 minutes. The argon flow was then kept above the solution at lower rate during the whole course of experiments. Obtained voltammograms were processed with PeakFit (Jandel Sci Software, San Rafael, California) to get first derivative (to find half wave potentials) using Savitzki-Golay 1^{st} derivative function at 4.0% - 8.0% level.

In the thermodynamic measurements (half wave potentials at varied peptide concentrations), Ag/AgCl reference electrode was checked against saturated calomel electrode (SCE) (Bioanalytical Systems, Inc) daily with the same phosphate-tartrate buffer used in the cyclic voltammetry experiments. The potential of employed Ag/AgCl electrode were -12 to -14 mV against SCE in all measurements.

Visible spectra were taken with a HP 8453 spectrometer (Hewlett and Packard, USA) using a 1 cm quartz cuvette (Starna Cells, Inc., Atascadero, California). The buffer was used as blank. Spectra were all taken at 5 second integration and reported either as original or sampled every 5 points.

5.4. Results

Diffusion coefficient of a redox active species is important in analyzing its voltammograms. The value of aqueous Cu(II) ion at 37 °C can be calculated from the constant $D\eta/T = 2.23 \pm 0.37 \times 10^{-10}$ cm^2poise/sK [27]. Using dynamic viscosity values of water at 35 and 40 °C (797.7 and 653.2 $\times 10^{-5}$ poise) the kinematic diffusion coefficients were calculated to be 8.47×10^{-6} and 10.7×10^{-6} cm^2/s. By assuming linear increasing of D with temperature between 35 and 40 °C, calculated D value at 37 °C is $10.0 \pm 1.6 \times 10^{-6}$ cm^2/s.

5.4.1. Oxidation of Ac-PHGGGWGQ-NH_2

On a 1 mm diameter glassy carbon electrode, the peptide in pH 7.4 aCSF gives an irreversible oxidation peak at 0.80 V (Figure 5-1). This potential is within the reported potential range of Trp and the peak shape also agrees with available literature [26].

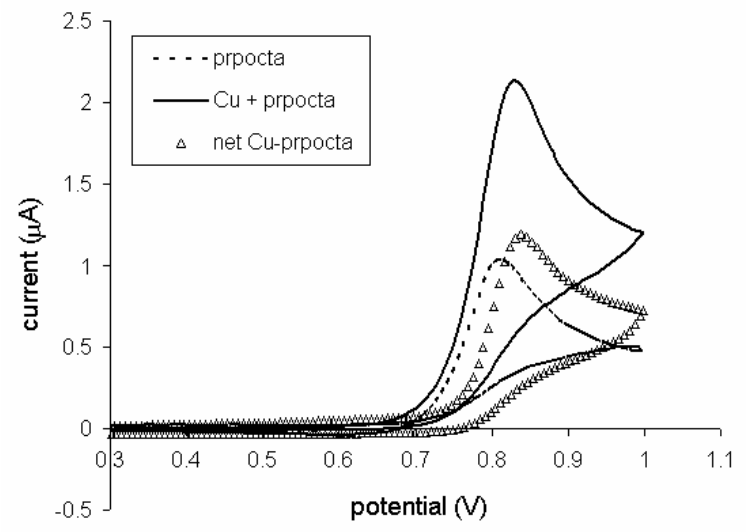

Figure 5-1. Cyclic voltammograms of Cu(II) and Ac-PHGGGWGQ-NH_2 in aCSF on 1 mm glassy carbon electrode.

All concentrations were 0.50 mM. Scan rates were 200 mV/s.

5.4.2. Oxidation of Cu(II) ion and Ac-PHGGGWGQ-NH_2 mixture

At a 1 mm diameter glassy carbon electrode, an equimolar solution of Cu(II) and Ac-PHGGGWGQ-NH_2 in pH 7.4 aCSF displays an irreversible oxidation with a peak potential of 0.82 V (Figure 5-1). The peak current corresponds to more than a 1 electron transfer, considering that the diffusion coefficient of Cu(II)-Ac-PHGGGWGQ-NH_2 is on the order of 10^{-6} cm^2/s. After subtraction of the peptide voltammogram from the mixture voltammogram, a "net" oxidation peak is obtained at 0.825 V. This should be ascribed to the oxidation of the complex [29, 30]. The peak current is still higher than 1 electron transfer. No reversed signals have been observed.

Similar phenomena have been reported with peptide ligands bearing Tyr residue, another electroactive residue [31]. According to the authors, the oxidation of Cu(II) to Cu(III) and of the Tyr residue are additive. The peptide oxidizes at a potential less positive than the Cu(II)-peptide complex. Its oxidation products rapidly reduce Cu(III)-peptide. These homogeneous reactions consume Cu(III) complex, resulting in the absence of a cathodic signal in the voltammetry of the complex. The Oxidation potential of Trp is less positive than the Cu(II) complex. A similar interpretation may be imposed on the Cu(II)-Ac-PHGGGWGQ-NH_2 complex. Products of oxidized Ac-PHGGGWGQ-NH_2 rapidly react with Cu(III) species thus no cathodic wave is seen on the reverse sweep.

5.4.3. Cu(II)-Ac-PHGGGWGQ-NH_2 binding

The coordination of Cu(II) and Ac-PHGGGWGQ-NH_2 can be verified by the color of the complex. Cu(II)-peptide complexes often display characteristic bands in blue to violet region. Bonomo et al. reported maximum absorption (λ_{max}) at 614 nm of the complex at pH 6-8 [25]. Luczkowski et al. reported 621 nm for the species $CuH_{-2}L$ (L = Ac-PHGGGWGQ-NH_2) with $\log\beta = -8.87 \pm 2$ [32], which accounted for 90% of total Cu(II) species at pH 7.4. The λ_{max} is

high for a set of equatorial ligands: imidazole, 2 amide, carbonyl (NNNO), but low for an NNOO environment [33, 34]. The crystal structure [35] shows that there is an axial water hydrogen-bonded to the Trp side chain. The axial bond distorts the square planar structure of Cu(II) toward a square pyramid structure. According to Billo [34], such axial bonding in a Cu(II) complex destabilize the complex and red-shifts the λ_{max}.

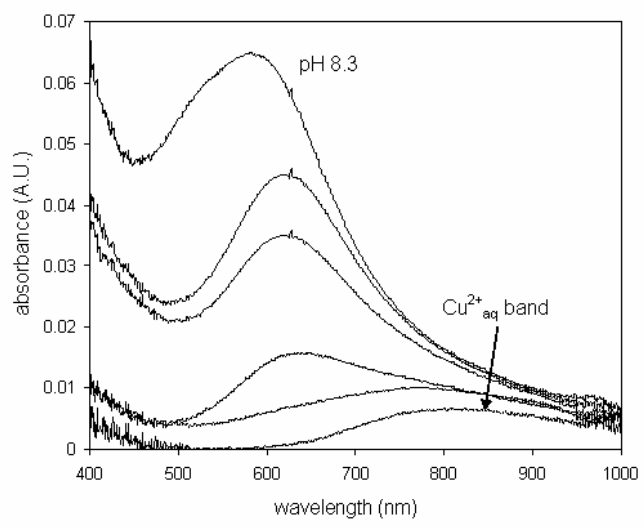

Figure 5-2. Visible spectra of Cu(II)- Ac-PHGGGWGQ-NH_2 mixture titrated with NaOH.

Starting volume is 960 μl. Each additional curve indicates one aliquot of 2 μl 0.050 M NaOH added.
Only pH of last solution has been measured and annotated. At beginning,
[Cu(II)] = [Ac-PHGGGWGQ-NH_2] = 0.30 mM.
Solution also contained 0.10 M KNO_3.

The imidazole moiety of His residue is basic. Its pKa is 6.0 when forming $CuH_{-2}L$ complex [32]. Cu(II) starts to interact with Ac-PHGGGWGQ-NH_2 when pH is above 5.3 or so [11], when the His imidazole starts getting deprotonated. In non-buffered solutions the imidazole moiety remains protonated, unless external OH^- is added. Figure 5-2 shows in non-buffered solution, gradually added OH^- shift the Cu(II) absorption band from aqueous free ion to Ac-

PHGGGWGQ-NH_2 bounded state. The further blue shift beyond 600 nm at pH 8.3 is possibly a $CuH_{-3}L$ species [32].

5.4.4. Reduction of Cu(II) in presence of Ac-PHGGGWGQ-NH_2

Ac-PHGGGWGQ-NH_2 binds Cu(II) under certain circumstances. Interaction of Ac-PHGGGWGQ-NH_2 with Cu(I) has not been looked into to date.

Reduction of aqueous Cu(II) leads to solid Cu deposition [36]. On a microelectrode, the presence of Cu° is deduced from the presence of a stripping peak. If the reduction of Cu(II) does not yield a stripping peak, we infer that the product is a soluble Cu(I) species.

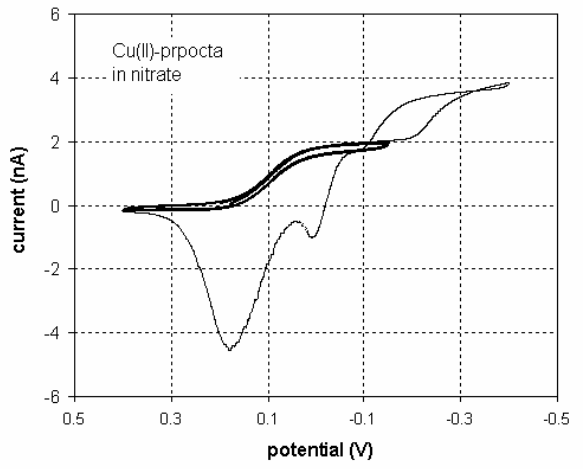

Figure 5-3. Cyclic voltammograms of Cu(II) reduction in presence of Ac-PHGGGWGQ-NH_2 in un-buffered solution.

Cu(II) and Ac-PHGGGWGQ-NH_2 are 0.30 mM each in 0.10 M KNO_3. Darker and lighter lines indicate different scanning range.

Shown in Figure 5-3, Cu(II) is reduced at a microelectrode in presence of equimolar Ac-PHGGGWGQ-NH_2 in unbuffered KNO_3 solution. In this solution there is no Cu(II) complex of Ac-PHGGGWGQ-NH_2 formed, as indicated in Figure 5-2. The CV scanned from 0.4 V to -0.15 V gives a diffusion-controlled wave at 0.096 V. No oxidation wave is observed indicating no

deposition occurs during reduction process. The potential is much more positive than that of Cu(II) ion, -0.056 V vs. Ag/AgCl. The limiting current corresponds to 1-electron transfer with diffusion coefficient $1x10^{-5}$ cm^2/s. This value is in good agreement with that of aqueous Cu(II) ion at 37 °C [27]. A second reduction wave occurs at -235 mV. This wave features a slightly lower steady state current than the first one. This wave is accompanied by an anodic stripping peak.

The simplest explanation for the data is that Cu(II) is reduced to a Cu(I)-peptide complex at the first wave. This complex is reduced to Cu(0) at the second wave

Cu(I) ion is a soft Lewis acid. It binds "soft" ligands better. Among its most well known ligands are the phenanthroline family to which the Cu(I) indicator bathocuproine belongs [22-24]. A mixed-ligand complex of Cu(I) with a member of this family and triglycine existed transiently when reduced by cyclic voltammetry, which called for at least two soft nitrogen donors to form a relatively stable Cu(I) complex [37]. In the case of Ac-PHGGGWGQ-NH_2, the Trp may play a role as a potential nitrogen donor. Figure 5-4 shows the voltammograms of the Cu(II)-Ac-PHGGG-NH_2 system. The stripping-free curve (bold) shows that Ac-PHGGG-NH_2 also prevents Cu(I) disproportion, possibly by binding Cu(I), too. The first half-wave potential is 0.041 V, less positive compared to that of the Ac-PHGGGWGQ-NH_2 (0.096 V). The second half wave potential is -0.141 V, more positive compared to that of Ac-PHGGGWGQ-NH_2 (-0.235 V). The separation of the two reduction steps is less than in the case of the octa-peptide. These observations are consistent with a weaker interaction of Cu(I) with Ac-PHGGG-NH_2 than with Ac-PHGGGWGQ-NH_2. The Trp residue is most likely responsible. In other words, the Trp side chain, or more exactly the indole nitrogen, may be capable of interacting with Cu(I)..

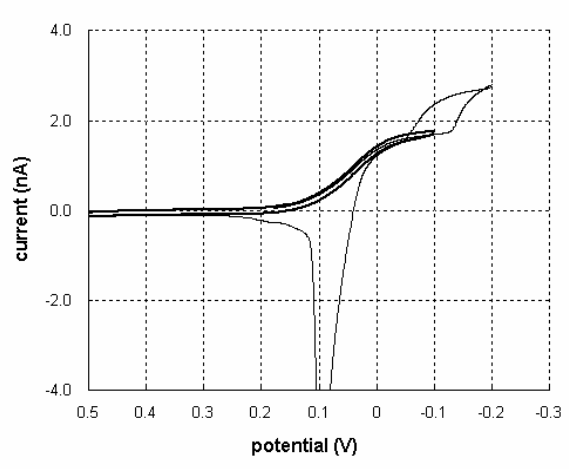

Figure 5-4. Cyclic voltammograms of Cu(II) in presence of pentapeptide Ac-PHGGG-NH_2 in un-buffered solution.

Cu(II) and Ac-PHGGG-NH_2 are 0.30 mM each. Solutions contain 0.10 M KNO_3.

The reduction half-wave potential is useful to evaluate the binding of Ac-PHGGGWGQ-NH_2 with Cu(II) and Cu(I). Regression of $E_{1/2}$ against ligand concentration at equilibrium provides information of formation constants ratio of the two oxidation states in its intercept, and information of difference in ligand numbers in the two complexes in its slope (see Eq. (5-6)). The Cu(II)- Ac-PHGGGWGQ-NH_2 system is then put in phosphate buffer with large excess of tartrate with respect to copper species. In this fashion Cu(II) ion will not precipitate because of coordination with tartrate. It also mimics the physiological condition in which Cu(II) is bound and virtually no free aqueous Cu(II) ion exists.

Figure 5-5 shows the voltammograms of Cu(II) in the presence of varying concentrations of peptide. The backward scan has been checked for Cu(II) to peptide ratio 3:4 and 3:30 to make sure no deposition forms within certain potential range (data not shown). At least two waves are seen in each voltammogram. Taking the first derivative of each voltammogram reveals another wave in between the two clearly seen ones. The current of this wave is low. It indicates a low abundance copper species. Figure 5-6 shows how half-wave potentials of the three waves vary

with Ac-PHGGGWGQ-NH_2 concentration. The first reduction wave features wider differential peaks than a reversible 1-electron redox process. They are typically asymmetrical and composed of multiple components. An "overall" $E_{1/2}$ is found for each voltammogram, which is the lowest point of the differential peak (Differential peaks are downward). The overall $E_{1/2}$ shifts toward *positive* potentials with increasing Ac-PHGGGWGQ-NH_2 concentration, meaning that Cu(I) is ligated to more peptide ligands than Cu(II). The second wave is not affected by Ac-PHGGGWGQ-NH_2 concentration, meaning the oxidized and reduced forms contain same number of Ac-PHGGGWGQ-NH_2 ligands. The third wave shifts toward *negative* potentials. Its differential peak is sharp with a relaxation resembling an exponential decay. This shape is a sign of insoluble redox product formation. Consistently it indicates Ac-PHGGGWGQ-NH_2 as a Cu(I) ligand stabilizes Cu(I) from being reduced to Cu(0).

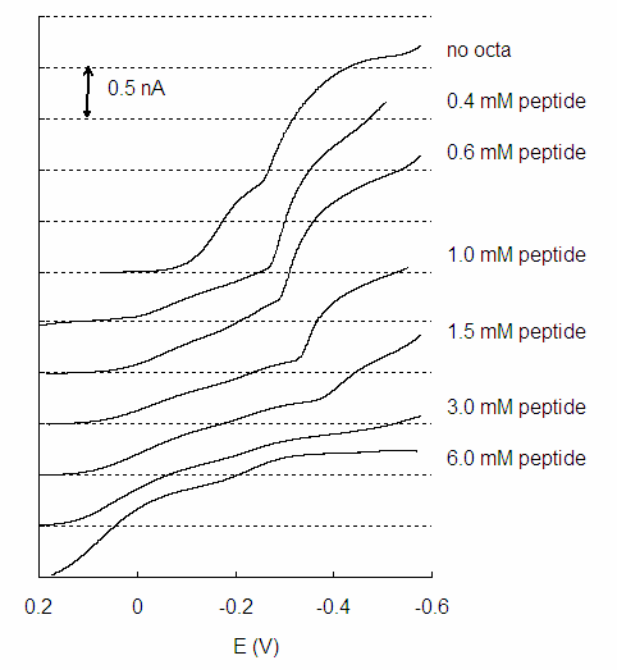

Figure 5-5. Cu(II) reduction in presence of varied Ac-PHGGGWGQ-NH_2 concentrations.

Cu(II) is 0.30 mM in 10.0 mM phosphate buffer (pH 7.43) with 3.0 mM tartrate.
Buffer blank is subtracted from each voltammogram.

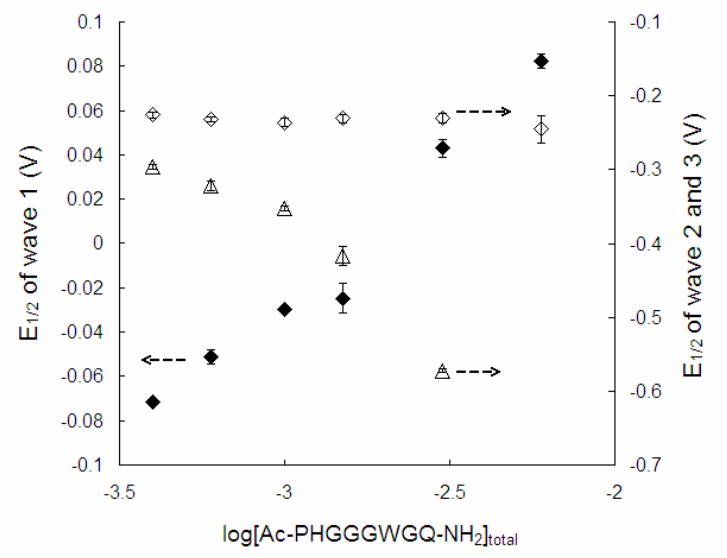

Figure 5-6. Half-wave potential shift of Cu(II) reduction with varied Ac-PHGGGWGQ-NH_2 concentration.

Cu(II) is 0.30 mM in each solution. All in 10.0 mM pH 7.43 phosphate buffer with 3.0 mM KNaTar.

♦: first wave, ◊: second wave, △: third wave.

To analyze these potential data we need to know the coordination profile of Cu(II) in the system. Visible spectra of same composed solutions show blue-shifting of maximum absorption bands (λ_{max}) as peptide concentration increases (Figure 5-7). With presence of large excess tartrate, Ac-PHGGGWGQ-NH_2 at this pH is not competitive enough compared to tartrate. The equilibrium

$$Cu^{2+} + \text{Ac-PHGGGWGQ-}NH_2 \rightarrow Cu^{2+}\text{- Ac-PHGGGWGQ-}NH_2$$

becomes

$$Cu^{2+}\text{-Tar} + \text{Ac-PHGGGWGQ-}NH_2 \rightarrow Cu^{2+}\text{-Ac-PHGGGWGQ-}NH_2 + \text{Tar}$$

The Cu(II)-Tar complexation system is a complicated multi-components system involving multi-nuclear species [35]. The above equations do not show actual stoichiometry related to these complexes.

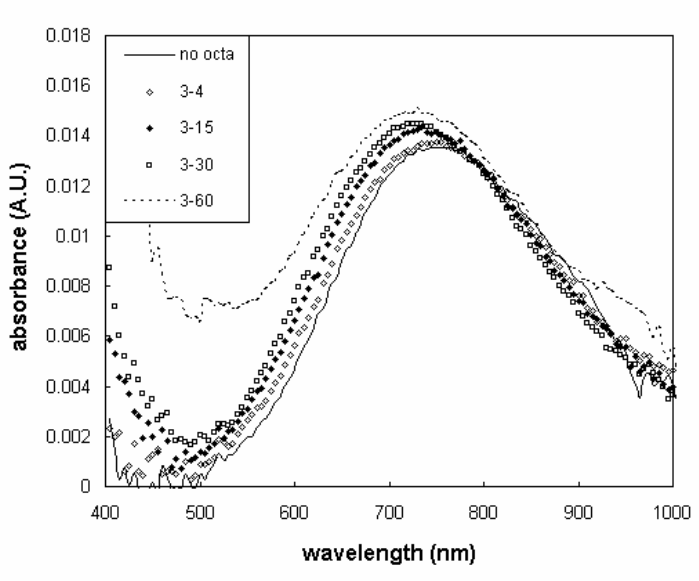

Figure 5-7. Visible spectra of 0.30 mM Cu(II) in presence of varied concentrations of Ac-PHGGGWGQ-NH_2**.**

Solution contains 10.o mM phosphate buffer (pH 7.4) and 3.0 mM tartrate.
Legends indicate molar ratio of Cu(II) to Ac-PHGGGWGQ-NH_2.

By subtracting the Cu(II)-tar spectrum from each with Ac-PHGGGWGQ-NH_2, we get spectra representing A/b = [Cu(II)-Ac-PHGGGWGQ-NH_2]$\cdot\left(\varepsilon_{Cu-Ac-PHGGGWGQ-NH_2}\right)$, where b is the path length. The "net" spectra all have λ_{max} at 630 nm, which should represent the Cu(II)-Ac-PHGGGWGQ-NH_2 complex. Calculated using $\varepsilon_{\text{Cu-PHGGGWGQ, 621nm}}$ from reference [32] and $\varepsilon_{\text{Cu-Tar, 630nm}}$ from our experimental data, the Cu(II)- Ac-PHGGGWGQ-NH_2 formed at pH 7.4 with tartrate present is no more than 15% of total Cu(II) when Ac-PHGGGWGQ-NH_2 is 1.50 mM, 5 times the total Cu(II). For all the Ac-PHGGGWGQ-NH_2 concentrations investigated, the Cu(II)-Ac-PHGGGWGQ-NH_2 complex formed only accounts for at most a few percent of total peptide

The data in Fig 5 consistently indicate that the first wave in the Cu(II)-Ac-PHGGGWGQ-NH_2 system is the reduction of Cu(II)-Tar to Cu(I)-Ac-PHGGGWGQ-NH_2. The second wave we believe is the reduction of Cu(II)-Ac-PHGGGWGQ-NH_2 to Cu(I)-Ac-PHGGGWGQ-NH_2, based

on its low current. The third wave corresponds to reduction of Cu(I) complexes of Ac-PHGGGWGQ-NH_2 to Cu(0).

For the reduction

$$Cu(II)_m Tar_n^{2(m-n)} + me^- + mpL = mCu(I)L_p + nTar^{2-}, \qquad \text{Eq. (5-8)}$$

half wave potential is expressed as

$$E_L = E_{Tar} + \frac{RT}{mF}\ln[L]^{mp} = E_{Tar} + p\frac{RT}{F}\ln[L] \qquad \text{Eq. (5-9)}$$

In Eq. (5-9), E_L stands for the half wave potential of the Cu(II) reduction in presence of L (i.e., Ac-PHGGGWGQ-NH_2), E_{Tar} stands for the half wave potential of Cu(II) reduction with presence of tartrate only, and p stands for number of peptide ligands per Cu(I) (generally, it is the difference in numbers of ligand L per metal at the reduced and oxidized forms.. We will be able to used $[L]_{total}$ instead of $[L]_{eq}$. The slope of the regression of E_L against $log[L]_{total}$ is the value of RT/F (0.0615 V at 37 °C) multiplied by p. By regression of $E_{1/2}$ of a wave vs. $log[L]$, the value p can be obtained..

Though the $E_{1/2}$ of the first wave displays some linearity against $\log[L]_{total}$, the broad differential peaks of the waves prevent us from using the $E_{1/2}$ values to determine the actual p value. The wave is associated with various ligand exchange processes. Any quantitative regression is meaningless. Nevertheless, it is still a firm indication that Ac-PHGGGWGQ-NH_2 as a Cu(I) ligand stabilizes Cu(I) from disproportion or precipitation. The number of Ac-PHGGGWGQ-NH_2 ligand per Cu(I) could be 1 and up, which is not resolved under current conditions. Consistently, the $E_{1/2}$ of the third wave is neither linear against logrism of ligand concentration, representing the reduction of multiple forms of Cu(I)-Ac-PHGGGWGQ-NH_2 to Cu(0) metal.

5.5. Discussion

We have demonstrated that the Cu-prion octarepeat has a rich electrochemistry. As others have observed, Cu(II) forms a complex with Ac-PHGGGWGQ-NH_2 at pH 7.4 in buffered aCSF. This complex is oxidizable at a potential near 0.8 V vs Ag/AgCl (3M NaCl). The natural peptide's tryptophan residue is oxidized at a similar potential.

The reduction of Cu(II) in the presence of Ac-PHGGGWGQ-NH_2 is more complicated. Our data are not consistent with the idea that the peptide reduces Cu(II) to Cu(I). If it did so, we would not see the spectrum in the 6 – 700 nm range, and we would not see a wave for the reduction of Cu(II) to Cu(I). If the product were a stable complex of a peptide or oxidized peptide and Cu(I), then the only reduction wave would be to Cu(0). We see reduction waves corresponding to products other than Cu(0) (i.e., freely diffusing products) .

In unbuffered solutions, Ac-PHGGGWGQ-NH_2 stabilizes Cu(I). The pentapeptide Ac-PHGGG-NH_2 stabilizes Cu(I) as well, but not as much as the octapeptide. Thus, the tryptophan stabilizes Cu(I) to a degree. In phosphate-buffered tartrate at pH 7.43 there are three reduction waves, one of which is the reduction of Cu(I) to Cu(0). The presence of tartrate avoids precipitation of copper ions as oxides/hydroxides but adds a competitive ligand. On the other hand, the presence of tartrate is at least qualitatively similar to the situation *in vivo* where Cu is protein-bound. The first two waves apparently correspond to tartrate-bound Cu(II) and peptide-bound Cu(II). Under the conditions of this experiment (excess peptide), multiple forms of complex are formed upon reduction of Cu(II) to Cu(I). The third wave has the characteristic shape of a reduction to metal, and corresponds to Cu(I) to Cu(0).

Using bathocuproine as a Cu(I) indicator to monitor Cu(I) level could cause methodological artifact [39], as its much stronger binding to Cu(I) than to Cu(II) increases the

oxidizing power of Cu(II) [40]. Under physiological conditions, there are reducing reagents such as ascorbic acid and GSH. Though the presence of Ac-PHGGGWGQ-NH_2 brings the potential to reduce Cu(II) to Cu(I) to more positive values, it is still not conclusive to assign a copper-reducing capability to the peptide. The peptide Ac-PHGGGWGQ-NH_2 is capable of stabilizing Cu(I) reduced by other reducing reagents. This means the Cu(I) can become less reactive with presence of the peptide. In other words, the oxidation of Cu(I) state to Cu(II) state, as in Habor-Weiss reaction, is unfavorably affected. Very possibly, the full length prion protein possesses similar ability, which supports the anti-oxidative stress function of the protein.

5.6. Conclusions

The peptide Ac-PHGGGWGQ-NH_2 mimics a Cu(II) binding unit in the prion protein octarepeat region. The electrochemical property of Ac-PHGGGWGQ-NH_2 does not enable it to reduce Cu(II). However, its coordinating property with Cu(I) may facilitate the reduction. Ac-PHGGGWGQ-NH_2 interacts with both Cu(II) and Cu(I). It binds electrically generated Cu(I) to prevent it from disproportion. The tryptophan side chain may be involved in the binding. Our work supports the of anti-copper toxicity function of the prion protein.

BIBLIOGRAPHY

[1]. Prusiner, S. B., *Science*, **1997**, 278, 245-251.

[2]. Prusiner, S. B., *Proc. Nat. Acad. Sci. US*, **1998**, 95, 13363-13383.

[3]. Dobson, C. M., *Tr. Biochem. Sci.*, **1999**, 24, 329-332.

[4]. Jones, C. E., Abdelraheim, S. R., Brown, D. R.,Viles, J. H., *J. Biol. Chem.*, **2004**, 279(31), 32018-32027.

[5]. Gaggelli, E. B., Francesca; Molteni, Elena; Pogni, Rebecca; Valensin, Daniela; Valensin, Gianni; Remelli, Maurizio; Luczkowski, Marek; Kozlowski, Henryk., *J. Am. Chem. Soc.*, **2005**, 127(3), 996-1006.

[6]. Stockel, J., Safar, J., Wallace, A. C., Cohen, F. E.,Prusiner, S. B., *Biochemistry*, **1998**, 37(20), 7185-7193.

[7]. Zong, X. H., Zhou, P., Shao, Z. Z., Chen, S. M., Chen, X., et al., *Biochemistry*, **2004**, 43(38), 11932-11941.

[8]. Wopfner, F., Weidenhofer, G., Schneider, R., Brunn, A. v., Gilch, S., et al., *J. Mole. Biol.*, **1999**, 289(5), 1163-1178.

[9]. Whittal, R. M., Ball, H. L., Cohen, F. E., Burlingame, A. L., Prusiner, S. B., et al., *Protein Sci.*, **2000**, 9(2), 332-343.

[10]. Viles, J. H., Cohen, F. E., Prusiner, S. B., Goodin, D. B., Wright, P. E., et al., *Proc. Nat. Acad. Sci. US*, **1999**, 96(5), 2042-2047.

[11]. Aronoff-Spencer, E., Burns, C. S., Avdievich, N. I., Gerfen, G. J., Peisach, J., et al., *Biochemistry*, **2000**, 39(45), 13760-13771.

[12]. Chattopadhyay, M., Walter, E. D., Newell, D. J., Jackson, P. J., Aronoff-Spencer, E., et al., *J. Am. Chem. Soc.*, **2005**, 127, 12647-12656.

[13]. Burns, C. S., Aronoff-Spencer, E., Dunham, C. M., Lario, P., Avdievich, N. I., et al., *Biochemistry*, **2002**, 41(12), 3991-4001.

[14]. Brown, D. R., *Neurobiology of Disease*, **2004**, 15(3), 534-543.

[15]. Jackson, G. S., Murray, I., Hosszu, L. L. P., Gibbs, N., Waltho, J. P., et al., *Proc. Nat. Acad. Sci. US*, **2003**, 98(15), 8531-8535.

[16]. Nishimura, T., Sakudo, A., Nakamura, I., Lee, D. C., Taniuchi, Y., et al., *Biochem. Biophys. Res. Commun.*, **2004**, 323(1), 218-222.

[17]. Chacon, M. A., Barria, M. I., Lorca, R., Huidobro-Toro, J. P.,Inestrosa, N. C., *Mole. Psych.*, **2003**, 8(10), 853-862.

[18]. Bremner, I., *Am. J. Clin. Nutri.*, **1998**, 67(5), 1069s-1073s.

[19]. Kadiiska, M. B., Hanna, P. M., Jordan, S. J.,Mason, R. P., *Mole. Pharmacol.*, **1993**, 44(1), 222-227.

[20]. Buettner, G. R., *Arch. Biochem. Biophys.*, **1993**, 300(2), 535-543.

[21]. Shiraishi, N., Ohta, Y.,Nishikimi, M., *Biochem. Biophys. Res. Commun.*, **2000**, 267(1), 398-402.

[22]. Ruiz, F. H., Silva, E.,Inestrosa, N. C., *Biochem. Biophys. Res. Commun.*, **2000**, 269, 491-495.

[23]. Opazo, C., Barria, M. I., Ruiz, F. H.,Inestrosa, N. C., *BioMetals*, **2003**, 16(1), 91-98.

[24]. Miura, T., Sasaki, S., Toyama, A.,Takeuchi, H., *Biochemistry*, **2005**, 44(24), 8712-8720.

[25]. Bonomo, R. P., Impellizzeri, G., Pappalardo, G., Rizzarelli, E.,Tabbi, G., *Chem. Eur. J.*, **2000**, 6(22), 4195-4202.

[26]. Konopka, S. J.,McDuffie, B., *Anal. Chem.*, **1970**, 42(14), 1741-1746.

[27]. Arvia, A. J., Bazan, J. C.,Carrozza, J. S. W., *Electrochim. Acta*, **1966**, 11(7), 881-889.

[28]. Harriman, A., *J. Phys. Chem.*, **1987**, 91, 6102-6104.

[29]. Chen, J.-G., Logman, M.,Weber, S. G., *Electroanalysis*, **1999**, 11(5), 331-336.

[30]. Meng, R., Becker, J., Lin, F.-T., Saxena, S.,Weber, S. G., *Inorg. Chim. Acta*, **2005**, 358(10), 2933-2942.

[31]. Tsai, H.,Weber, S. G., *Anal. Chem.*, **1992**, 64(23), 2897-2903.

[32]. Luczkowski, M., Kozlowski, H., Stawikowski, M., Rolka, K., Gaggelli, E., et al., *J. Chem. Soc. Dalton Trans.*, **2002**, 11, 2269-2274.

[33]. Sigel, H.,Martin, R. B., *Chem. Rev.*, **1982**, 82, 385-426.

[34]. Billo, E. J., *Inorg. Nucl. Chem. Lett.*, **1974**, 10, 613-617.

[35]. Millhauser, G. L., *Acc. Chem. Res.*, **2004**, 37(2), 79-85.

[36]. Bard, A. J., Lund, H.,Editors, *Encyclopedia of Electrochemistry of the Elements, Vol. 2: As, O, B, Re, Cu, Ta, Nb, Tc*. 1974. 512 pp.

[37]. Youngblood, M. P.,Margerum, D. W., *J. Coord. Chem.*, **1981**, 11(2), 103-110.

[38]. Blomqvist, K.,Still, E. R., *Inorg. Chem.*, **1984**, 23(13), 3730-3734.

[39]. Sayre, L. M., *Science*, **1996**, 274, 1933-1934.

[40]. Lappin, A. G., Youngblood, M. P.,Margerum, D. W., *Inorg. Chem.*, **1980**, 19(2), 407-413.